The subsurface structure of oblique impact craters

Dissertation vorgelegt von

Dipl.-Geol. Michael H. Poelchau

vom Fachbereich Geowissenschaften
der Freien Universität Berlin

zur Erlangung des akademischen Grades
doctor rerum naturalium
(Dr. rer. nat.)

Berlin, 2010

The subsurface structure of oblique impact craters

Dissertation vorgelegt von

Dipl.-Geol. Michael H. Poelchau

vom Fachbereich Geowissenschaften
der Freien Universität Berlin

zur Erlangung des akademischen Grades
doctor rerum naturalium
(Dr. rer. nat.)

Berlin, 2010

Gutachter: 1. PD Dr. Thomas Kenkmann

2. Prof. Wolf-Uwe Reimold

Tag der Disputation: 23.02.2010

Statement regarding the contributions of the author and others to this thesis

This thesis is comprised of three published, peer-reviewed articles and one submitted manuscript, which each form separate chapters within this thesis. The chapters “Introduction” and “General Conclusions” were written especially for this thesis. The PhD candidate is the first author of two of these articles, and the second author of the third article. The PhD candidate is also the first author of a manuscript currently submitted to Earth and Planetary Science Letters. Therefore, these four chapters have their own introduction, methodology, discussion, conclusions and references. The articles and manuscripts used in this thesis are the following:

Poelchau, M. H., and T. Kenkmann, 2008. Asymmetric signatures in simple craters as an indicator for an oblique impact direction, Meteoritcal and Planetary Science, 43, 2059-2072.

Poelchau M. H., Kenkmann T. and Kring D. A., 2009. Rim uplift and crater shape in Meteor Crater: the effects of target heterogeneities and trajectory obliquity. Journal of Geophysical Research, 114, E01006, doi:10.1029/2008JE003235.

Kenkmann, T. and Poelchau, M. H., 2009. Low-angle collision with Earth: The elliptical impact crater Matt Wilson, Northern Territory, Australia. Geology 37, 459-462.

Poelchau, M.H., and T. Kenkmann, 2010. Feather Features: A Low Shock Pressure Indicator in Quartz. Submitted to Earth and Planetary Science Letters.

Hans Knöfler and Ulli Raschke (MfN Berlin) prepared the thin sections used in this thesis. Sebastian Quart and Dirk Scherler (formerly MfN Berlin) acquired samples and data points from Wolfe Creek Crater, Australia. David A. Kring (LPI Houston) assisted in field work in Meteor Crater, Arizona. Alex Kurta (MfN Berlin) assisted in the generation of the map of Martin Crater, Mars. Thomas Kenkmann (MfN Berlin) created the map of Matt Wilson crater, Australia. All field work was performed by the candidate under the supervision and assistance of his supervisor, Thomas Kenkmann. All other maps, diagrams, microscope and u-stage measurements were generated by the candidate unless noted otherwise. This thesis was funded by the DFG, project KE 732/11-1.

Summary

In this thesis, several terrestrial and Martian impact craters were the subject of detailed structural field and remote sensing analysis, with a strong focus on structural deformation related to oblique impacts. Additional microstructural analysis of shear induced features in quartz grains from samples of several impact structures was performed and their role as shock metamorphic features was evaluated.

In the introduction of this thesis (chapter 1), the many facets of impact craters and their usefulness in different scientific and industrial fields is stressed. The structural processes of impact cratering are then briefly reviewed, and the prevalence of impacts caused by projectiles obliquely striking target surfaces is discussed.

Wolfe Creek crater, Australia, was the initial subject of structural analysis (chapter 2). The hypothesis is tested that the asymmetrical, non-radial distribution of the ejecta blanket commonly seen in oblique impacts on other planets can be followed back to an internal structural signal of deformed rock beds in terrestrial crater rims. A new method of strike and dip data evaluation is devised, and Wolfe Creek's bedding data is compared to structural asymmetries inferred from the ejecta blanket of Tooting crater Mars. The resulting non-radial signal in Wolfe Creek is used to infer the direction of impact.

For comparison, the results of Wolfe Creek crater are tested on a second terrestrial crater, Meteor Crater in Arizona, USA (chapter 3). The evaluation of bedding data from Meteor Crater shows that the expected signal of an oblique impact is weak and has been overprinted by deformational effects caused by the pre-impact target heterogeneities of an orthogonal joint set pattern. These deformational features, in particular so-called "radial corner faults" and "interthrust wedges" are observed in detail, and mechanisms of their generation are suggested that solidify the proposed connection of Meteor Crater's polygonal shape to the orthogonal joint sets.

Based on recent discoveries of central peaks that display non-radial structural deformation (e.g., Upheaval Dome, Utah, USA, Gosses Bluff, Australia), detailed mapping of the Matt Wilson impact structure, Australia, is performed (chapter 4). Mapping results reveal that Matt Wilson is the first elliptical crater found on Earth with a central uplift. The structural deformation of the central uplift is strongly non-radial and displays a preferred direction of thrusting and imbrication that coincides with the long axis of the eroded elliptical rim. Thus, for the first time, two independent indicators of non-radial deformation are found in the same impact structure, which infer an impact direction.

The promising results of Matt Wilson crater suggest that similar structural deformation must occur in impact craters on other planets, too. The central uplift of Martin Crater, Mars, is therefore structurally mapped, based on new, high-resolution HiRISE imagery (chapter 5). Results show that the orientation of structural deformation is at a ~180° angle to the direction

of impact inferred by the ejecta blanket. Recently published numerical models are used to devise a model for asymmetrical central uplift formation based on a chain of events initiated by oblique impact, and the relationship of the orientation of structural deformation to the impact direction is discussed.

Initiated by microstructural analysis of samples collected from the Matt Wilson impact structure, a recently discovered type of planar microstructure in quartz, termed “feather features”, is systematically analysed in samples from several impact craters (chapter 6). Feather features are shear induced structures that are formed by shock metamorphic deformation of quartz in low-shock pressure regimes, and give insights into the differential stresses that occur during the passage of the shock wave in the early stages of crater formation. Their use as indicators for impact craters is suggested.

Kurzfassung

In dieser Dissertation wurden sowohl mehrere terrestrische als auch Mars-Krater Gegenstand detaillierter struktureller Gelände- und Fernerkundungsanalysen, wobei der Focus auf struktureller Deformation schiefwinkliger Einschläge liegt. Zusätzliche mikrostrukturelle Analysen scherinduzierter Strukturen in Quarzkörnern aus Proben verschiedener Impaktstrukturen wurden durchgeführt, und ihre Bedeutung als stoßwellenmetamorphe Strukturen wurde evaluiert.

In der Einleitung dieser Dissertation (Kapitel 1) werden die zahlreichen Facetten von Impaktkratern und deren Nutzen in unterschiedlichen wissenschaftlichen und industriellen Bereichen beleuchtet. Die strukturellen Prozesse der Kraterbildung werden kurz erläutert, und das Überwiegen von Impakten, die durch schiefwinklige Einschläge entstehen, diskutiert.
Wolfe Creek, Australien, war der ursprüngliche Gegenstand struktureller Untersuchungen (Kapitel 2) Die asymmetrische, nicht-radiale Verteilung der Ejektadecke, wird häufig auf anderen Planeten beobachtet. Die Hypothese, ob sie auch auf der Erde zu einem internen strukturellen Signal des deformierten Gesteins in Kraterrändern zurückverfolgt werden kann, wurde getestet. Eine neue Methode der Evaluierung von Streich- und Einfallwerten wurde entwickelt. Die Schichtwerte von Wolfe Creek wurden mit strukturellen Asymmetrien, die aus der Ejektadecke des Tootingkraters, Mars, stammen, verglichen. Das resultierende, nicht-radiale Signal in Wolfe Creek wurde benutzt, um eine Einschlagsrichtung anzugeben.
Vergleichsweise wurden die Ergebnisse von Wolfe Creek an einem zweiten terrestrischen Krater geprüft; Meteor Krater in Arizona, USA (Kapitel 3). Die Evaluierung der Schichtwerte vom Meteor Krater zeigt, dass das erwartete Signal eines schiefwinkligen Einschlags nicht ausreichend detektierbar ist, und von den Deformationseffekten überprägt wurde, die durch präimpakt-Targetheterogenitäten eines rechtwinklig ausgeprägten Kluftsystems entstanden sind. Diese Deformationsstrukturen, insbesondere sogenannte „radiale Eckstörungen“ und „zwischengeschobene Keile“, sind im Detail observiert worden. Außerdem sind Mechanismen ihrer Generierung vorgeschlagen worden, die zusätzlich den vorgeschlagenen Zusammenhang zwischen der polygonalen Form des Meteor Krater und des rechtwinkligen Kluftsystems verfestigen.
Basierend auf jüngsten Entdeckungen von Zentralbergen, die nicht-radiale strukturelle Deformation aufweisen (z.B. Upheaval Dome, Utah, USA, Gosses Bluff, Australien) wurde eine detaillierte strukturelle Kartierung der Matt Wilson Impaktstruktur durchgeführt (Kapitel 4). Kartierergebnisse enthüllen, dass Matt Wilson der erste elliptische Krater der Erde ist, der eine Zentralaufwölbung aufweist. Die strukturelle Deformation der Zentralaufwölbung ist nicht-radial ausgerichtet. Ihre Überschiebungs- und Verschuppungsrichtung zeigt eine Vorzugsrichtung, die mit der langen Achse des erodierten, elliptischen Kraterrandes übereinstimmt. Dies bedeutet, dass zum ersten Mal zwei unabhängige Indikatoren

nichtradialer Deformation in ein und derselben Impaktstruktur gefunden wurden, die die Einschlagsrichtung anzeigen.

Die vielversprechenden Ergebnisse des Matt Wilson-Kraters suggerieren, dass ähnliche strukturelle Deformation auch in Impaktkratern anderer Planeten auftreten muss. Die Zentralaufwölbung des Martin-Kraters auf dem Mars ist aus diesem Grund auf der Basis von neuen, hochauflösenden HiRISE Bilddaten kartiert worden (Kapitel 5). Die daraus gewonnenen Ergebnisse zeigen, dass Ausrichtung der strukturellen Deformation in einem ~180° Winkel zur durch die Ejektadecke angezeigten Einschlagsrichtung steht. Jüngst publizierte numerische Modellierungen wurden verwendet, um ein Modell asymmetrischer Zentralbergsaufwölbung zu erarbeiten, die auf einer Kette von Ereignissen basiert, welche durch schiefwinkligen Einschlag eingeleitet wurden. Des Weiteren wird das Verhältnis der Orientierung der strukturellen Deformation zur Einschlagsrichtung diskutiert.

Ausgelöst durch die mikrostrukturelle Analyse von Proben aus der Matt Wilson Impaktstruktur, wurde systematisch in Proben mehrerer Impaktstrukturen eine jüngst entdeckte Art planarer Mikrostrukturen in Quarz, die als „feather features“ oder „Federelemente“ bezeichnet werden, analysiert (Kapitel 6). Federelemente sind scherinduzierte Strukturen, die durch stoßwellenmetamorphe Deformation von Quarz im Niedrigstoßwellen-Druckregime gebildet werden. Sie geben Einsichten in die differentiellen Spannungen, die während des Durchlaufs der Stoßwellen in den frühen Phasen der Kraterbildung auftreten. Ihr Nutzen als Impaktindikatoren wird vorgeschlagen.

1. Introduction

The importance of impact craters

Virtually all solid bodies in the solar system share the common trait of being scarred by impact craters. In the early solar system, as the accretion of matter progressed to form planetesimals and then planets and moons, impacts were commonplace, with the impactors shaping, altering and adding to the bodies they struck. It has been proposed that the Earth's Moon was formed by the oblique collision of a Mars-sized object with the proto-Earth (Hartmann and Davis, 1975). The rate of impacts has been roughly constant for the last 3.5 Ga (Neukum et al., 2001) and they are still observed in present times, with the impact of comet Shoemaker-Levy 9 into Jupiter in 1994 (e.g., Roulston and Ahrens, 1997) and the Carancas cratering event in Peru in 2007 (Kenkmann et al., 2009) as two prominent examples. Thus, the predominance of these features has led numerous researchers to propose that impact cratering has been „a fundamental geological process … since the formation of the solar system" (Stöffler and Langenhorst, 1994), or even „the most fundamental process that has taken place on the terrestrial planets" (Shoemaker, 1978).

Practical applications and uses of impact craters are manifold. Terrestrial craters have proven their economic use as natural resource deposits. For example, the Sudbury impact structure in Ontario, Canada, has one of the world's largest reservoirs of nickel and copper ores, which segregated from the melt sheet formed by the impact (Dressler et al., 1987). Impact structures are also often drilled as hydrocarbon reservoirs, as for example in the case of the Chicxulub and Ames structures (e.g., Curtiss et al., 1998). In planetary science, the size-frequency distribution of craters is commonly used for dating planetary surfaces, due to the exposure of older surfaces to a larger flux of impacting projectiles (Neukum et al., 2001). The geological timescale of the Moon, for example, is based on cratering events (the Nectarian, Imbrian, Copernican, etc. periods; Stöffler and Ryder, 2001). Impact craters on Mars show effects that suggest varying levels of liquid content present during the individual cratering events, and thus can be used as indicators for paleoclimate change (Boyce and Mougins-Mark, 2006). The excavation of subsurface material through cratering gives valuable insights into the structure and composition of otherwise concealed rock layers. This process is even actively applied in space programs like the Deep Impact or LCROSS missions, in which the ejecta expelled by the collision of artificial projectiles into the comet Tempel 1 (A'Hearn et al., 2005) or the lunar south pole (Colaprete et al., 2008) was analyzed.

By far the most important aspect necessitating impact crater research is the inherent danger of future impacts on Earth. At least one global extinction event has been proven to be caused by the impact of a ~10 km bolide into the Yucatán peninsula 65 Ma ago (Hildebrandt et al., 1991). Younger impacts like the 50 ka old, 1.2 km diameter Barringer Crater in Arizona are

estimated to have had lethal effects up to ~24 km in radius from the point of impact (Kring 1997), while the Tunguska event in 1908 flattened an area of the Siberian forest over 20 km in diameter (e.g., Boyarkina, 1964). Even the Carancas event in 2007 that created a 15 m diameter crater in Peru showed that the Earth's atmosphere provides less protection from projectiles than previously thought (Kenkmann et al., 2009). It is therefore vital not only to predict the trajectories of these so called "Near Earth Objects" (NEOs) that threaten the Earth, but also to understand as many details as possible involved in this violent, highly complex and dynamic, and not the least, fascinating process.

The impact cratering process

Hypervelocity impacts on planetary surfaces typically occur at speeds of tens of kilometers per second. The average impact velocity for the Earth is suggested to be at ~17 km/s, based on the escape velocity from the Earth's surface (11.2 km/s) plus the average differential component of cosmic velocity of the projectile relative to Earth (Melosh, 1989). The actual impact process is divided into three stages, based on the dominance of different physical phenomena at different times of the process (Gault et al., 1968, Melosh, 1989). These stages are contact and compression, excavation, and modification.

The first stage is initiated upon contact of the projectile with the target surface. The kinetic energy of the projectile is then released in the form of an extremely high pressure pulse, the shock wave. This shock wave expands from the point of impact through both the target and the projectile, and can reach peak pressures of several hundred GPa. As it passes through, the shock wave plastically deforms the medium and can even melt or vaporize the affected material upon unloading. The duration of the pressure pulse is dictated by the projectile diameter. Pressure release occurs as the shock wave is reflected from the back of the projectile in the form of a rarefaction wave. The unloading of the projectile from high pressure ends the contact and compression stage.

During the following excavation stage, the shock wave expands hemispherically through the target rock and weakens as it progresses further outward. In combination with the trailing rarefaction wave, the target rock is set in motion in the form of a subsonic excavation flow, which opens up the crater cavity below the target surface and ejects rock material upward and outward above the target surface (Fig. 1). The final result of the excavation flow is a bowl shaped „transient crater" many times the diameter of the projectile (typically 10-20x for terrestrial craters, depending on the size of the projectile), and an ejecta blanket of excavated rock surrounding the crater.

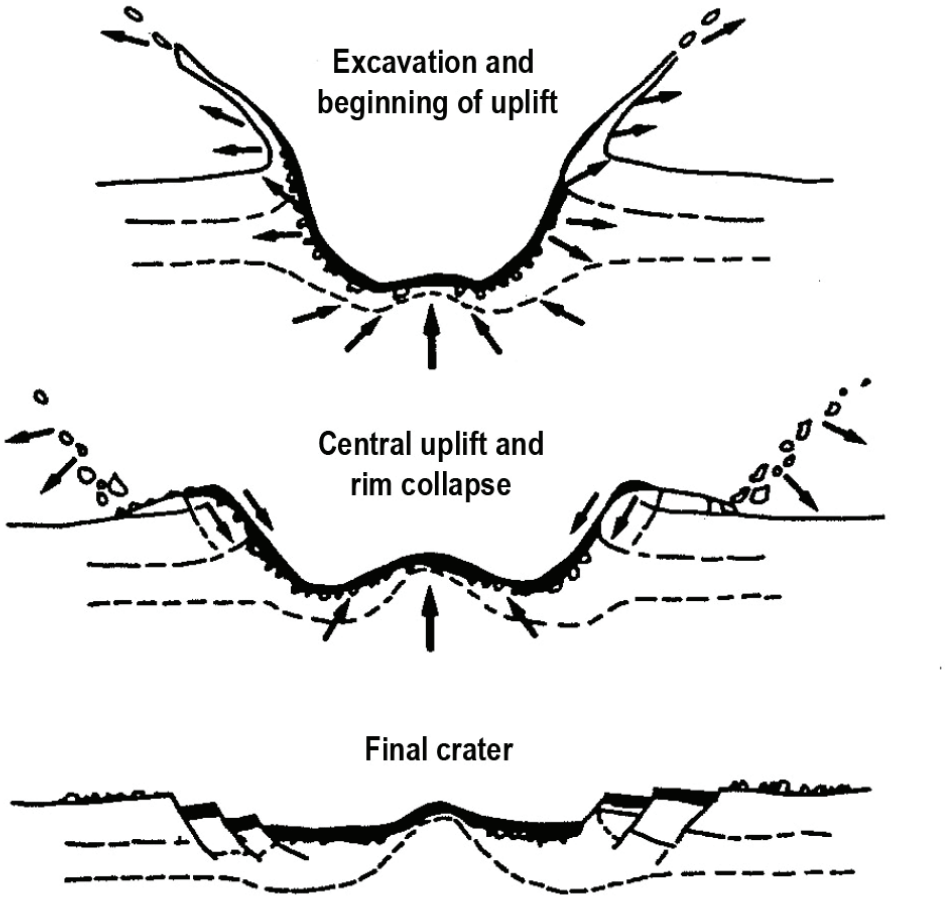

Fig. 1: Simplified sketches of the excavation and modification stages during the formation of a complex impact crater (from Melosh, 1989).

During the modification stage, the transient crater begins to collapse under the effect of gravity. Loose material begins to slide inwards from the crater walls. In larger craters (>2-4 km diameter on Earth) the crater walls slump inwards to form radial terraces, while a central uplift forms as the crater floor rises, forming so-called complex craters (Fig. 1).

The plastic deformation of the target rock during the transgression of the shock wave can leave characteristic signatures visible on both microscopic and hand-specimen scale, known as shock metamorphic features, some of which are unique to impact cratering. Macroscopically, shatter cones that occur as multiple sets of striated conical fractures are used as a diagnostic impact criterion (Dietz, 1959). They can occur in different lithologies on a cm to m-scale. Microscopically, planar microstructures in minerals are induced by shock (e.g., Stöffler and Langenhorst, 1994). The most important shock indicators among these microstructures are planar deformation features (PDFs), which occur as intersecting sets of thin, narrowly spaced amorphous lamellae that permeate mineral grains and are most easily recognized in quartz. PDF formation in quartz requires pressures above 10 GPa. Other shock features that can occur below 10 GPa include planar fractures. Their use as diagnostic criteria

is still under debate (e.g. Grieve et al., 1996), although French and Koeberl (2010) suggest planar features can be used to diagnose impacts under certain circumstances. The use of feather features as an additional, low shock pressure diagnostic microstructure is discussed in chapter 6.

Oblique Impacts

Over a century ago, Gilbert (1892) calculated that, statistically, the chances of a projectile striking a spherical body at vertical angle are highly improbable, whereas a 45° angle is the most common angle. These calculations are based on a simple model in which a hemisphere is exposed to a stream of projectiles flying in the same direction (Fig. 2). For a vertical impact (90°) to occur, the hemisphere must be struck exactly in the center, while near horizontal impacts glance the hemisphere's edges. This results in the equation $P = \sin^2 \Theta$, where Θ is the angle of the projectile trajectory to the surface and P is the probability of an impact occurring between 0° and Θ. Therefore, half of all impacts onto spherical surfaces should occur at angles $\leq 45°$ (i.e., $P = 0.5$ for $\Theta = 45°$). Additional calculations by Shoemaker (1962) showed that the addition of gravitation to the model has no effect on the statistical relationships.

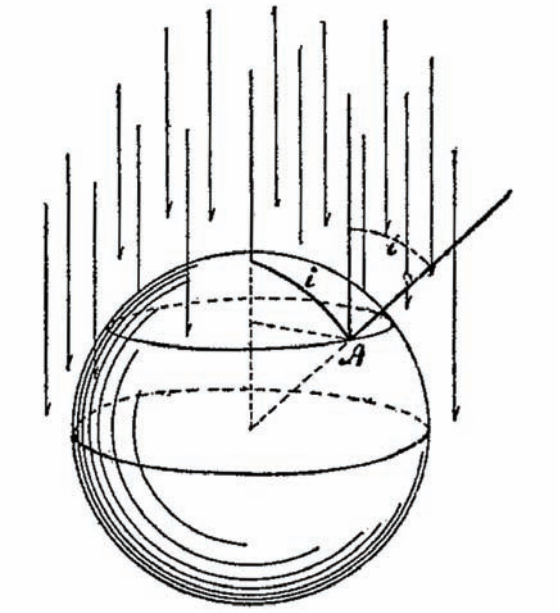

Fig. 2: Theoretical model from Gilbert (1892) explaining the statistical distribution of impact angles onto a spherical body. The model assumes a homogenous stream of particles in one direction that strike different regions of the hemisphere, resulting in different impact angles.

Early planetary scientists observing the moon were puzzled that nearly all craters are circular in shape, despite Gilbert's proposed predominance of oblique impacts, as oblique impacts were originally thought to produce elliptical craters. A recent survey of the Moon, Mars and Venus in fact shows that only ~5% of craters are elliptical (with an aspect ratio ≥ 1.2, Bottke et al., 2000). This apparent contradiction can be explained by the high kinetic energy of the

projectile. The impacting projectile, instead of simply pushing target material away, causes a shock wave-induced excavation flow field. This results in a crater 10-20 times the size of the projectile and therefore normally makes the asymmetry of an obliquely striking projectile insignificant.

Despite the circularity of crater rims, signatures of oblique impacts are most readily visible in the shape of the ejecta blanket. Based on experimental data (Gault and Wedekind, 1978), at angles below 45° the ejecta blanket begins to shift downrange and departs from radial symmetry. With increasing obliqueness, a wedge-shaped "forbidden zone" begins to form uprange (Fig. 3), and is then followed by a second forbidden zone downrange, leading to a bilaterally symmetric "butterfly pattern" at very shallow angles (Fig. 3). The question of how far these asymmetric ejecta patterns can be followed inwards to the proximal ejecta blankets and the internal structure of the circular crater rim is addressed in chapters 2 and 3.

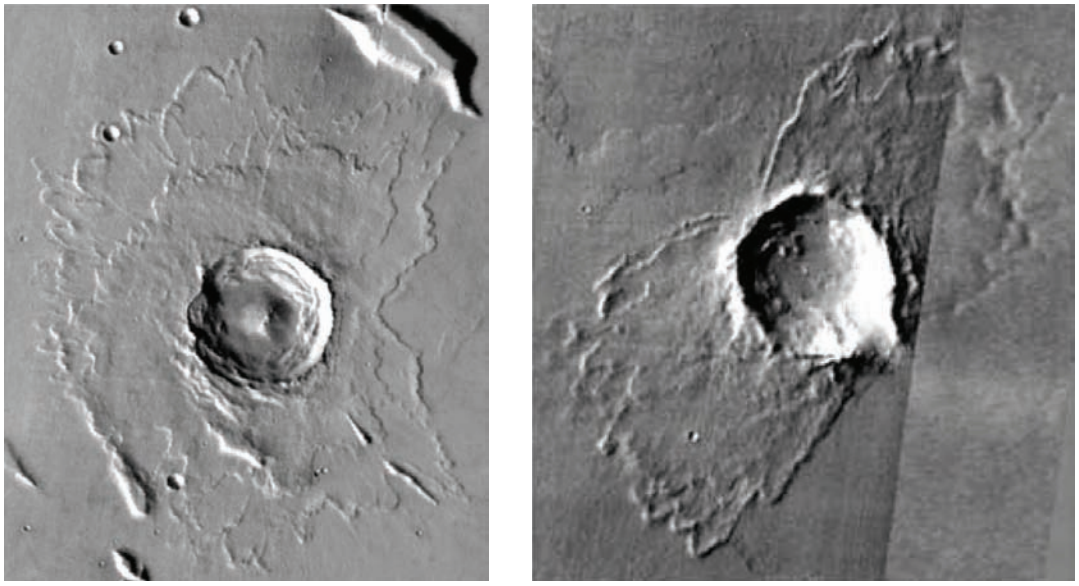

Fig. 3: Ejecta patterns from two Martian craters. Left: an uprange forbidden zone is visible to the right of the crater rim, indicating that the impactor came from the right. Right: a butterfly pattern, formed by a highly oblique impact. The breached rim on the lower left indicates that the impactor came from the upper left. THEMIS infrared imagery (from Herrick and Hessen, 2006).

Recent results of structural mapping of terrestrial impact craters show that beyond the asymmetric patterns of ejecta blankets in oblique impacts, central uplifts also display strong non-radial internal deformation (Scherler et al., 2006). Figure 4 displays structural maps of the Upheaval Dome, Spider, and Gosses Bluff impact structures. In all three cases preferential deformation in one direction is visible based on folding, thrusting and imbrication of rock layers. This deformation is suggested to be directly connected to obliquely striking projectiles. This hypothesis is explored further in chapters 4 and 5. A more detailed review of research on oblique impacts can be found in the introduction of chapter 2.

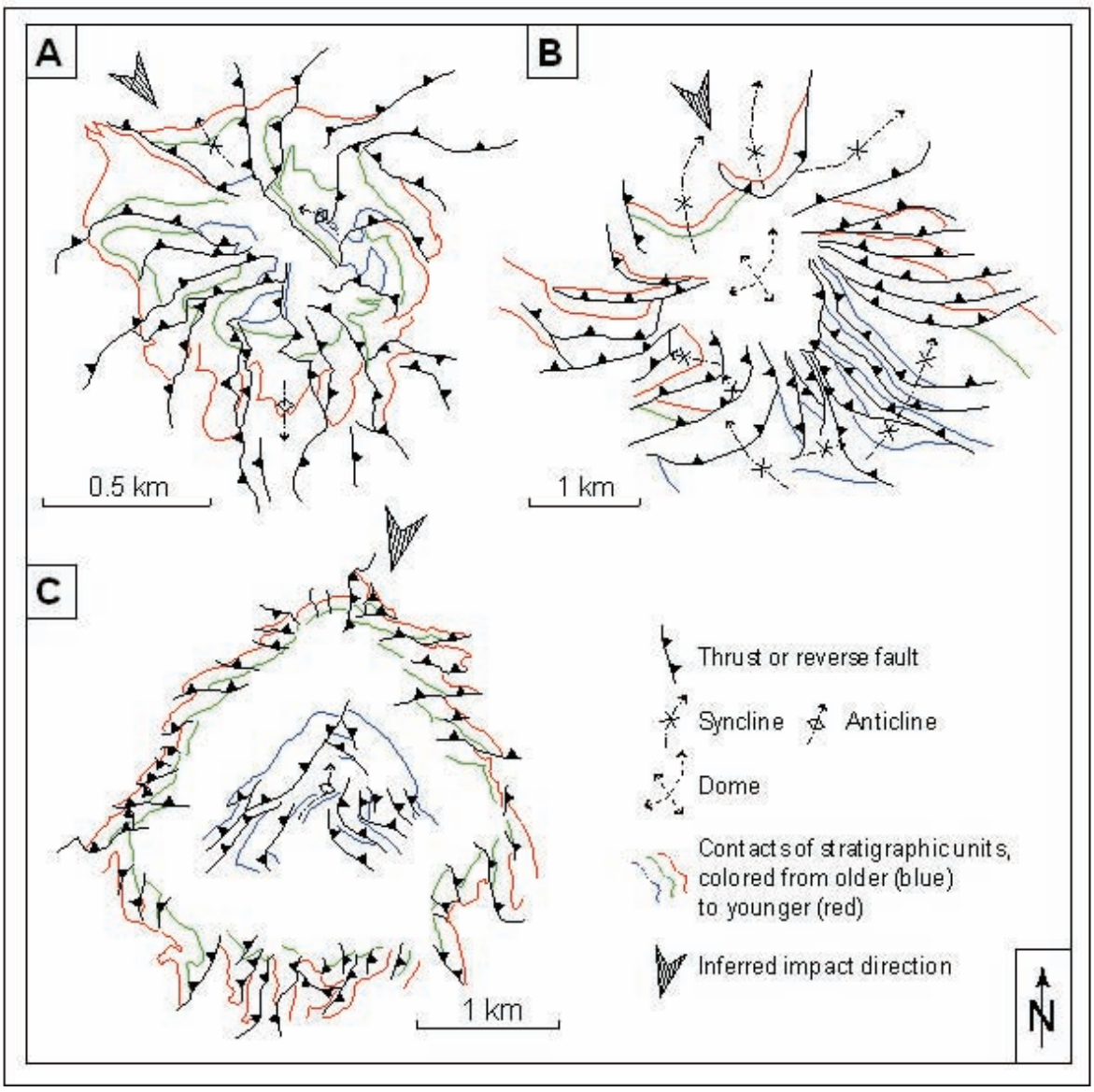

Fig. 4: Structural sketch maps of central uplifts in three terrestrial craters, showing a strong non-radial component of deformation linking to oblique impacts. A: Upheaval Dome, Utah, USA, B: Spider Crater, Australia, C: Gosses Bluff, Australia (from Scherler et al., 2006).

References

A'Hearn, M. F., M. J. S. Belton, W. A. Delamere, J. Kissel, K. P. Klaasen, L. A. McFadden, K. J. Meech, H. J. Melosh, P. H. Schultz, J. M. Sunshine, P. C. Thomas, J. Veverka, D. K. Yeomans, M. W. Baca, I. Busko, C. J. Crockett, S. M. Collins, M. Desnoyer, C. A. Eberhardy, C. M. Ernst, T. L. Farnham, L. Feaga, O. Groussin, D. Hampton, S. I. Ipatov, J.-Y. Li, D. Lindler, C. M. Lisse, N. Mastrodemos, W. M. Owen, Jr., J. E.

Richardson, D. D. Wellnitz, R. L. White, 2005. Deep Impact: Excavating comet Tempel 1. Science, 5746: 258–264. doi:10.1126/science.1118923

Bottke, W.F., S. G. Love, D. Tytell, T. Glotch, 2000. Interpreting the elliptical crater populations on Mars, Venus, and the Moon: Icarus, 145: 108–121, doi: 10.1006/icar.1999.6323.

Boyce, J. M., P. J. Mouginis-Mark, 2006. Martian craters viewed by the THEMIS instrument: Double-layered ejecta craters, J. Geophys. Res., 111, E10005, doi:10.1029/2005JE002638.

Boyarkina, A. P., D. V. Demin, I. T. Zotkin, W. G. Fast, 1964. Estimation of the blast wave of the Tunguska meteorite from the forest destruction. – Meteoritika, 24: 112-128.

Colaprete, A., G. Briggs, K. Ennico, D. Wooden, J. Heldmann, L. Sollitt, E. Asphaug, D. Korycansky, P. Schultz, A. Christensen, K. Galal, and the LCROSS Team, 2008. An Overview of The Lunar Crater Observation and Sensing Satellite (LCROSS) Mission – A Mission to Investigate Lunar Polar Hydrogen. (abstract #1838). 39th Lunar and Planetary Science Conference. CD-ROM.

Curtiss, D. K., D. A. Wavrek, 1998. Hydrocarbons in meteorite impact structures: Oil reserves in the Ames feature. Journal of the Minerals, Metals and Materials Society, 50: 35-37.

Dietz, R.S., 1959. Shatter cones in cryptoexplosion structures (meteorite impact?). Journal of Geology, 67: 496–505.

Dressler, B. O., G. G. Morrison, W. V. Peredery, B. V. Rao, 1987. The Sudbury structure, Ontario, Canada - A review. In: Pohl, J., (Ed.), Research in Terrestrial Impact Structures. Friedr.Vieweg and Sohn, Braunschweig/Weisbaden, 39-68.

French, B.M., C. Koeberl, 2010. The convincing identification of terrestrial meteorite impact structures: What works, what doesn't, and why. Earth-Science Reviews, 98: 123-170.

Gault, D. E., 1968. Impact cratering mechanics and structures. In: French, B.M., N.M. Short, (Eds.), Shock Metamorphism of Natural Materials. Mono Book Corp, Baltimore, 87-100.

Gault, D. E., J. A. Wedekind, 1978. Experimental studies of oblique impact. 9th Lunar and Planetary Science Conference, 3843 - 3875.

Gilbert, G. K. 1892. The Moon's Face; a study of the origin of its features. Bull Phil. Soc., 12: 241 - 292.

Grieve, R.A.F., F. Langenhorst, D. Stöffler, 1996. Shock metamorphism of quartz in nature and experiment: II. Significance in geoscience. Meteoritics and Planetary Science, 31: 6–35.

Hartmann, W. K., D. R. Davis 1975. Satellite-Sized Planetesimals and Lunar Origin. Icarus, 24:505-515.

Herrick, R. R., K. K. Hessen, 2006. The planforms of low-angle impact craters in the northern hemisphere of Mars. Meteoritics and Planetary Science, 41:1483-1495.

Hildebrand, A. R., G. T. Penfield, D. A. Kring, M. Pilkington, A. C. Zanoguera, S. B. Jacobsen, W. V. Boynton, 1991. Chicxulub Crater; a possible Cretaceous/Tertiary boundary impact crater on the Yucatán Peninsula, Mexico. Geology, 19: 867–871.

Kenkmann, T., N. A. Artemieva, K. Wünnemann, M. H. Poelchau, D. Elbeshausen, H. Núñez del Prado, 2009. The Carancas meteorite impact crater, Peru: geologic surveying and modeling of crater formation and atmospheric passage. Meteoritics and Planetary Science, 44: 985-1000.

Kring, D. A., 1997. Air blast produced by the Meteor Crater impact event and a reconstruction of the affected environment, Meteoritics and Planetary Science, 32: 517-530.

Melosh, H.J. 1989. Impact Cratering: A Geologic Process. Oxford University Press, U.K. Paperback, 245 pp.

Neukum, G., B. A. Ivanov, W. K. Hartmann, 2001. Cratering records in the inner solar system in relation to the lunar reference system. In: Kallenbach, R., J. Geiss, W. K.Hartmann, (Eds.), Chronology and Evolution of Mars, International Space Science Institute, Bern, 87-104.

Roulston, M.S., T. Ahrens, 1997. Impact Mechanics and Frequency of SL9-Type Events on Jupiter. Icarus, 126: 138–147. doi:10.1006/icar.1996.5636

Scherler, D., T. Kenkmann, A. Jahn, 2006. Structural record of an oblique impact. Earth and Planetary Science Letters, 248:43-53.

Shoemaker, E. M. 1962. Interpretation of lunar craters. In: Kopal, Z., (Eds.), Physics And Astronomy of the Moon. New York/London: Academic, 283-359.

Shoemaker, E. M. 1978. Why study impact craters? In: Impact and explosion cratering: Planetary and terrestrial implications; Proceedings of the Symposium on Planetary Cratering Mechanics, Flagstaff, Ariz., September 13-17, 1976. New York, Pergamon Press, Inc., 1-10.

Stöffler, D., F. Langenhorst, 1994. Shock metamorphism of quartz in nature and experiment: I. Basic observation and theory. Meteoritics 29: 155-181.

Stöffler D., G. Ryder, 2001. Stratigraphy and isotope ages of lunar geological units: chronological standards for the inner solar system. Space Sci. Rev. 96: 9–54. doi:10.1023/A:1011937020193.

2. Asymmetric signatures in simple craters as an indicator for an oblique impact direction

This chapter has been published as the following peer-reviewed article:

Poelchau, M. H., and T. Kenkmann, 2008. Asymmetric signatures in simple craters as an indicator for an oblique impact direction, Meteoritcal and Planetary Science, 43, 2059-2072.

Abstract

In oblique impacts with an impact angle under 45° the bilateral shape of the distal ejecta blanket is used as the strongest indicator for an impact vector. This bilateral symmetry is attenuated and is superimposed by radial symmetry towards the crater rim, which remains circular for impact angles down to 10-15°. The possibility that remnants of bilateral symmetry might still be present in the most proximal ejecta, the overturned flap and the crater rim was explored with the intention of deducing an impact vector. A model is presented that postulates bilateral patterns using proximal ejecta trajectories and predicts these patterns in the orientation of bedding planes in the crater rim. This model was successfully correlated to patterns described by radial grooves in the proximal ejecta blanket of the oblique Tooting crater on Mars. A new method was developed to detect structural asymmetries by converting bedding data into values that express the deviation from concentric strike orientation in the crater rim relative to the crater center, termed “concentric deviation”. The method was applied to field data from Wolfe Creek crater, Western Australia. Bedding in the overturned flap implies an impactor striking from the east, which refines earlier publications, while bedding from the inner rim shows a correlation with the crater rim morphology.

Introduction

The majority of craters are formed by oblique impacts. Statistically, the most probable impact angle is 45° for planetary bodies (Gilbert 1892; Shoemaker 1962), and half of all impacts should strike at angles of 45° or lower, without regarding atmospheric effects. Despite the prevalence of oblique impacts, crater shapes remain circular for impact angles steeper than 10-15° from horizontal (Gault and Wedekind 1978; Bottke et al. 2000) and thus normally do not give any implications for the direction of impact.

The ejecta pattern is affected in a much stronger fashion by oblique impacts than the final crater shape. With decreasing impact angle the ejecta blanket first shows a preferential concentration downrange. At angles less than 30°, a wedge-shape forbidden zone (Gault and Wedekind 1978) develops uprange. This zone expands with decreasing angle. At 20° a second

forbidden ejecta zone develops downrange of the crater. At very shallow impact angles this leads to the formation of a bilaterally symmetric "butterfly" pattern (Gault and Wedekind 1978; Herrick and Forsberg-Taylor 2003; Herrick and Hessen 2006), in which the ejecta dominantly expands sideways. The characteristic bilateral symmetry of the ejecta around craters has become an important diagnostic feature for the recognition of craters formed by oblique impacts on planetary surfaces (Pierazzo and Melosh 2000a) and has been used for the determination of the impact vector for example on the Moon (e.g. Gault and Wedekind 1978; Bottke et al. 2000; Herrick and Forsberg-Taylor 2003), on Venus (e.g. Schultz 1992a; Herrick and Phillips 1994; Ekholm and Melosh 2001), and on Mars (e.g. Schultz and Lutz-Garihan 1982; Herrick and Hessen 2006). Two examples of bilateral symmetry in ejecta blankets on Venus and Mars can be seen in Fig. 1, from which an impact direction can easily be deduced.

On Earth the ejecta blanket is the first part of the crater that is eroded, therefore difficulties arise with the recognition of the impact vector in terrestrial craters. Nonetheless, numerous efforts have been made to determine the impact direction of the impacting projectile in craters on Earth using different methods and aspects of the cratering process. For example, distribution of tektites E of the Nördlinger Ries, the WSW-ENE alignment of the Steinheim and Ries craters and the preferential distribution of impact melt in the eastern sector of the Ries led to the postulation of an impactor coming from the WSW (Stöffler et al. 2002), and similarly the distribution of tektites around the Bosumtwi crater led to the proposal of the impactor coming from the N-NE (Artemieva et al. 2004).

Furthermore, in lack of ejecta, morphological, structural and geophysical data in craters have also been used as diagnostic features to derive an impact vector. Early attempts by Barringer (1910) on Barringer Meteorite Crater were based on morphology and tectonic uplift, while later Shoemaker and Kieffer (1974) stated that thrust faults in the crater wall might indicate the direction of motion of the impacting projectile. Schultz and Anderson (1996) examined the offset and asymmetry of the central peak, rim uplift and distribution of shock disruption in the Manson impact structure, from which they suggested an impact direction from the southeast. However, in a study on oblique Venusian craters, Ekholm and Melosh (2001) suggest that the offset distribution of central peaks relative to the impact direction is random and that there may not be a correlation between impact angle and central peak diameter. Asymmetry displayed in seismic and gravity data of the Mjølnir crater in combination with structural features and crater elongation imply an impactor traveling from the south/southwest (Tsikalas 2005). The Chicxulub crater has been subject to numerous attempts at finding a direction. Proposed directions from the SE (Schultz and D'Hondt 1996) and from the SW (Hildebrandt et al. 1998) were based mainly on structural aspects of the crater, while Morgan et al. (2006) suggested an impactor coming from the NW based on distribution of shocked quartz. Gulick et al. (2008) suggest that target heterogeneities (e.g. variable water depth) have an effect on crater structures like Chicxulub and that this can distort some of the indicators used for an impact direction. Recent studies have shown that an impact vector is indicated in

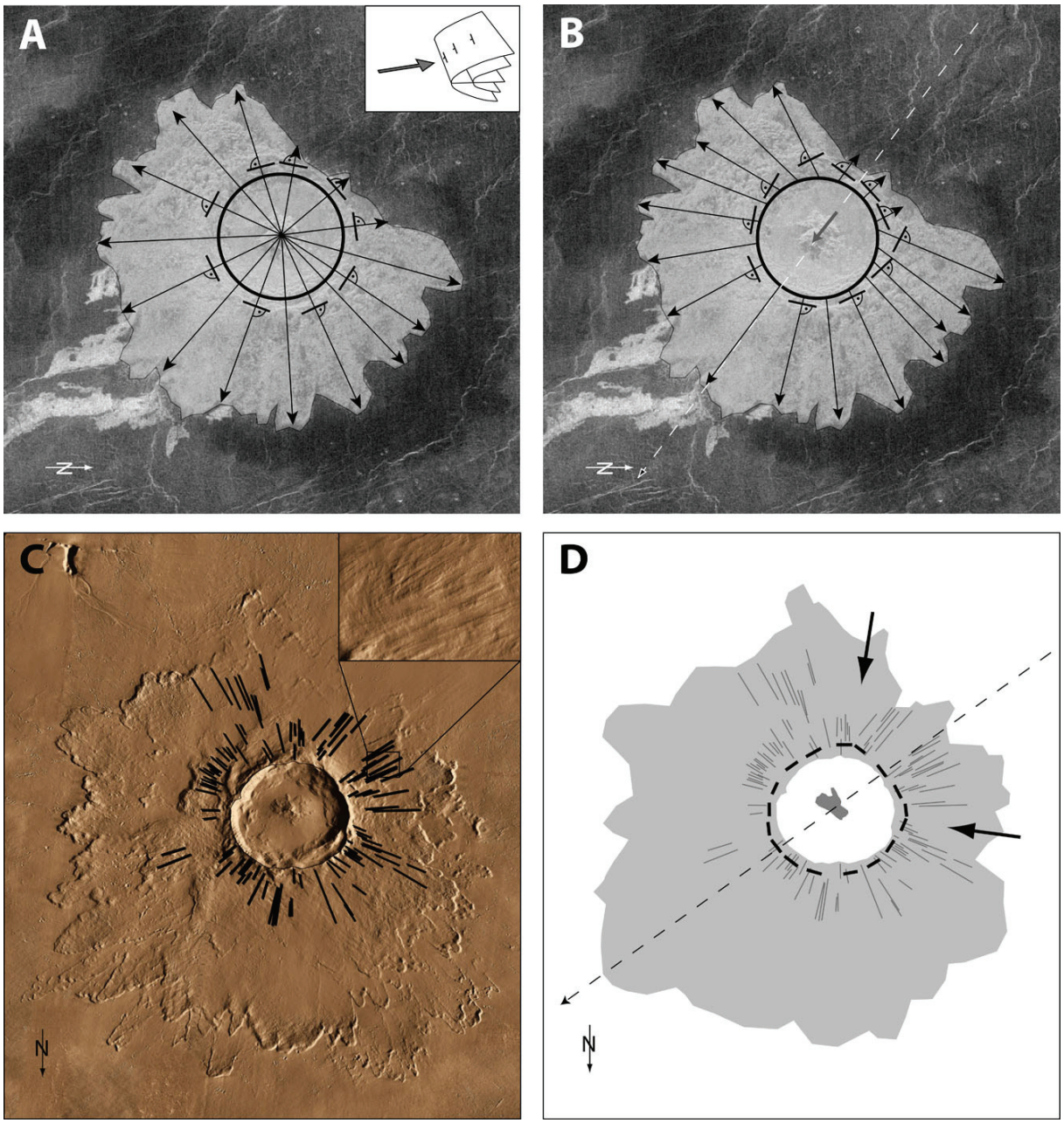

Fig. 1. Asymmetric ejecta blankets of two oblique impacts. Top: Aurelia crater, Venus (Magellan Imaging Radar, courtesy NASA/JPL-Caltech); bottom: Tooting crater, Mars (THEMIS mosaic). (a) and (b) contrast two models of ejecta trajectories (black arrows) and the resulting strike (black bars). Strike of folded bedding in the overturned flap is always orthogonal to the ejecta trajectories for originally horizontal target bedding (inset Fig. 1a). (a) shows a radially symmetric "point source" or stationary center of the ejection flow field with the resulting concentric strike pattern of ejected bedding. (b) shows non-radial, bilaterally symmetric "line source" or downrange shifting center of the ejection flow field with a resulting bilaterally symmetric strike pattern. The non-radial deviation of strike correlates with the assumed impact vector (white dashed line). Tooting crater in (c) exhibits grooves and ridges in its ejecta blanket (inset) that were mapped as indicators for ejecta trajectories (black lines). In (d), assumed strike (black bars) is orthogonal to the mapped ejecta trajectories and displays a non-radial, bilaterally symmetric pattern, similar to (b), which indicates an impact vector coming from the top right. Black arrows mark "corners" in the strike pattern as the strongest uprange indicators. Note: all images are rotated from north to depict the impactor coming from the top right.

the subsurface structures of central peaks of craters on Earth, which show preferential directions of folding and faulting that indicate a preferred transport direction, as seen in Upheaval Dome (Kenkmann et al. 2005; Scherler et al. 2006) and also proposed in Spider crater, Gosses Bluff crater (Scherler et al. 2006) and the Matt Wilson structure (Kenkmann and Poelchau 2008).

Experimental studies of oblique hypervelocity impacts give further insights into the cratering process. Early work by Gault et al. (1968) suggests that obliquity influences the flow pattern of target material, and shows a departure from axial symmetry of the structural pattern, e.g. the form of the overturned flap. Later work done by Gault and Wedekind (1978) has shown that while highly oblique angles are necessary to affect the crater circularity, ejecta deposits become asymmetric below 45°, and start displaying bilateral patterns, which are used as a strong criterion for determining the impact vector. More recently, Dahl and Schultz (2001) measured the asymmetry of shock waves in oblique impact experiments, revealing an elevation of shock pressures downrange.

Anderson et al. (2003) imaged ejecta particle vectors during oblique impact experiments into particulate targets, showing that during oblique impacts a very obvious non radial, bilaterally symmetric pattern of these vectors can be observed that is oriented according to the impact direction of the projectile. This is especially obvious during the initial stages of crater formation. The flow pattern is compatible with a downrange moving crater center. The original asymmetry decreases as the cratering progresses, but is still visible after 50% of the final crater size is reached. Ejecta formed in the final phases of excavation was not imaged. Based on these results, Anderson et al. (2004) stated that a stationary point source of ejection, as approximated in Maxwell's *Z* model (Maxwell 1977), does not sufficiently describe the process of excavation, and suggested a new model based on the downrange migration of the flow field center.

Numerical modeling supports and confirms the non-radial cratering aspects documented in planetary observations and experiments. First systematic 3D modeling work on oblique impacts was done by Pierazzo and Crawford (1998). Analysis of these results in Pierazzo and Melosh (1999, 2000b) showed that shock pressure, shock temperature and melt production decrease with decreasing impact angle and that the strength of the shock front in the target is asymmetric, with the strongest shock in the downrange direction. In 3D hydrocode runs of oblique impacts Artemieva and Ivanov (2001) showed that during cratering the flow velocity field is asymmetric up to the beginning of cavity collapse, with larger downrange velocities in the cavity wall compared to uprange velocities. The component of initial horizontal momentum is present until the start of the crater floor uplift. 3D numerical simulations of the crater floor flow in oblique impacts by Shuvalov and Dypvik (2004) strongly support the assumption of an asymmetric crater flow structure indicative for the impact vector. They also state that "late" or proximal ejecta near the crater rim still shows slight asymmetry.

Elbeshausen et al. (2007) used tracers placed in the ejecta curtain of 3D models from which the paths of ejecta trajectories were reconstructed. The ejecta distribution shows obvious non-radial behavior and an uprange forbidden zone for a 30° impact.
Based on the bilateral pattern of oblique ejecta blankets and on the asymmetry prevalent in the excavation flow field, as shown in latest research on oblique impacts, we have developed a new model for the structure of the crater rim, which will be discussed in detail. Bedding strike, one of the main structural features that can be systematically measured in the field, is used as an indicator for non-radial symmetry. A new means of quantifying strike in the crater rim was developed which displays angular deviation from concentric strike relative to the crater center, referred to as "concentric deviation". We expect patterns revealed in the concentric deviation that should indicate an impact direction for oblique impacts.

Proposed "two corners" pattern

In this study, we propose that the strike of bedding planes in the proximal ejecta blanket of the overturned flap and crater rim can be used as an indicator for the orientation of excavation flow field trajectories in well-preserved simple craters on Earth, especially near the crater rim, where the ejecta forms still coherent sheets. Strike, which is defined as an intersecting line between the bedding plane and a hypothetical horizontal plane, remains orthogonal to the trajectory during rotation or overturning of layered rocks, as long as the bedding was originally horizontal (Fig. 1a inset, Fig 2). During excavation bedding is rotated around an axis that remains perpendicular to the force of the flow field exerted on the rock (best visualized by the shape of the overturned flap). While the strike of bedding in the distal ejecta blanket is most likely too chaotic due to transport to reflect trajectories, continuous, coherent blocks of bedding planes are expected in the proximal parts of the ejecta blanket, including the overturned flap and parts of the inner rim (Fig. 2), which can be used to display asymmetrical behavior of the excavation flow.
In Figs. 1a and 1b, two possible excavation flow field models are contrasted. In the first model, the origin of the flow field is located in the center of the crater and remains in this position for the duration of cratering. This has been described in Maxwell's *Z* model (Maxwell 1977), which is used as an approximation for vertical impacts. In this case, the trajectories are purely radial with respect to the final crater, and the asymmetry of the ejecta blanket is controlled by the magnitude of the ejecta flow. Therefore pure concentrical striking along the crater rim and overturned flap is expected that bears no information of the impact vector.

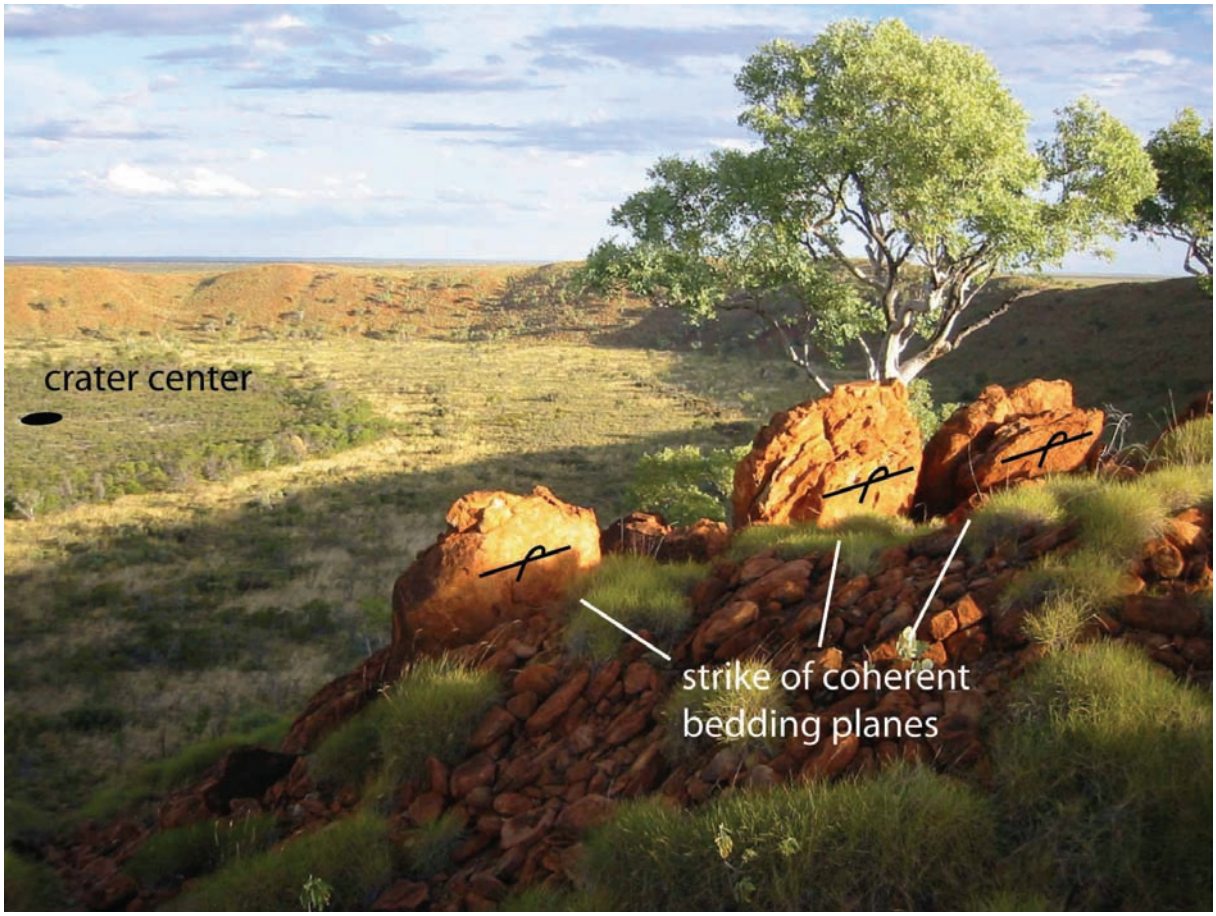

Fig. 2. Exposed beds of the overturned flap in the Wolfe Creek crater rim. Strike of bedding planes is roughly perpendicular to the crater center and was only measured when it was consistent over several meters, as marked in the picture.

However, the ejecta trajectories forming asymmetric or bilaterally symmetric ejecta blankets of oblique impacts should deviate from a strictly radial orientation with respect to the final crater center (Fig. 1b) and could probably be traced at the rim and overturned flap of simple craters in layered targets on Earth, which represent the most proximal part of the ejecta. If the mechanism of ejection is described by a modified *Z* model approach (Anderson et al. 2004; Anderson and Schultz 2006) with the ejection flow field center shifting from uprange to downrange (Fig. 1b), the flow field should be non-radial and bilaterally symmetric.

We particularly expect a hypothetical pattern of strike along the rim to show mostly concentric behavior downrange, while stronger deviations should occur between the downrange and crossrange sectors of the rim, with strike forming a pattern with two "corners", due to abrupt changes in strike orientation. This "two corners" pattern should begin to form at angles below 45° and become stronger the shallower the angle gets. The uprange

zone, defined by the two corners, should also become wider for shallower angles. Based on qualitative assessments of ejecta patterns, the two corners pattern should approximate impact angles at around 40-20°. This pattern is closely related to the heart-shaped "cardioid pattern" that Schultz et al. (2007) have postulated for non-radial ejecta trajectories, based on observations of ejecta behavior during the Deep Impact cratering experiment and hypervelocity laboratory experiments (Anderson and Schultz 2006). The cardioid pattern predicts radial ejecta trajectories downrange and an uprange "zone of avoidance", which should coincide with the two corners suggested in this paper.

Observations of craters and their ejecta blankets on other terrestrial planets show patterns on which the "two corners" pattern is based. THEMIS images of the Martian Tooting crater were used for a quantitative evaluation of ejecta trajectories. Tooting crater is a young, well-preserved double-layer ejecta (DLE) crater, which, like all fresh DLE craters, has straight, radial grooves carved into the inner ejecta layer. Boyce and Mouginis-Mark (2006) suggest these grooves can be caused by a high-velocity outflow of materials following in the wake of the advancing ejecta curtain, based on models of atmospheric interaction proposed by Schultz (1992b) and Barnouin-Jha et al. (1999a, b). Grooves on the inner ejecta layer (the first of the two layers to be deposited) show no signs of being influenced by topography. We assume that an asymmetrically advancing ejecta curtain of an oblique impact should affect the radial orientation of the grooves that follow it in DLE craters, and possibly reflect the impact trajectory. This appears to be the case in Tooting's ejecta blanket, which shows a stronger concentration of ejecta deposits and radial orientation of grooves in the proposed downrange direction (Mouginis-Mark and Garbeil 2007), while in uprange direction a weaker distribution of ejecta and non-radial groove orientation coincide (Fig. 1c, d). Although more research is needed to solidify these observations, we believe this correlation is further supported by the fact that non-radial behavior of grooves in DLE craters with radially symmetric ejecta distributions has not been observed. Therefore, in this study, grooves were used as basic indicators for non-radial behavior of ejecta trajectories, which, as discussed above, should in turn be perpendicular to the strike of rotated bedding planes in the crater rim and proximal ejecta blanket.

Both grooves and implied resulting strike show bilateral symmetry and two "corners" in the transition from the uprange to the crossrange sector (Fig. 1d), which correlate with an impactor coming from the southwest, as suggested by Mouginis-Mark and Garbeil (2007). Data from a model based on the "two corners" pattern and from Tooting crater was evaluated further and compared with strike data from the Australian Wolfe Creek crater, as is presented below.

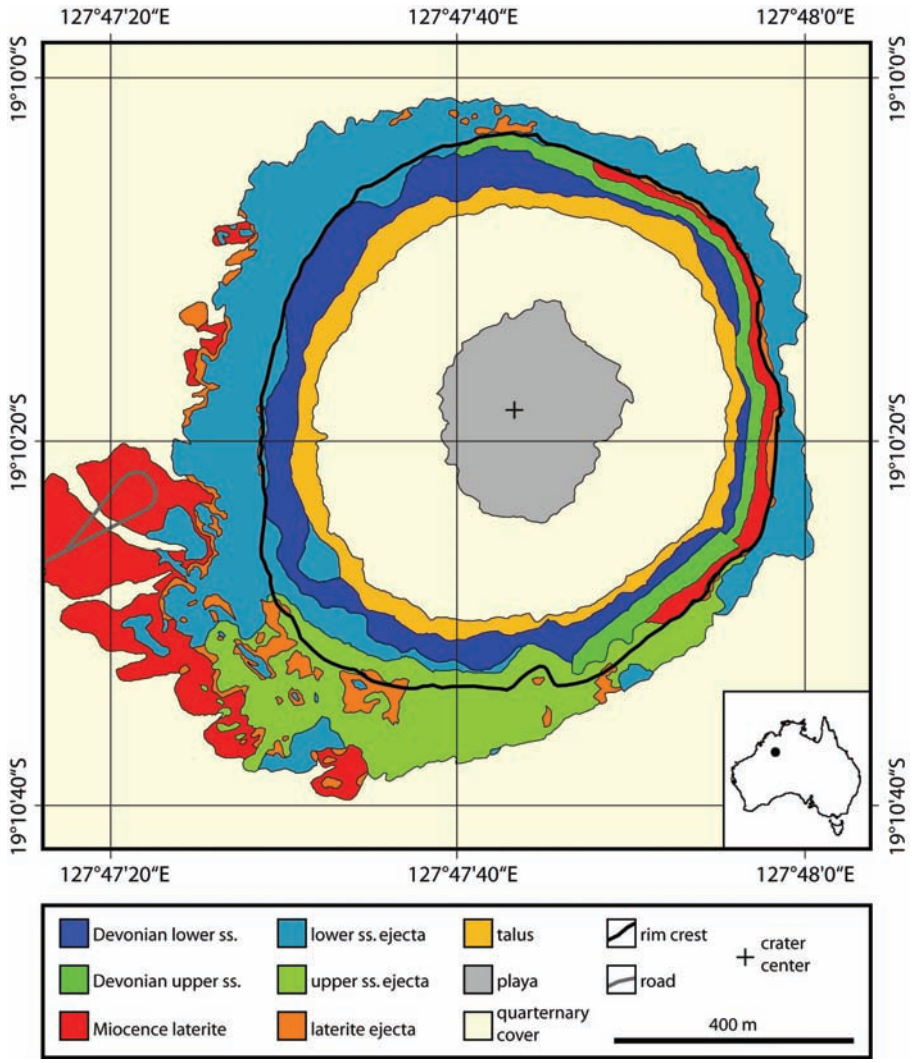

Fig. 3. Geological map of Wolfe Creek crater (from Shoemaker et al. 2005).

Geological Setting of Wolfe Creek Crater

Wolfe Creek Crater in Western Australia was used as a study object to test our hypothesis on field data (Figs. 2, 3). We collected and systematically analyzed striking of strata in the crater rim. Wolfe Creek Crater is a relatively young, simple impact crater with an average diameter of 880 m (Hawke 2003) that was formed 0.3 Ma ago (Shoemaker et al. 1990) by an iron meteorite (a medium octahedrite; Buchwald 1975). It was formed in flat-lying Devonian sandstones that are overlain by a layer of Miocene laterites. The crater is well preserved, recent erosion rates are calculated at $2*10^{-3}$ cm/a (Shoemaker et al. 1990), based on ^{10}Be-^{26}Al dating which yielded exposure ages of ~30 000 years. This suggests an average amount of 6m of erosion when extrapolated to the time of impact. Shatter cones are found in the SSW rim of the crater (O'Neill and Heine 2005), oxidized iron shale is found predominantly on the SW rim in the form of shale balls (LaPaz 1954; McCall 1965). O'Neill and Heine (2005) state that

beds in the crater rim dip gently at 40-60° in the ENE crater rim and show strongest overturn of 135° in the WSW. They also remark that in the N and S, overturned bedding shows irregular strike, described as “undulations”. Hawke (2003), O’Neill and Heine (2005) and Shoemaker et al. (2005) agree on an impactor coming from the NE, based on the distribution of shatter cones, meteoritic material and ejecta, along with the orientation of the elliptical axes of the crater shape and a qualitative assessment of dip data in the crater rim.

Methodology

The collected field data consists of strike and dip values along with latitude and longitude. The bedding data was divided into two groups. “Autochthonous” values consist of normal layered bedding that is located in the inner, upper part of the crater wall, as opposed to “ejecta” values, which consist of overturned layers measured in the overturned flap that is regarded as the most proximal ejecta, generally located in the outer parts of the crater wall (Fig. 2). This data was combined with published data from Shoemaker et al. (2005) who also performed the same division into two groups.

The collected field data from Wolfe Creek crater and data derived from THEMIS images of Tooting crater on Mars were translated from a geographic reference system to a radial system with the point of origin situated in the crater center (Fig. 4a). For data conversion, the precise latitude and longitude of the crater center and measurement points are necessary. The crater center was defined by determining the geometric center of the crater rim crest with the aid of GIS software. Coordinates were then converted by approximating the angle x between two geographical points and north:

$$x = \arctan \frac{lat_c - lat_d}{(lon_c - lon_d)\cos lat_c} \tag{1}$$

with lat_c and lon_c as the latitude and longitude of the crater center and lat_d and lon_d as the latitude and longitude of the data point, all in degrees. This results in values ranging from –90 to +90°. To convert these values into the azimuth a with a range of 0 to 360°, the following conditions must be distinguished:

$$a = \begin{cases} x + 360°; & lat_c - lat_d < 0°; \quad x < 0° \\ x; & lat_c - lat_d < 0°; \quad x > 0° \\ x + 180°; & lat_c - lat_d > 0° \end{cases} \tag{2}$$

The azimuth a thus gives an angular value in relation to the crater center, e.g. a data point directly north of the center has a value of 0°, east has a value of 90°, etc.

The strike of rock layers in the rim was then compared to the tangential orientation, or "concentric strike", of a circle with a point of origin in the crater center (Fig. 4b). The difference between the two produces an angular value for each measurement, which is either positive or negative depending on the orientation of strike. This value is referred to as the angular deviation from concentric strike or short, the concentric deviation, *cd*. In a first step, the angle *y* is calculated as:

(3) $$y = -(x + 90° - s)$$

with *s* as the measured strike value, which ranges from 0 to 180°, and *x* as defined in Eq. 1. As *s* and *x* are cyclic for a range of 180°, the final conversions for the concentric deviation *c* must be made:

(4) $$cd = \begin{cases} y + 180°; & y < -90° \\ y; & -90° < y < 90° \\ y - 180°; & y > 90° \end{cases}$$

The concentric deviation *cd* is plotted against the azimuth *a*. This can be done in a standard x-y plot or in a polar plot (Figs. 5, 6). In the case of the Wolfe Creek datasets, and to a lesser degree in the Tooting dataset, plots display scattering and therefore require smoothing to get a better overview of possible average deviations.

The preferred method of smoothing is referred to as the "overlapping bins" method, where all data within a defined sector is averaged. By default a bin size of 30° was used and the position of this bin was varied in steps of 10°. Starting directly north of the crater center (azimuth = 0°), all values within a 30° range from 345° to 15° are collected. The arithmetical average is calculated and displayed for 0°. For a step size of 10°, the next value is calculated for all data between 355° and 25° and displayed at 10°, then from 5° to 35° for 20°, etc., yielding 36 points of average concentric deviation (Fig. 5). This method is useful if there are larger sectors of the crater that only yield a few data points. If the data is good, then one point can represent a large section. On the other hand, if the data is erratic and unreliable due to noise or similar factors, it can be overrepresented by this method and distort the graph in that sector.

An alternative method utilizes the central moving average of data points (i.e. arithmetical average of points 1-5, 2-6, 3-7, etc.). This smoothes outliers, but can also dilute sectors with scarce data. This method shows only minor deviations from the overlapping bins method. When the appropriate amount of smoothing was chosen, major trends remained the same.

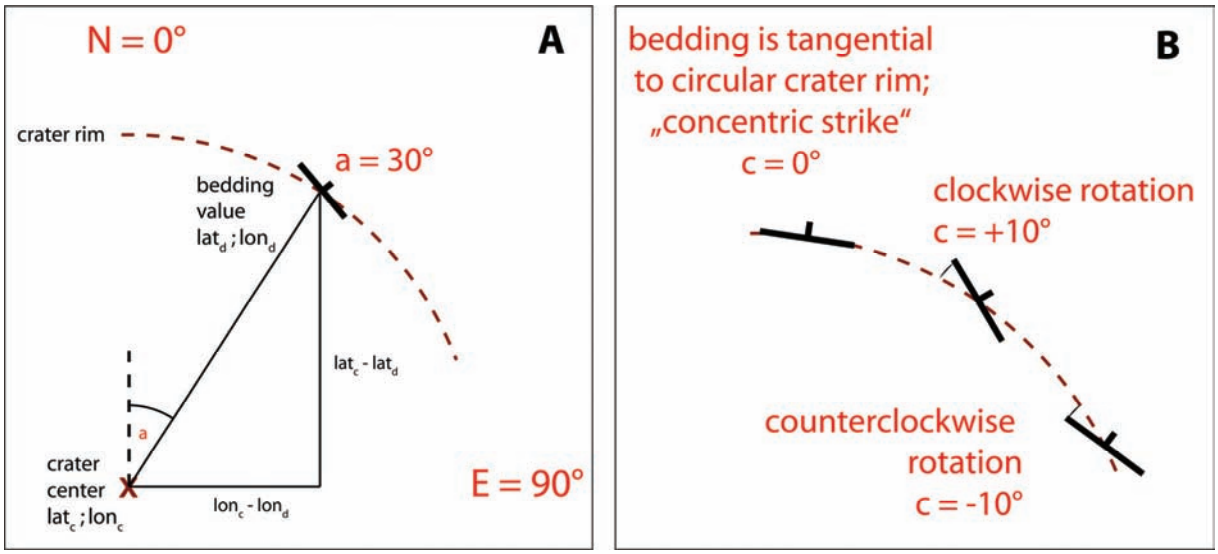

Fig. 4. The method of data conversion for analysis of strike deviation. (a) Conversion of latitude and longitude to a radial reference scheme based on the crater center (azimuth). (b) Angular quantification of strike orientation relative to a hypothetical circle based on the crater center. These values are referred to as "concentric deviation".

To give a better spatial sense of the data, the X-Y-diagrams were converted to polar plots (Figs. 5 and 6). These plots display the data more intuitively from an azimuthal perspective (similar to "map view") and show which values are juxtaposed to each other. Negative values are located on the inside of the circular X-axis, positive ones are on the outside. The conversion to polar plots does distort the visual depiction of the curve to a certain degree, compared to the X-Y-diagram, stretching the display of positive parts of the curve and shortening the negative parts.

To improve the interpretation of the data, 36 bars of average strike were added around the polar plot in steps of 10°, oriented according to the concentric deviation after smoothing with the overlapping bins method. To enhance the visualization of non-concentric behavior, strike can be displayed with an exaggeration factor, e.g. a strike bar with an azimuth of 90°, an angular deviation of -5° and an exaggeration factor of 3 is displayed in the polar plot with a strike value of 75° instead of 85°. The exaggeration factor is constant for a single plot and typically an exaggeration factor of 2 is used.

Further analytical methods

The detection of bilateral symmetry is of great importance for narrowing down the direction of impact. A quantitative method was devised to confirm the qualitative interpretation and determine the azimuthal orientation of the highest degree of bilateral symmetry (Fig. 8). In the method we applied, the 36 values calculated in the overlapping bins method were divided into

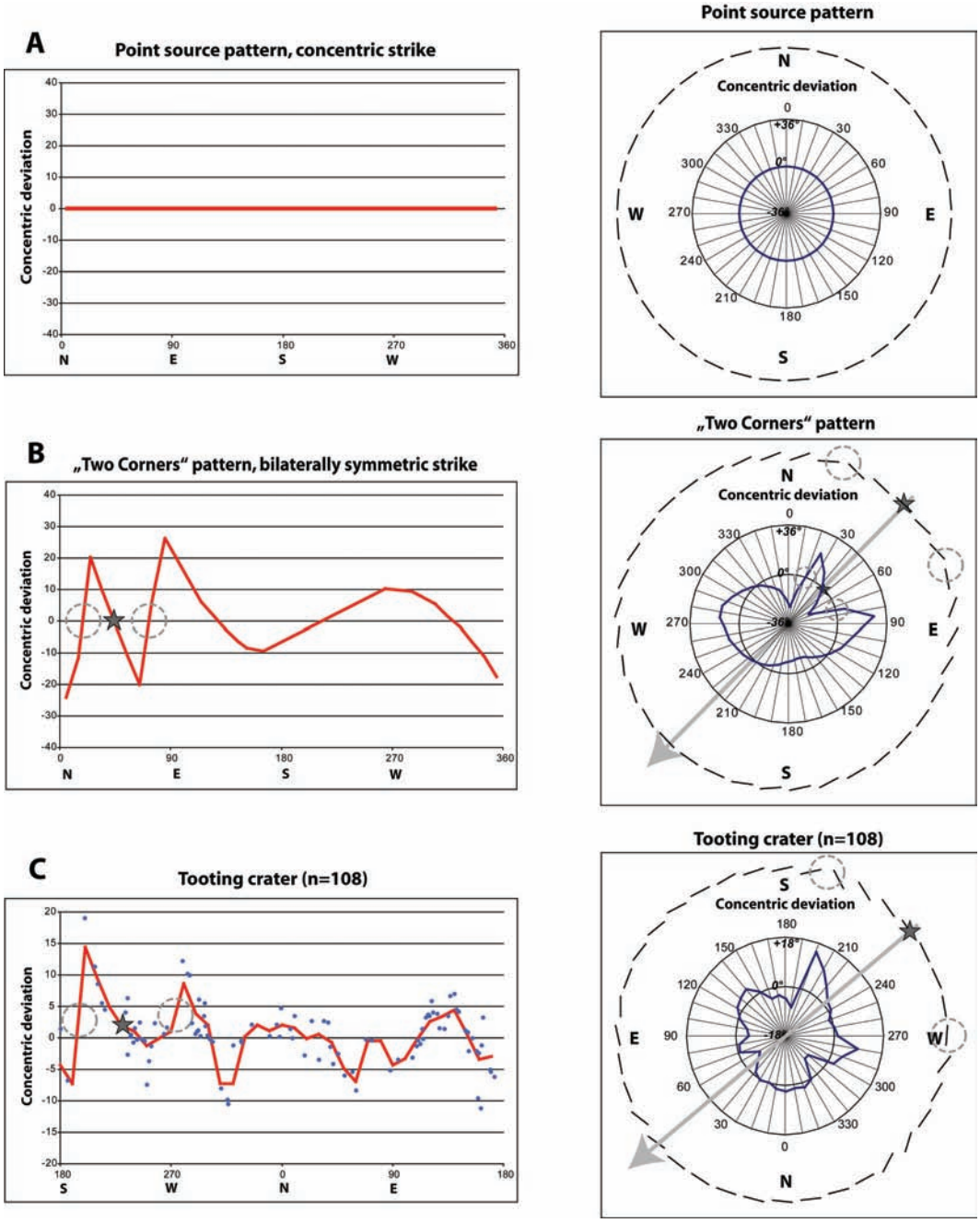

Fig. 5. X-y plots of concentric deviation values plotted against their azimuth relative to the crater center (left) and corresponding polar plots (right). Positive concentric deviation values represent clockwise rotation from concentric strike, negative values display counterclockwise rotation. Curve for Tooting crater is an average of data smoothed with the overlapping bins method (bin size 15°, step size 10°, see text for further explanation). Bars of average strike around polar plots are based on the values of the concentric deviation curve and are used to enhance the interpretation of the data. Strike bars in (c) are exaggerated by a factor of 3. (a) and (b) are based on the two hypothetical models shown in Figs. 1a and b. (a) depicts concentric strike, expected from a model with a "point source" of ejection, where the ejection flow field center does not move. No concentric deviation is visible. (b) shows bilaterally symmetric strike, as expected from "line source" ejection in which the ejection flow field center migrates downrange, with an impactor coming from the northeast. The concentric deviation curve shows two prominent peaks that result from the "corners" the strike bars show uprange, while downrange strike shows a more concentric pattern. (c) consists of data from Tooting crater, Mars. Strike orientation was derived from radial grooves in the ejecta blanket, which are assumed to indicate ejecta trajectories. The concentric deviation curve correlates well with the suggested "line source" model, showing two prominent peaks and a strike bar pattern with "corners", indicating an impact vector from the upper right. Note: Tooting data were rotated by 180° for a better comparison with Figs. 5b and 6.

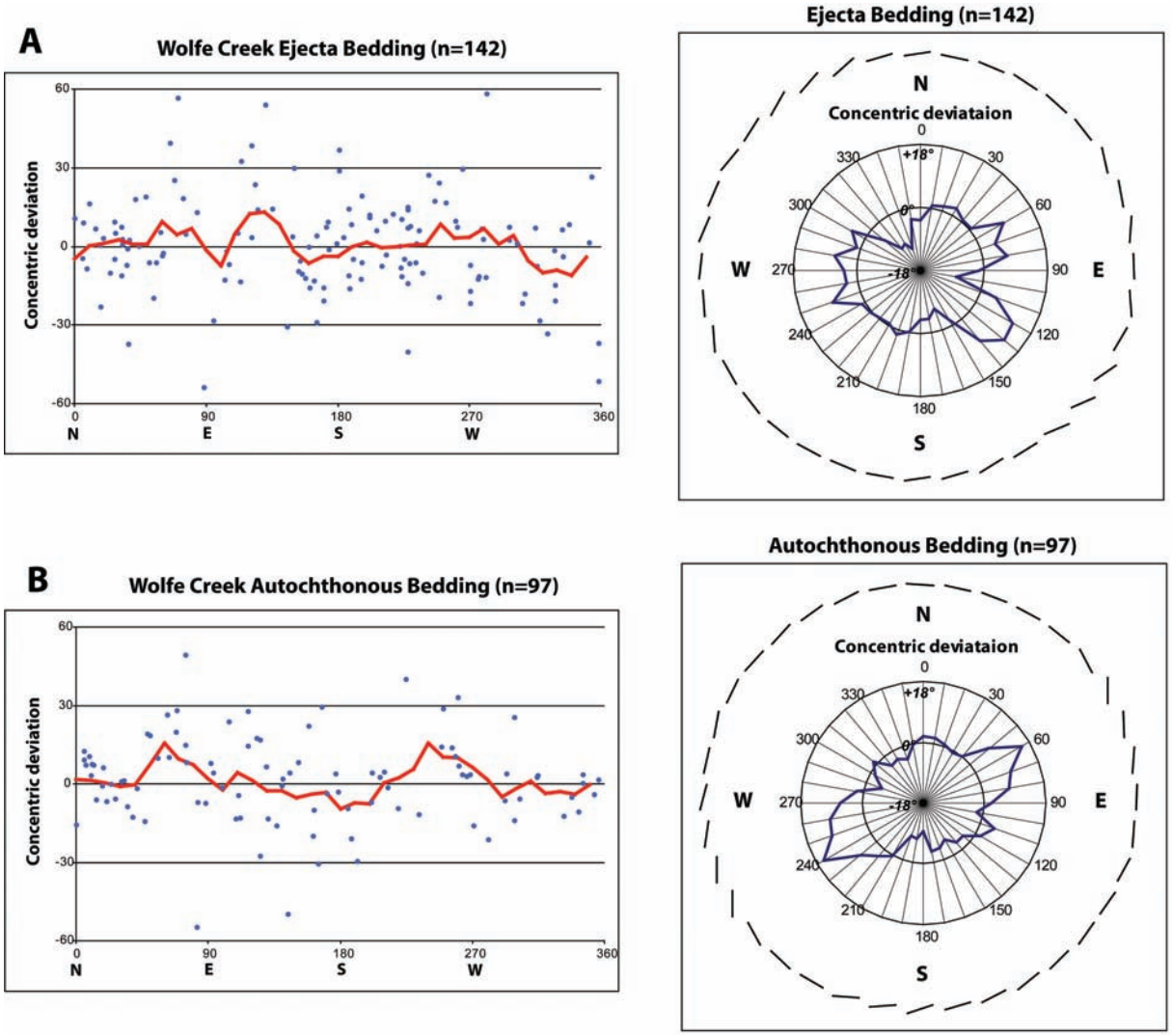

Fig. 6. Concentric deviation values of the Wolfe Creek crater rim and corresponding polar plots. Curves are smoothed with the overlapping bins method (bin size 40°, step size 10°); strike bars are exaggerated by a factor of two. Ejecta values are bedding values from the overturned flap and proximal ejecta blanket. Autochthonous values are from the inner part of the crater rim consisting of normal layered strata. See text and Fig. 5 for further explanation.

two halves and compared to each other. This was done in an iterative manner in steps of 5°. Starting at 0°, a possible axis of bilateral symmetry running N to S was assumed. Then the concentric deviation values at 350° and 10° were compared and added up, e.g. (+4°) + (-11°) = -7°, then the values at 340° and 20°, etc. The sum of all of these compared values is an expression of how well the proposed axis of bilateral symmetry fits, with an ideal axis of symmetry at a sum of 0°, and a higher sum expressing a poorer fit. The axis of potential symmetry was then rotated clockwise by 5° and compared the concentric deviation at 0° and 10°, 350° and 20°, etc. (NB: For even azimuthal orientations, e.g. 0°, 10°, 20°…, single concentric deviation values at 0° and 180°, 10° and 190°, etc. were used in the sum of compared values.) This led to 36 values, each expressing a relative amount of symmetry for a specific azimuthal orientation, which was plotted in an X-Y-diagram. Minima in this diagram

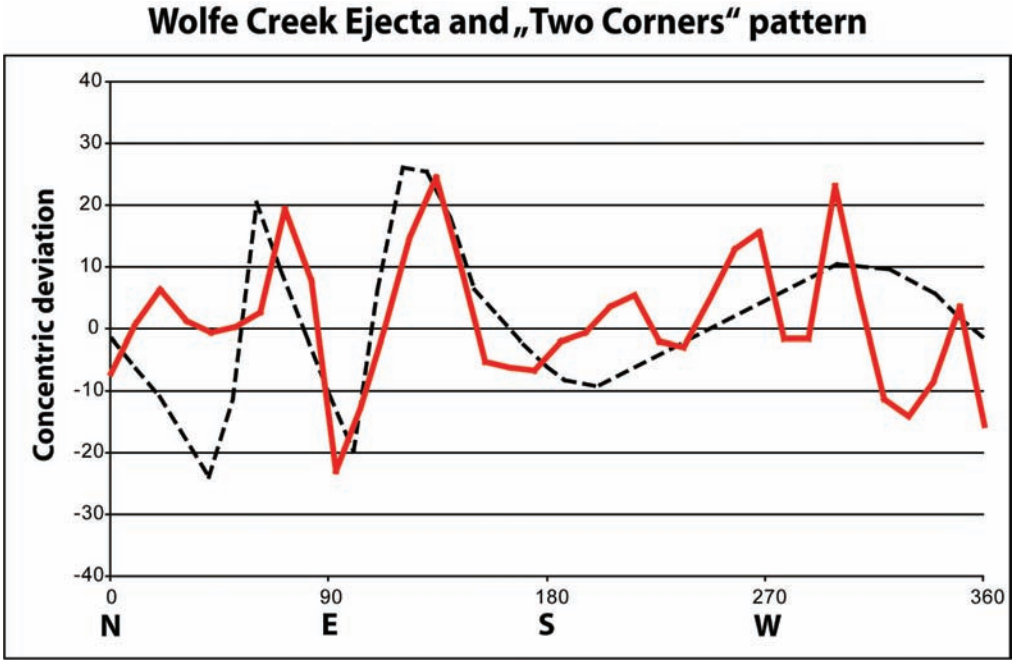

Fig. 7. Comparison of smoothed concentric deviation data (bin size 20°, step size 10°) from Wolfe Creek ejecta (bold curve) with the proposed curve from the “two corners” pattern (dashed curve; see also Figs. 1b and 5b). Based on this fit, the impact direction for Wolfe Creek should be at 80-90°, which revises previous publications and interpretation of bilateral symmetry that suggest 45°.

are interpreted as the best possible axis of bilateral symmetry, implying two possible directions from which the impactor came.

Dip data from the autochthonous inner rim were converted in the same manner as strike data to display their azimuth. Instead of concentric deviation, the dip value, ranging from 0-90° was used. Innermost values in the polar plot are defined as 0°, or horizontal, outermost as 90° (Fig. 9). While dip values are not intended to be used as an indicator for trajectory, azimuthal distribution of varying dip can give further insights into rim structure and symmetry.

Results

Concentric deviation data is presented in Fig. 5 for (a) an ideal point source crater with pure concentrical strike, (b) the ideal “two corners” pattern, and (c) Tooting crater. Concentric deviation curves expected in the point source and “two corners” patterns, which are explained above and depicted in Figs. 1a and b, are shown in a generalized form in Fig. 5a and b.

Concentric strike of the point source pattern shows no concentric deviation, therefore the curve in the X-Y plot is a straight line and a simple circle in the polar plot with a value of 0°. The two corners pattern (Fig. 5b) on the other hand shows strongest concentric deviation at the two corners between the uprange and crossrange sectors, visible in the strike bars around the polar plot, which results in a distinctive pair of peaks in the left part of the X-Y plot that constrain the impact direction. These peaks are the result of the abrupt change in strike

orientation at the corners from counterclockwise to clockwise rotation, which is seen as an abrupt change from negative to positive concentric deviation. The angle between the two corners is a yet uncalibrated function of the impact angle.

Tooting crater

The pattern of concentric deviation data in Tooting crater shows a resemblance to the predicted two corners pattern (Fig. 5c). Two corners in the strike pattern are located uprange at 190° and 280°, showing the strongest amount of deviation, as can also be seen in the smoothed curve (bin size 15°, bin steps of 10°). This is in agreement with the bilateral shape of the distal ejecta blanket, which indicates an impactor coming from 230°, or the southwest.

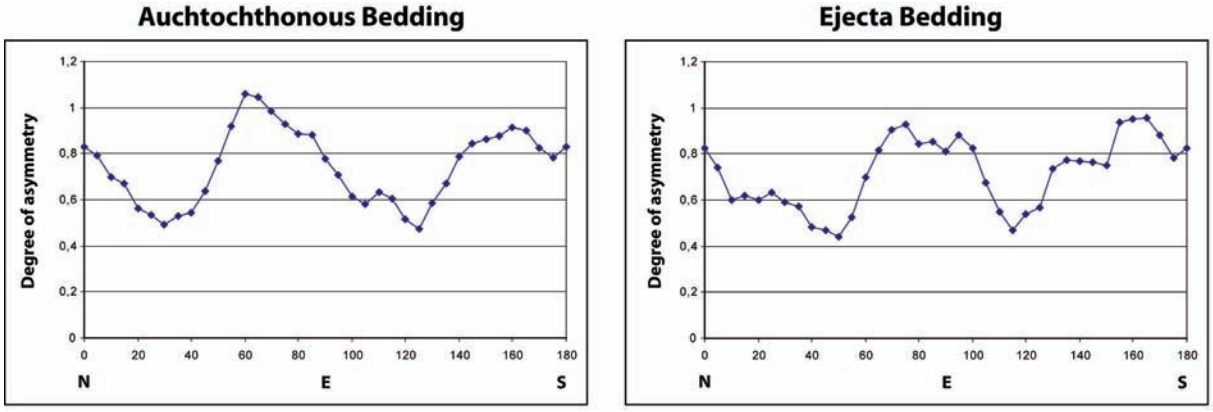

Fig. 8. Degree of asymmetry plotted against the azimuth for Wolfe Creek data. Curves express a relative amount of bilateral symmetry, comparing one half of the concentric deviation data to the other, with the divisional axis aligned to the azimuth. The highest degree of bilateral symmetry is located in the minima of the curves at 30 and 115° for the autochthonous data and 50 and 115° for the ejecta data.

Wolfe Creek Ejecta

The average curve of the concentric deviation of proximal ejecta of the overturned flap of Wolfe Creek, after smoothing with the overlapping bins method (bin size 40°, bin steps of 10°), shows areas of stronger average concentric deviation, located at azimuths of 60-90°, 110-150° and 310-340°, with maximum concentric deviation values of +10° and –10° (Fig 5a). Areas with low concentric deviation are found at 10-50° and 190-240°. Fig. 7 compares the two corners pattern with the ejecta curve (bin size 20° for smoothing) and shows a fit if the two corners pattern curve is rotated to 80-90°, which would imply an impactor coming from the east. This shifts the impact vector from northeast to east. Evaluation of bilateral symmetry of the proximal ejecta (values smoothed with overlapping bins, bin size 40°, bin

steps of 10°) shows two minima at 50° (NE) and 115° (Fig. 8). The first value coincides with the direction of impact suggested in previous publications and might reflect bilateral symmetry of eroded distal ejecta. The second minimum is caused by bilateral symmetries between the proposed downrange and uprange sectors.

Wolfe Creek Autochthonous Rim

The average curve of the concentric deviation of the autochthonous rim (smoothed, bin size 40°, bin steps of 10°, Fig. 5b) does not fit the two corners pattern in Fig. 5b well. Two areas of strong clockwise rotation with maximum values of +15° can be seen at 50-80° and 220-280°, while areas of counterclockwise rotation are located at 130-200°, reaching maximum deviation values near –10°, and to a lesser degree at 320-340°. A larger area of more or less concentric strike is at 350-40°. The strike follows a more elliptical shape, with the long axis running NE to SW, which is along the direction of impact proposed in earlier publications (Hawke 2003; O'Neill and Heine 2003; Shoemaker et al. 2005). The bilateral symmetry curve (smoothed with overlapping bins, bin size 40°, bin steps of 10°) displays minima along the axes of the rough ellipse described by the strike pattern, lying at 30° and 125° (Fig. 8).
The elliptical shape the strike of the autochthonous bedding describes appears to show a similar orientation to the shape of the crater morphology. To investigate this, we compared the strike of the autochthonous bedding with the orientation of the crater rim crest, as mapped by Shoemaker et al. (2005, Fig. 3). Basically, the theoretical line following the rim crest was digitized; each digitized segment was treated as a strike value and converted in the same manner as the bedding values described above. When plotted, the concentric deviation curve of the rim crest orientation coincides surprisingly well with the autochthonous bedding, implying a connection between the internal crater rim structure and its surface expression as rim morphology (Fig. 10).
Our quantitative analysis of dip data of autochthonous rocks in the inner crater rim slope confirms qualitative assessments from an earlier publication by O'Neill and Heine (2003). The NE sector shows data dipping shallowly, from 0-45°. All other sectors show an even distribution of dip values ranging from 0-90° (Fig. 9). This asymmetrical distribution coincides with the NE impact trajectory suggested in other publications.

Discussion

The ejecta deposits of oblique craters on Mars and the Moon suggest that when extrapolated into the crater, the ejecta trajectories do not merge in the crater center. Instead, they merge in a line, suggesting that the ejecta flow field center migrates downrange with time. Based on these observations we proposed a hypothetical and phenomenological model, exhibiting the

so-called “two corners” pattern, which is characterized by its bilateral symmetry and specific “corners” in the transition from the uprange to the crossrange sectors.

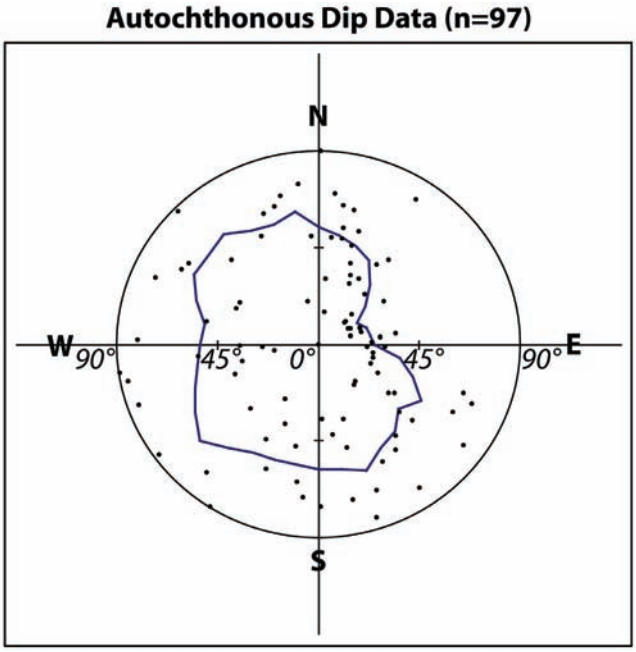

Fig. 9. Dip data of Wolfe Creek autochthonous bedding displayed in a polar plot. Steepest dip values of 90° are located furthest from the center of the plot, the center itself is 0°, or horizontal layering. Curve is an average of data smoothed with the overlapping bins method (bin size 40°, step size 10°). Note the lack of steep bedding in the NE sector of the crater.

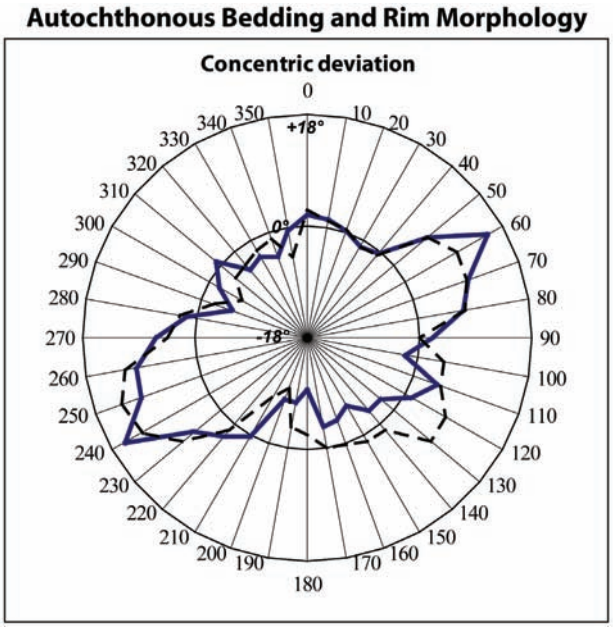

Fig. 10. A comparison of Wolfe Creek autochthonous concentric deviation bedding (solid curve) with the morphology of the crater rim (dashed curve), displayed in a polar plot. Rim morphology was compared to a perfect circle and treated in the same way as bedding strike. Both curves were smoothed with the overlapping bins method (bin size 40°, step size 10°). Note the similarity between the two curves. This implies a strong correlation between bedding structure and rim morphology in Wolfe Creek crater.

The application of our hypothetical model to structural features in the proximal ejecta blanket of Tooting crater was successful. The main features predicted in the concentric deviation curve of the two corners pattern can be easily correlated to Tooting's data, as shown in Fig. 5. Tooting therefore gives evidence for the existence of non-radial behavior in the proximal parts of the ejecta blanket, where otherwise radial symmetry should be expected to dominate due to the circularity of the crater rim.

Concentric deviation curves of Wolfe Creek ejecta and autochthonous bedding are more complex and difficult to interpret (Tab. 1). Data of the inner slope ("autochthonous data") express an interesting interaction between the elliptical shape of the crater morphology and its internal structure, which appear to correlate to a large degree (Fig. 10). In other words, strike of strata influences the orientation of the geomorphologically visible ridge.

Table 1. Summary of impact directions inferred by different methods.

Crater	Method	Figure	Azimuth of incoming impactor
Tooting	Ejecta pattern	Fig. 1d	~240°
	"Two corners"	Fig. 5c	~230°
Wolfe Creek	"Two corners"	Fig. 7	~85°
Ejecta	Bilateral symmetry	Fig. 8	50°, 115° (230°, 295°)
Wolfe Creek	"Two corners"	Fig. 6b	no fit
Autochthonous	Bilateral symmetry	Fig. 8	30°, 125° (210°, 305°)
	Dip data	Fig. 9	~45°, ~225°
	Elliptical rim shape	Fig. 10	~45°, ~225°

Ejecta data can be interpreted in two different ways. Based on the bilateral symmetry of a strongly smoothed concentric deviation curve (bin size 40°), an impact vector is seen coming from the SW or NE, with the latter in agreement with three recent papers (Hawke 2003, O'Neill and Heine 2003, Shoemaker et al., 2005) in which all authors agree on an impactor coming from the NE. Autochthonous concentric deviation data and dip data also support this direction. On the other hand, Fig. 7 shows that the concentric deviation curve for ejecta shows a striking resemblance to our hypothetical model when smoothing is reduced (bin size 20°). This would lead to an impact direction from the east, which slightly modifies previous results including our own. The reason for this is not readily clear, but seems to depend on the chosen bin size.

The large degree of scattering makes it difficult to assess whether the signatures seen in concentric deviation are meaningful or not. It appears that we are close to the limit of resolution that scattering allows. Standard deviations lie at ± 20° for the ejecta and ± 17° for the autochthonous data, compared to only ± 5° for the Tooting data. One possible factor that

contributes to the scattering in Wolfe Creek is an error in measurement when using the field compass, which is estimated around ± 3°.

While any field geologist can avoid measuring small-scale undulations in bedding, meter-scale and larger variations are more difficult to avoid and harder to detect. The lower of the two Devonian sandstones is of assumed fluviatile origin, and an ideal stratigraphic datum cannot be found that can be traced around the crater (Shoemaker et al. 2005). Therefore, although the bedding is subhorizontal on average (dipping gently to the South), one must consider the possibility of local variations in the bedding and the effect this has on our model. If, for example, an originally horizontal bedding plane is rotated during the excavation process by 45° to the north, the new dip direction is 0°. If a neighboring plane, which was not originally horizontal but dipped to the East at 5° is rotated the same way, its new dip direction is at 7.05°, as calculated in a stereoplot. If the same plane is rotated by 60°, its new dip direction is at 5.77°. Rotational values of 45 and 60° represent the average dip for ejecta (45.3°) and autochthonous bedding (58.0°). Thus slight variations in the initial bedding orientation could be biased due to rotation.

While large-scale variation of bedding surfaces explains the scattering observed to a certain degree, other mechanisms might be involved that additionally contribute to the noise. Lithologic heterogeneities in sandstone beds, including variations in density, pore space, and rock strength may play a small role in the final crater structure, but it is beyond the scope of this paper to quantify these factors. Further change in bedding orientation during the crater modification stage may occur, but probably plays a minor role for our model. In simple craters, the final crater differs little from the state of the transient crater. Some brecciated rock will have slid into the crater center, while the stable part of the rim should remain unaltered. Portions of the rim that show small scale slumping were avoided during collection of field data. Generally, in the field lithological boundaries are used to make out large-scale rim deformation and possible post-impact slumping. Displacements and faulting that could reveal rim collapse or back wasting were not observed in the field and are also not present in Shoemaker et al.'s (2005) map (Fig. 3).

The effect of joint sets on the cratering process has already been shown in Barringer Meteorite Crater (Roddy 1978; Poelchau et al. forthcoming) where two prominent, orthogonal joint sets aligned to the diagonals of the square-shaped crater rim enabled the propagation of the cratering flow. Wolfe Creek Crater on the other hand has a recognizable elliptical shape. Shoemaker et al. (2005) believe this is caused by the impactor striking at an oblique trajectory of around 45-30°, based on experiments with oblique impacts by Gault and Wedekind (1978). Apparently in Wolfe Creek, this mechanism dominates over the effect joints sets have on the crater shape. The eastern half of the crater does show a somewhat hexagonally shaped rim, which could be caused by joint sets (Öhman et al. 2006). Joint sets may also play a role in the orientation of bedding in the rim after impact, as has been shown in our study by the striking

correlation between the shape of the rim crest and the strike of autochthonous bedding (Fig. 10).
Even though numerous factors may influence the deformation of bedding during crater excavation and a large degree of scattering is prevalent in the strike data of Wolfe Creek, it must be stressed that after smoothing, patterns in the concentric deviation data are revealed that can be analyzed and subjected to further interpretation with respect to a possible impact direction.

Conclusions

We developed a quantitative technique that allows structural asymmetries in impact craters to be deciphered. The technique consists of (i) the conversion of structural data from a geographic into a radial reference scheme, (ii) the illustration of "concentric deviation" in x-y diagrams and specific polar plots and (iii) the iterative analysis of symmetry patterns. This new technique allows a fast, quantitative analysis of field data, which was lacking beforehand. Based on the latest insights from recent numerical models and from remote sensing data of the ejecta blankets of planetary craters, we suggest a simple hypothetical and phenomenological model, the "two corners" model, that uses patterns observed in the ejecta blankets on planetary surfaces to predict structural features in the crater rim. This model has shown its relevance for the Tooting crater on Mars and has implications for simple craters on Earth, as was shown in Wolfe Creek, although these results deviate slightly from other findings. Nonetheless, while radial symmetry dominates in the crater rim, non-radial patterns have been revealed that can be interpreted as indicators for an impact direction.
At present, our model is intuitive and needs a sound explanation. Our model would be greatly enhanced by further experiments on visualization of particle trajectories in oblique impacts. So far, resolution of the final stages of crater excavation has not been published. Also, verification through 3D modeling of oblique impacts is needed. The situation that our model describes, the final stage of crater excavation, requires specific modeling for a precise replication. So far, little work has been done in this area. First attempts made with 3D models show promising results that confirm our hypothesis (D. Elbeshausen and K. Wünnemann, pers. communication), but require more work for a reliable verification that supports our model to a larger degree of certainty.

Acknowledgements

We would like to thank Pete Schultz and Jennifer Anderson for their encouraging, thoughtful reviews. Thanks also to Peter Haines and Franco Pirajno from the GSWA and Phil Palmer from the Department of Indigenous Affairs, Derby, Australia, for their advice and logistical help in the course of our field campaign. We are grateful to Dirk Scherler and Sebastian Quart

for their field assistance in Australia. Fruitful discussions with Dirk Elbeshausen and Kai Wünnemann helped to improve the concepts introduced in this paper. Funding was provided by DFG project KE 732-11/1.

Literature

Anderson J. L. B., Schultz P. H. and Heineck J. T. 2003. Asymmetry of ejecta flow during oblique impacts using three-dimensional particle image velocimetry. *Meteoritics & Planetary Science* 108:13-1.

Anderson J. L. B., Schultz P. H. and Heineck J. T. 2004. Experimental ejection angles for oblique impacts: Implications for the subsurface flow-field. *Journal of Geophysical Research* 108:1-10.

Anderson J. L. B. and Schultz P. H. 2006. Flow-field center migration during vertical and oblique impacts. *International Journal of Impact Engineering* 33:35-44.

Artemieva N. A. and Ivanov B. A. 2001. Numerical simulation of oblique impacts: impact melt and transient cavity (abstract #1288). 32nd Lunar and Planetary Science Conference. CD-ROM.

Artemieva N. A., Karp T. and Milkereit B. 2004. Investigating the Lake Bosumtwi impact structure: Insight from numerical modeling. *Geochemistry Geophysics Geosystems* 5.

Barnouin-Jha O. S., Schultz P. H. and Lever J. H. 1999a. Investigating the interactions between an atmosphere and an ejecta curtain, 1, Wind tunnel tests. *Journal of Geophysical Research* 104:27105 -27115.

Barnouin-Jha O. S., Schultz P. H. and Lever J. H. 1999b. Investigating the interactions between an atmosphere and an ejecta curtain, 2, Numerical experiments. *Journal of Geophysical Research* 104:27117–27131.

Barringer D. M. 1909. Meteor Crater in Northern Central Arizona. *Pap., Autumn Meeting of the National Academy of Sciences at Princeton Univ.*

Bottke W. F., Love S. G., Tytell D. and Glotch T. 2000. Interpreting the Elliptical Crater Populations on Mars, Venus, and the Moon. *Icarus* 145:108-121.

Buchwald V. F. 1975. Handbook of iron meteorites (Mer-Z): University of California Press, Berkeley.

Dahl J. M. and Schultz P. H. 2001. Measurement of stress wave asymmetries in hypervelocity projectile impact experiments. *International Journal of Impact Engineering* 26:145-155.

Ekholm A. G. and Melosh H. J. 2001. Crater features diagnostic of oblique impacts: The size and position of the central peak. *Geophysical Research Letters* 28:623-626.

Gault D. E. 1968. Impact cratering mechanics and structures, in: French, B.M., Short, N.M. (Eds), Shock Metamorphism of Natural Materials. Mono Book Corp, Baltimore, pp. 87-100.

Gault D. E. and Wedekind J. A. 1978. Experimental studies of oblique impact. *9th Lunar and Planetary Science Conference.* pp. 3843 - 3875.

Gilbert G. K. 1892. The Moon's Face; a study of the origin of its features. *Bulletin of the Philosophical Society*. 12:241 - 292.

Gulick S. P. S., Barton P. J., Christeson G. L., Morgan J. V., McDonald M., Mendoza-Cervantes K., Pearson Z. F., Surendra A., Urrutia-Fucugauchi J., Vermeesch P. M. and Warner M. R. 2008. Importance of pre-impact crustal structure for the asymmetry of the Chicxulub impact crater. *Nature Geoscience* 1:131-135.

Hawke, P. J. 2003. Geophysical investigation of the Wolfe Creek meteorite crater, *Geological Survey of Western Australia Record* 2003/10.

Herrick R. R. and Phillips R. J. 1994. Implications of a global survey of Venusian impact craters. *Icarus* 111:387-416.

Herrick R. R. and Forsberg-Taylor N. K. 2003. The shape and appearance of craters formed by oblique impact on the Moon and Venus. *Meteoritics & Planetary Science* 38:1551-1578.

Herrick R. R. and Hessen K. K. 2006. The planforms of low-angle impact craters in the northern hemisphere of Mars. *Meteoritics and Planetary Science* 41:1483-1495.

Hildebrand A. R., Pilkington M., Halpenny J., Cooper R., Connors M., Ortiz-Aleman C., Chavez R. E., Urrutia-Fucugauchi J., Graniel-Castro E., Camara-Zi A. and Buffler R. T. 1998. Mapping Chicxulub crater structure with overlapping gravity and seismic surveys (abstract #1821). 29th Lunar and Planetary Science Conference. CD-ROM.

Kenkmann T., Jahn A., Scherler D. and Ivanov B. A. 2005. Structure and formation of a central uplift: a case study at the Upheaval Dome impact crater, Utah. In *Large Meteorite Impacts III*, edited by Kenkmann T., Hörz F. and Deutsch A. Boulder: Geological Society of America Special Paper 384. p. 85-115.

Kenkmann T. and Poelchau M. H. 2008. Matt Wilson: an elliptical impact crater in Northern Territory, Australia (abstract #1027). 39th Lunar and Planetary Science Conference. CD-ROM.

LaPaz L. 1954. Meteoritic material from Wolf Creek, Western Australia, Crater. *Meteoritics* 1:200-203.

Maxwell D. E. 1977. Simple Z model of cratering, ejection, and the overturned flap. In *Impact and Explosion Cratering*, edited by Roddy D. J., Pepin R. O. and Merrill R. B. New York: Pergamon Press. p. 1003-1008.

McCall G. J. H. 1965. Possible meteorite craters - Wolf Creek, Australia and analogs: in Geological Problems in Lunar Research. *New York Academy of Science Annals* 123:970 - 998.

Morgan J., Smith A., Styles E., Surendra A. and Barton P. 2006. Chicxulub revealed with new seismic and gravity data (abstract #1626). 37th Lunar and Planetary Science Conference. CD-ROM.

Mouginis-Mark P. J. and Garbeil H. 2007. Crater geometry and ejecta thickness of the Martian impact crater Tooting. *Meteoritics and Planetary Science* 42:1615-1625.

Öhman T., Aittola M., Kostama V.-P., Hyvärinen M. and Raitala J. 2006. Polygonal impact

craters in the Argyre region, Mars: Evidence for influence of target structure on the final crater morphology. *Meteoritics and Planetary Science* 41:1163-1173.
O'Neill, C., and C. Heine, C. 2005. Reconstructing the Wolfe Creek meteorite impact: deep structure of the crater and effects on target rock. *Australian Journal of Earth Sciences*, 52:699-709.
Pierazzo E. and Crawford D. A. 1998. Modeling Chicxulub as an oblique impact event: results of hydrocode simulations (abstract #1704). 29th Lunar and Planetary Science Conference. CD-ROM.
Pierazzo E. and Melosh H. J. 1999. Hydrocode modeling of Chicxulub as an oblique impact event. *Earth and Planetary Science Letters* 165:163 - 176.
Pierazzo E. and Melosh H. J. 2000. Understanding oblique impacts from experiments, observations, and modeling. *Earth and Planetary Science Letters* 28:141-167.
Pierazzo E. and Melosh H. J. 2000. Hydrocode modeling of oblique impacts: The fate of the projectile. *Meteoritics & Planetary Science* 35:117 - 130.
Poelchau M. H., Kenkmann T. and Kring D. A. Forthcoming. Rim uplift and crater shape in Meteor Crater: the effects of target heterogeneities and trajectory obliquity. *Journal of Geophysical Research.*
Roddy D. J. 1978. Pre-impact geologic conditions, physical properties, energy calculations, meteorite and initial crater dimensions and orientations of joints, faults and walls at Meteor Crater, Arizona. *9th Lunar and Planetary Science Conference.* pp. 3891-3930.
Scherler D., Kenkmann T. and Jahn A. 2006. Structural record of an oblique impact. *Earth and Planetary Science Letters* 248:43-53.
Schultz P. H. 1992a. Atmospheric effects on ejecta emplacement and crater formation on Venus from Magellan. *Journal of Geophysical Research* 97:16,183-16,248.
Schultz P. H. 1992b. Atmospheric effects on ejecta emplacement. *Journal of Geophysical Research* 97:11,623-11,662.
Schultz P. H. and Anderson R. R. 1996. Asymmetry of the Manson impact structure: evidence for impact angle and direction. In *The Manson Impact Structure, Iowa: Anatomy of an Impact Crater*, edited by, Koeberl C. and Anderson R. R. Boulder: Geological Society of America Special Paper 302. p. 397-417.
Schultz P. H. and D'Hondt S. 1996. Cretaceous-Tertiary (Chicxulub) impact angle and its consequences. *Geology* 24:963-967.
Schultz P. H. and Lutz-Garihan A. B. 1982. Grazing impacts on Mars: a record of lost satellites. *Journal of Geophysical Research* 87:A84 - A96.
Schultz P. H., Eberhardy C. A., Ernst C. M., A'Hearn M. F., Sunshine J. M. and Lisse C. M. 2007. The Deep Impact oblique impact cratering experiment. *Icarus* 190:295-333.
Shoemaker E. M. 1962. Interpretation of lunar craters. In *Physics And Astronomy of the Moon*, edited by Kopal Z. New York/London: Academic. p. 283-359.
Shoemaker E. M. and Kieffer, S.W. 1974. Guidebook to the Geology of Meteor Crater,

Arizona. Center for Meteorite Studies, Ariz. State Univ., Tempe. 66 pp.
Shoemaker, E. M., C. S. Shoemaker, K. Nishiizomi, C. P. Kohl, J. R. Arnold, J. Klein, D. Fink, R. Middleton, P. W. Kubik, and P. Sharma 1990. Ages of Australian meteorite craters - A preliminary report (abstract). *Meteoritics*, 25:409.
Shoemaker E. M., MacDonald F. A. and Shoemaker C. S. 2005. Geology of five small Australian impact craters. *Australian Journal of Earth Sciences,* 52:529-544.
Shuvalov V. and Dypvik H. 2004. Ejecta formation and crater development of the Mjølnir impact. *Meteoritics & Planetary Science* 39:467- 479.
Stöffler D., Artemieva N. A. and Pierazzo E. 2002. Modeling the Ries-Steinheim impact event and the formation of the moldavite strewn field. *Meteoritics & Planetary Science* 37:1893-1907.
Tsikalas F. 2005. Mjølnir crater as a result of oblique impact: Asymmetry evidence constrains impact direction and angle. In *Impact Tectonics*, edited by, Koeberl C. and Henkel H. Berlin: Springer. p. 285-306.

3. Rim uplift and crater shape in Meteor Crater: the effects of target heterogeneities and trajectory obliquity

This chapter has been published as the following peer-reviewed article:

Poelchau M. H., Kenkmann T. and Kring D. A., 2009. Rim uplift and crater shape in Meteor Crater: the effects of target heterogeneities and trajectory obliquity. Journal of Geophysical Research, 114, E01006, doi:10.1029/2008JE003235.

Abstract

We have analyzed the rim structure of Meteor Crater, Arizona, in order to understand the mechanism of rim uplift in simple craters and the causes of the shape of polygonal impact craters. For this purpose, we systematically determined bedding orientation of the autochthonous crater wall and overturned flap and analyzed the kinematics of major radial faults. We found that rim uplift correlates with the crater shape and increases in the corners of the crater. The two main mechanisms of differential uplift are the formation of horizontal interthrust wedges, leading to the doubling of strata in the rim, and radial corner faults, or tear faults, that vertically displace bedrock. The development of Meteor Crater's quadrangular shape is caused by more effective crater excavation flow parallel to major joint sets. Additionally, we infer the impact direction with a newly developed technique, the two corners model, and review the arguments in favor of an oblique trajectory. While the dataset is ambiguous, several indicators suggest an impact direction from the NNW. We conclude that oblique impacts should have an effect on early cratering and excavation flow, whereas target heterogeneities like joints start to play a prominent role in later stages when the stresses induced by the excavation flow are in the same order of strength as the material involved.

Introduction

The Barringer Meteorite Crater, or Meteor Crater, is the prime example of a young, well-preserved and well-documented simple impact crater. As simple craters are among the most common morphological features on planetary surfaces in the solar system, understanding Meteor Crater is of major importance. While the outline of most simple craters is circular, the shape of Meteor Crater strongly deviates from a circle and resembles a quadrangle (Fig. 1). The quadrangular shape is generally attributed to the occurrences of joint sets running through the diagonals of the crater, although so far, little research has been performed on the details of the proposed process. Ground truth data are needed to better understand how the pre-impact target structure can affect the shape and internal deformation of the crater wall and crater rim. This knowledge in turn can be used to enhance our understanding of the cratering process and the implications crater morphology and structure

have on the configuration and composition of the surface and subsurface of other solid bodies in the solar system.

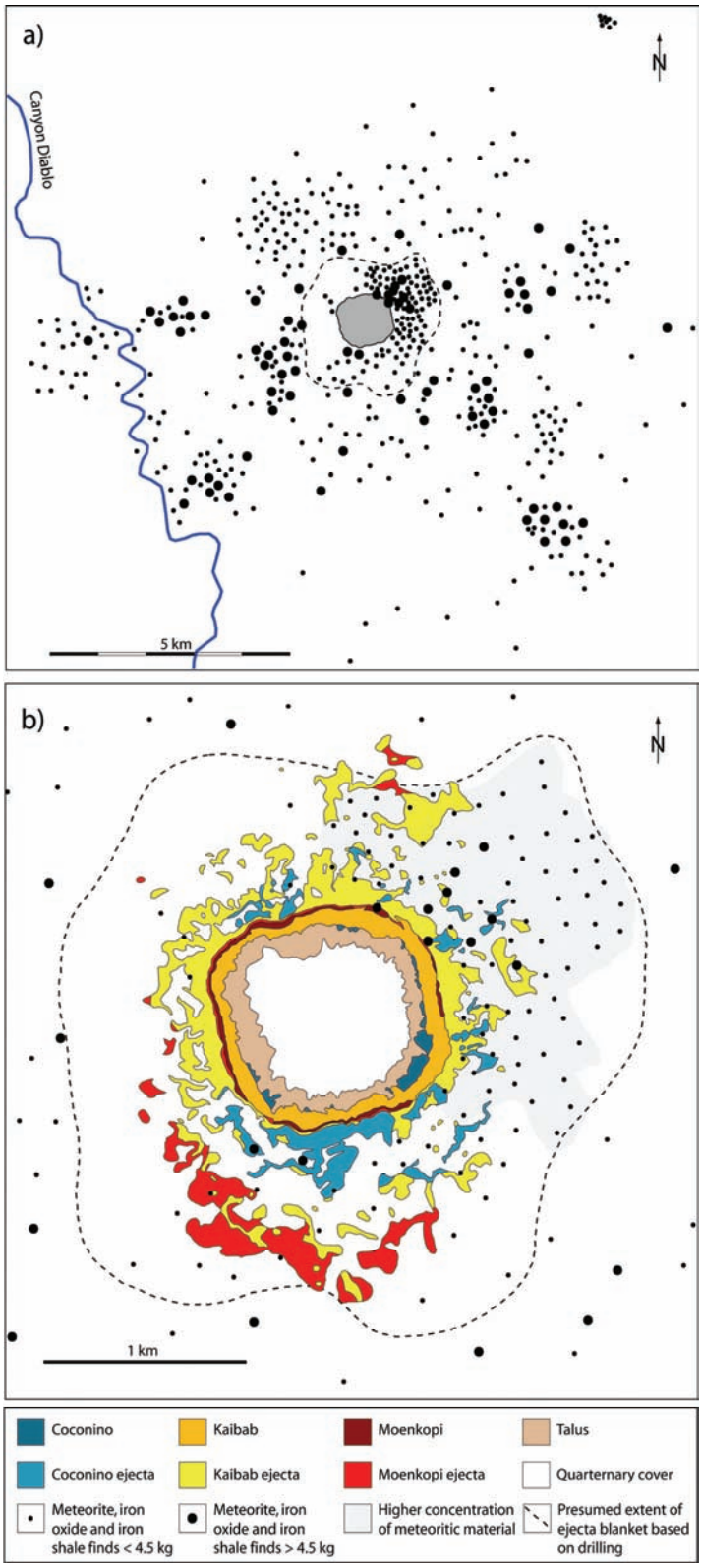

Figure 1: a) The distribution of the Canyon Diablo iron meteorite [after Barringer, 1909; also Kring, 2007]. Points in the map represent meteoritic iron, meteoritic iron oxide and iron shale. Finds < 4.5 kg were mostly only a few grams in weight. b) Geological map of Meteor Crater showing stratigraphic units of the crater wall and exposed ejecta blanket [from Shoemaker & Kieffer, 1974] and the presumed extent of the ejecta blanket based on drilling [Roddy et al., 1975], which shows slight discrepancies with the mapped ejecta in the N.

Meteor Crater

Meteor Crater was formed ~50,000 years ago in flat-lying sedimentary rocks of the Southern Colorado Plateau in Arizona by the iron Canyon Diablo meteorite. With a diameter of ~1.2 km, Meteor Crater is a simple, bowl-shaped crater that is surprisingly well preserved by terrestrial standards. Shoemaker and Kieffer [1974] estimate 15 to 20 m of erosion in the rim crest, while the crater floor shows ~30 m of post impact sedimentation of lake sediments and alluvium. Talus covers the lower segments of the inner crater wall, leaving 80-100 m of the stratigraphic sequence of the Southern Colorado Plateau exposed (Fig. 1). The lowest unit visible, the Permian Coconino sandstone, is only exposed in small areas of the crater wall, revealing white, fine-grained quartzose sandstone layers. It is overlain by 3 m of Toroweap Formation, consisting mainly of white to yellowish-brown calcareous sandstones. The main unit visible in the crater wall is the 80 m thick Kaibab Formation, with the older gamma member (white-yellowish dolomite) and beta member (yellow, massive dolomite) overlain by yellow, well-bedded dolomite and sandstone interbeds of the alpha member. The top unit of this sequence is the 8.5 m thick Permo-Triassic Moenkopi Formation, which follows unconformably. It is subdivided into the reddish brown, massive sandstone of the Wupatki Member and the reddish brown, fissile siltstone of the Moqui Member, which both form a marked contrast to the underlying yellow Kaibab units and are easily traced in the crater wall. The inverted sequence of these rocks can be observed in the hinge zone and overturned flap and further outwards in the ejecta blanket (Fig. 1b). For a detailed review of the geology of Meteor Crater, see Kring [2007].

Previous structural research in Meteor Crater

Structural aspects of Meteor Crater were first observed and published in the early 20th century by Barringer [e.g. 1905] among others, who described uplift of the crater rim and speculated that uplift is caused by crushed rock thrust into the crater walls. In his research on Meteor Crater, Shoemaker [1960, 1963; Shoemaker & Kieffer, 1974] also briefly focused on several structural aspects of the crater rim, noting (1) that joint sets coincide with the diagonals of the crater's roughly square-shaped outline, (2) that the joint sets additionally enable large scale vertical faulting with "scissor type displacement" in the crater wall, and (3) that coherent rock material has been emplaced in horizontal zones of weakness, resulting in thrusting and horizontal faulting in several areas of the crater rim. Roddy [1978] was the first to quantify structural features of the crater rim and showed how closely the crater diagonals are related to the orientation of joint sets. Until recently, no comprehensive quantitative structural data of the crater wall other than Roddy's concise data set of joints were available in peer-reviewed literature. Kumar & Kring [2008] measured over 1700 fractures. They were able to differentiate between impact induced, outward dipping "conical fractures" and pre-impact radial and concentric fractures. They conclude that a combination of faulting along joints oriented diagonally and "fracture-controlled motion" along the crater walls led to the

crater's square shape. It should be stated that Kumar & Kring's study was coordinated with our study. While Kumar and Kring's focus was on the orientation and generation of fractures, our study investigated kinematic processes of cratering, based on bedding and GPS measurements.

The effect of target structure, especially jointing, on the shape of craters has been discussed in several papers. Fulmer & Roberts [1963] concluded, from lunar observations and experiments with explosion cratering, that joint sets determine whether polygonal impact craters (PICs) are formed or not. They believe that PICs are not formed if an uppermost, unconsolidated target layer is at least ¼ as thick as the (transient) crater depth, or if the joint spacing is too large. Gault et al. [1968] report square shaped and hexagonal craters formed during hypervelocity impact experiments into "jointed" targets with a rather large spacing of 1/5 crater diameter, but do not quantify the experimental outcome in detail (e.g. orientation of crater walls to joints). Eppler et al. [1983] propose a model that differentiates between the crater shapes of simple and complex craters, based mainly on observations in Meteor Crater and publications of other authors. They suggest that in simple craters, excavation is more efficient parallel to joint sets, thus forming corners, while in complex craters, the dominant effect is slumping along joints during crater modification, resulting in walls that are parallel to the to the joint sets, not to the diagonals in simple craters. Interestingly, while tectonic regimes and structures have been inferred from PICs on the moon and other planets [e.g. Elston et al., 1971; Öhman et al., 2006; Aittola et al., 2007], to the best of our knowledge there are only two terrestrial PICs in which joints have been correlated with crater shape: Söderfjärden crater (an eroded, complex crater), and Meteor Crater.

This paper provides new structural data obtained from the crater rim of Meteor Crater. Based on these new data the effects of target heterogeneities as well as possible effects of oblique incidence are analyzed and discussed.

Can the impact vector be derived in simple craters? - A working hypothesis

Based on the probability P of an impact occurring below a certain angle θ above the horizon, given as $P = \sin^2 \theta$ [Shoemaker, 1962], one out of two impacts occurs below 45°, and one out three impacts occurs below 35°. Only highly oblique impacts of less than 10° incidence from the horizontal create elliptical craters, therefore the crater shape cannot normally be used as an indicator of an impact direction. The shape of the ejecta blanket, on the other hand, has proven its use in determining the impact vector in numerous studies if the impact angle is less than ~35° from the horizontal [e.g. Gault & Wedekind, 1978; Herrick & Hessen, 2006; McDonald et al., 2008]. The offset position of the blanket in the downrange direction and the v-shaped uprange forbidden zone are two indicators of the presence of the non-radial aspects that exist during oblique cratering (Fig. 2). This non-radial behavior of

ejecta has been analyzed in hypervelocity impact experiments by Anderson et al. [2003], in which the vectors of ejected particles were imaged. A strong, non-radial, bilaterally symmetric signature can be seen in their data, which weakens as cratering progresses but is still present in images of the late stages. On Earth the ejecta blankets are rarely preserved and thus no craters have been found with an ejecta blanket capable of giving unambiguous indicators for an impact direction. While distal ejecta with its asymmetric features is lacking in terrestrial craters, the most proximal parts of the ejecta blanket – the overturned flap and hinge zone of the crater rim – are preserved in a number of craters on Earth. The possibility that these proximal parts may preserve non-radial symmetry was explored by Poelchau & Kenkmann [2008] at Wolfe Creek crater. We refer to that paper for a comprehensive description of the so-called "two corners" model.

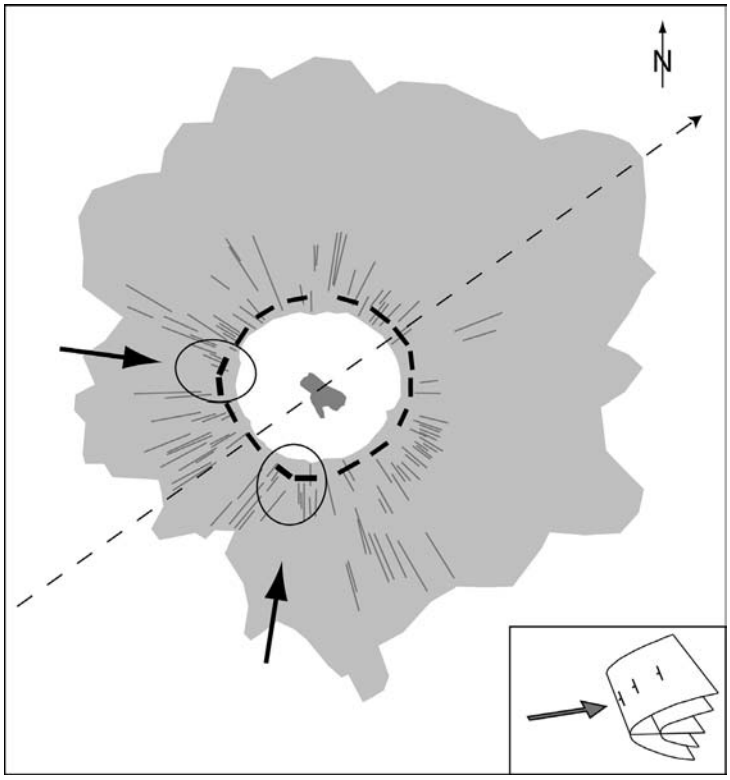

Figure. 2: Sketch map of Tooting crater on Mars (derived from THEMIS mosaic), which exhibits striations in its ejecta blanket that were mapped as possible indicators for ejecta trajectories (black lines). Assumed strike (black bars) is orthogonal to the mapped ejecta trajectories and displays a non-radial, bilaterally symmetric pattern with two corners, which indicates an impact vector coming from the SW. Black arrows mark corners in the strike pattern as the strongest uprange indicators. Strike of folded bedding in the overturned flap is always orthogonal to the ejecta trajectories for originally horizontal target bedding (inset).

Poelchau and Kenkmann's "two corners" model is based on the observation that the proximal and distal ejecta blankets of oblique craters on the Moon and Mars display deviations from pure radial flow (Fig. 2). When extrapolated backwards into the crater, striations on the ejecta blankets do not meet in the crater center but focus along a line running

from the uprange section of the crater to its center, suggesting non-radial, outward flow from a moving source of ejection, as also suggested from experiments [e.g. Anderson et al., 2003]. While these striations are a late-stage cratering phenomenon and on Mars may possibly indicate atmospheric interaction, the non-radial pattern the striations describe is believed to reflect early cratering asymmetries.

It is expected that the bedding orientation of blocks in the ejecta blanket is too chaotic to be used to derive any deviation from radial ejection patterns. However, near the crater rim in the hinge zone and within the overturned flap, strata are often coherent over large distances. In these settings it can be assumed that strata strike is perpendicular to the excavation flow direction (for originally horizontal bedding, Fig. 2, inset). Thus, deviations from radial flow should lead to a measurable deviation in strike from a concentric direction. The expected pattern of strike should be bilaterally symmetric to the direction of impact and, based on the analysis of Tooting Crater on Mars and Wolfe Creek, Australia, have two "corners" between the uprange and crossrange sector, in which an abrupt change in strike orientation occurs (Fig. 2).

In this paper we present new structural data of Meteor Crater and provide a kinematic model that is consistent with structural observations, in particular the quadrangular crater shape. We quantify the characteristic structural asymmetries of this crater and address the question as to whether these asymmetries could be exclusively caused by target heterogeneities or if they are additionally related to an oblique impact scenario. In the first part of this article (Results I) structural data are presented. The second part (Results II) critically reviews arguments in favor of an oblique impact scenario and applies the "two corners" model [Poelchau and Kenkmann, 2008] to Meteor Crater in order to derive a possible impact vector. In the discussion section phenomenological models are presented that bring rim uplift and shape into a causal context.

Methods

1. Measurement of bedding planes

Field data was collected in the upper part of the crater rim, when possible in the area of the overturned flap, where the transition from uppermost autochthonous rock layers to overturned proximal ejecta beds occurs (Fig. 3). The data set was subdivided into "autochthonous data" if normal bedding occurs (298 measurements) and "ejecta data" if strata are overturned (83 measurements). Data values consist of strike and dip of bedding planes along with their latitude, longitude, and altitude as measured with GPS. (Strike of a plane is defined as the crossing line between a theoretical, horizontal plane and the measured bedding plane. At the time of measurement, magnetic declination was at 11.2° E and was corrected afterwards by rotating strike values clockwise.) As layering in the ejecta becomes more chaotic the further away it is from the crater center, care was taken to measure only

overturned units that showed coherent behavior over tens of meters in length. Additionally, care was taken not to measure slumped blocks when measuring autochthonous bedding data.

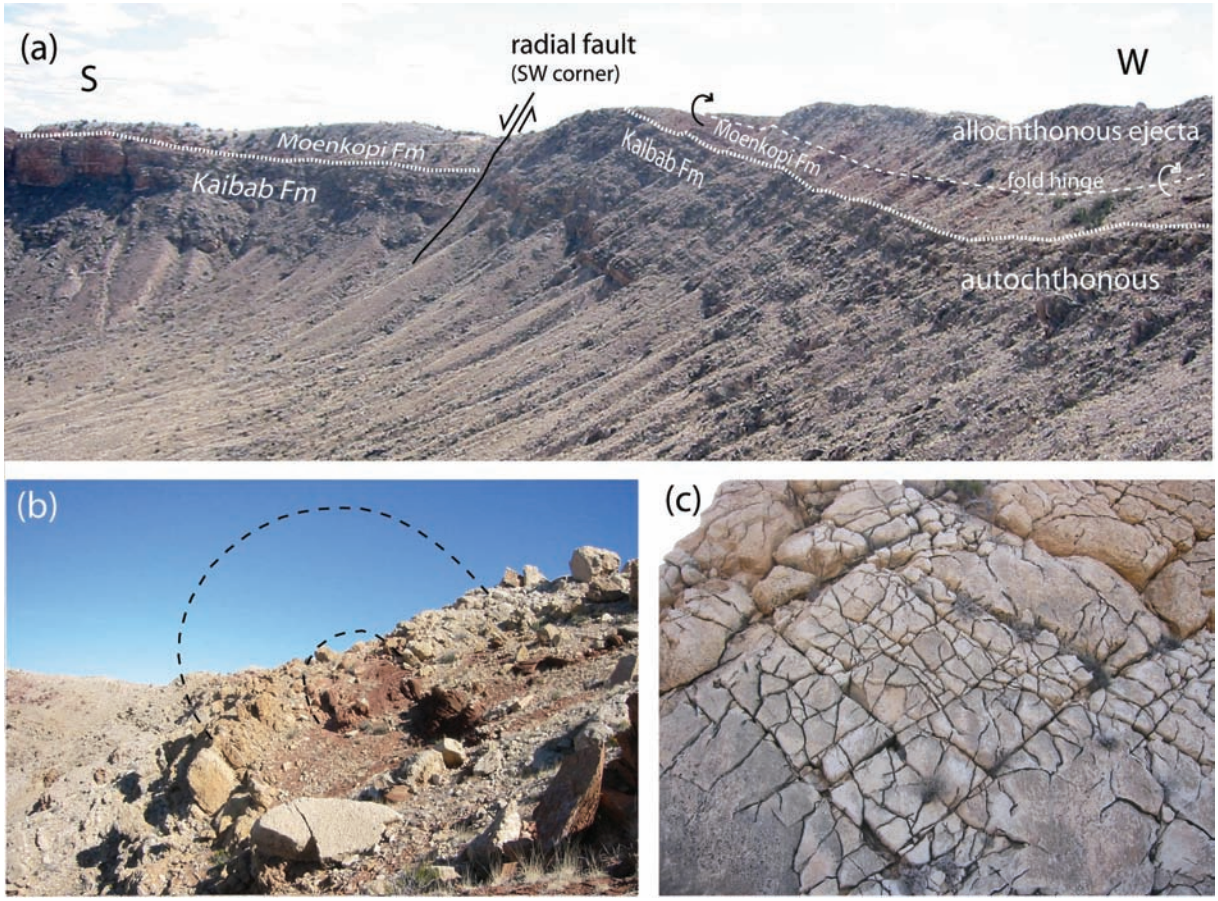

Figure 3: Field observations. a) Displacement of bedding by a radial corner fault. To the right one can see the beginning of the interthrust wedge at Barringer Point. b) Hinge zone and overturned flap, showing Kaibab alpha and Moenkopi beds. c) Orthogonal joint sets seen on the surface of “House Block”, an ejected Kaibab block on the east rim. Photo size is roughly 2x3 m.

We particularly focused our measurements on a single stratigraphic horizon, the contact bedding plane of the Kaibab and Moenkopi formations, which can be easily traced in the field (122 data values). Tracing this marker horizon allows differential rim uplift to be quantified. Due to differential uplift and erosion of the rim, parts of the highest strata and overturned flap are missing, particularly in the SE sector.

The GPS altitude data of the Kaibab-Moenkopi contact proved to be unreliable. To compensate, we used a georeferenced topographic map of the crater (as presented on the current USGS 7.5 minute quadrangle for Meteor Crater) in combination with the much more precise latitude and longitude GPS data to derive the altitude of our measurements. For these values we estimate an error of ±5 m altitude.

The Coconino-Kaibab contact was analyzed by combining the geological map compiled by Shoemaker [1960] with the topographic map of the crater for a more detailed overview of uplift. We estimate an error of ±10 m.

2. Conversion from a geographic to an azimuthal reference scheme – the concept of "concentric deviation"

For analysis of the strike data, methods were applied that have been developed in Poelchau and Kenkmann [2008], and we refer to that paper for a more comprehensive description. First, the position of each measurement was converted from its original geographic reference system to its azimuth based on the crater center, giving angular values from 0 to 360° (90° = east, Fig. 4). In a second step, the orientation of strike relative to the crater center was determined and given an angular value that we refer to as "concentric deviation" (Fig. 3). Strike that is tangential to a hypothetical circle around the crater center is defined as "concentric" and has a concentric deviation value of 0°. Strike that is rotated clockwise relative to the circle has positive concentric deviation values, while counterclockwise rotation produces negative values.

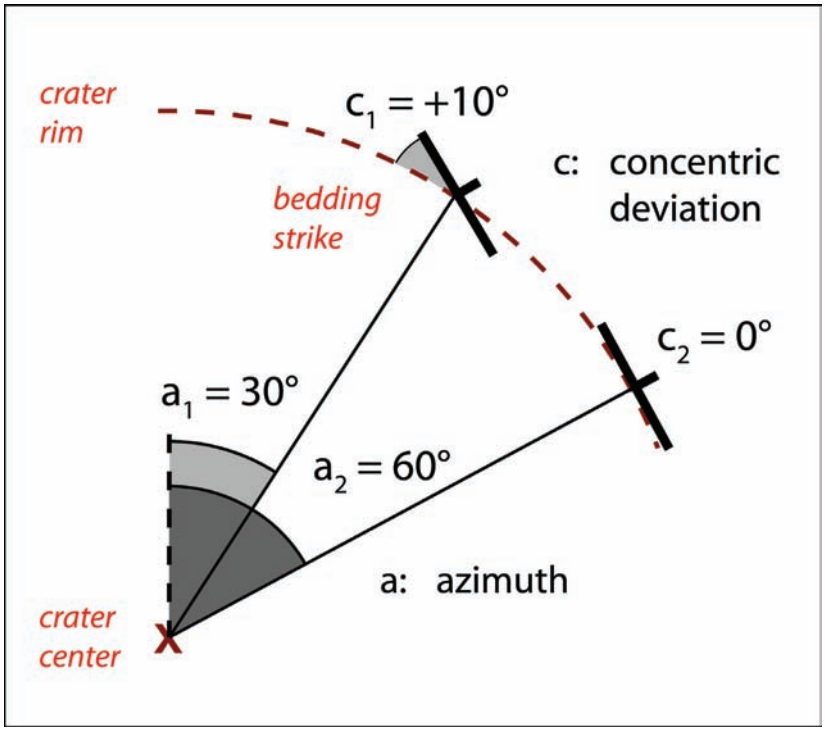

Figure 4: Determination of the azimuth and concentric deviation from the strike and location of bedding. The azimuth is the position of a measurement relative to the crater center, ranging from 0 to 360°. Concentric deviation defines the orientation of strike relative to the crater center, with concentric strike lying tangential to a hypothetical circle (dashed curve) around the crater center. Concentric deviation ranges from –90 to +90°; positive values indicate clockwise rotation.

3. Statistical treatment – the "overlapping bins" method

When concentric deviation is plotted against its azimuth in an x-y plot (e.g. Fig. 5), a large amount of scattering is displayed that requires smoothing for a better interpretation. We use the "overlapping bins" method, in which the arithmetic average of all concentric deviation

values in a defined azimuthal range, or "bin" (e.g. 0 to 30°) is calculated. This bin is then rotated by 10° and the average of all values in the bin is calculated again (e.g. 10 to 40°), and so on for each step, resulting in 36 smoothed concentric deviation values. For a better sense of spatial relationship, the data is also displayed in polar plots, showing the azimuth in "map view" and using the radial distance from the center of the plot to quantify the concentric deviation (Fig. 5).

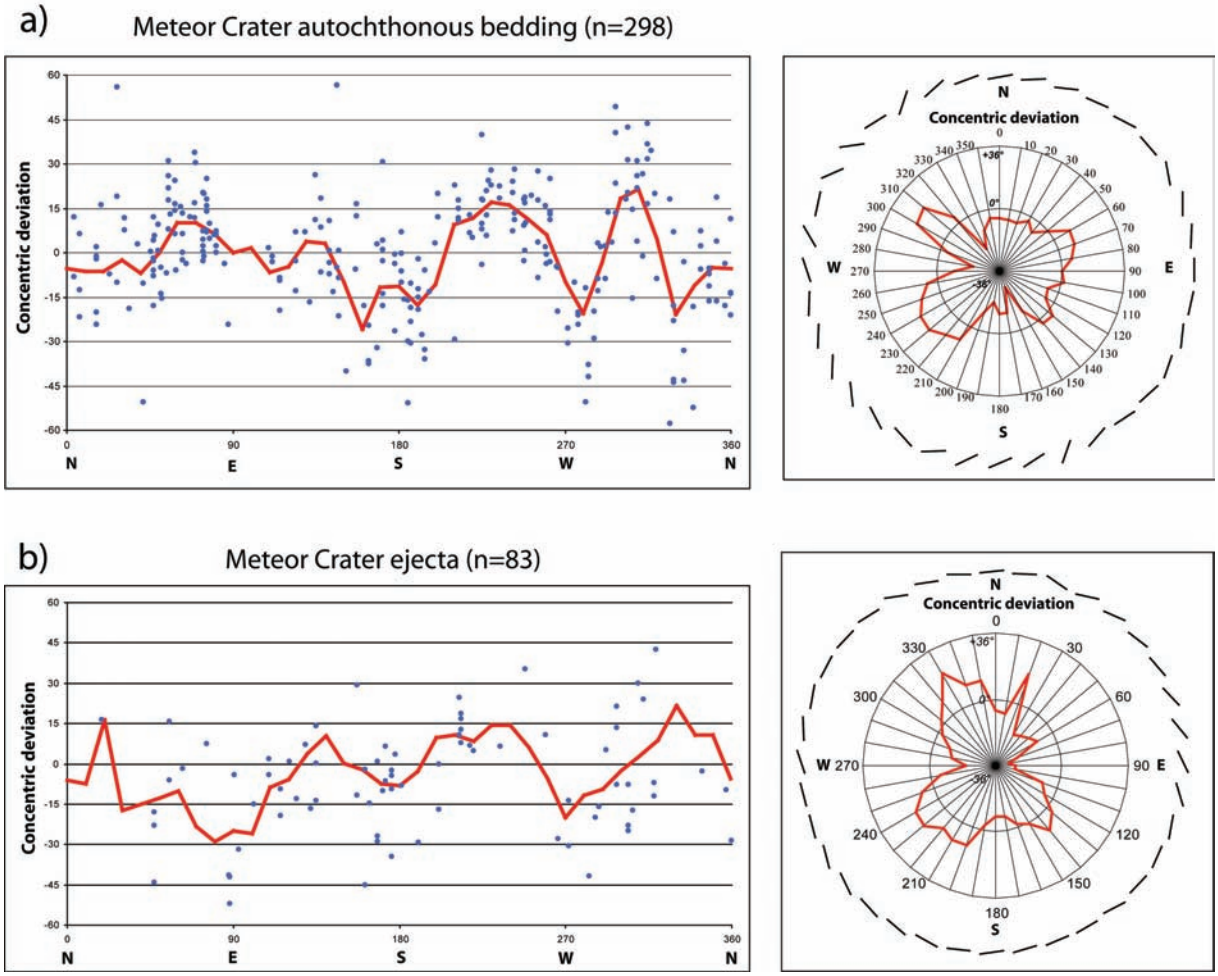

Figure 5: Deviation of bedding planes from concentric strike plotted against its azimuth, displayed in x-y-plots (left) and polar plots (right). Positive values quantify clockwise rotation of bedding strike (and vice versa). The curve displays data smoothed with the overlapping bins method (bin size 20°, step size 10°). The deviation from concentric strike can be most intuitively observed in the strike bars of the polar plots on the right, as seen in "map view". Strike bar orientation is exaggerated by a factor of two. The plots show that strike does not directly reflect the outline of the crater (compare Fig. 4), but infers more complex internal structural features of faulting and folding.

Results I: Strata orientation, joints, faults and uplift in Meteor Crater

1. Bedding data

For the display in a stereographic projection (stereo plot), the normal, autochthonous bedding data set was split into crater corners and sides, based on its square shape (Fig. 6). The data show four clusters of surface normals, or bedding plane poles, reflecting the four sides of the crater wall that accentuate the square shape of the crater. The N and S sides have more concentrated poles, compared to the more scattered E and W sides. This indicates rotation in the E and W sides. The S side dips more gently on average (the poles of bedding planes are nearer to the center of the projection) than the E and W sides, while the N side has the steepest dip. The NE and NW corners are more concentrated, while the SE and SW corners show strong scattering and rotation.

Although we believe that the data displayed in the stereographic projection directly reflects faulting and differential uplift in the crater, variations of the pole distributions in the stereo plot, e.g. the relatively flat lying south crater side, may in part be attributed to erosional effects. The steepest bedding is found in the hinge of the overturned flap (Fig. 3b). When this is removed by erosion, flatter surfaces remain. Also, care must be taken in interpreting stereo plots as certain areas of the crater can be over or underrepresented during sampling. Nonetheless, bedding data reveal non-radial behavior that is more complex than simple, square-shaped deviation. The structural and tectonic factors that we believe control this complex, non-radial behavior are discussed below.

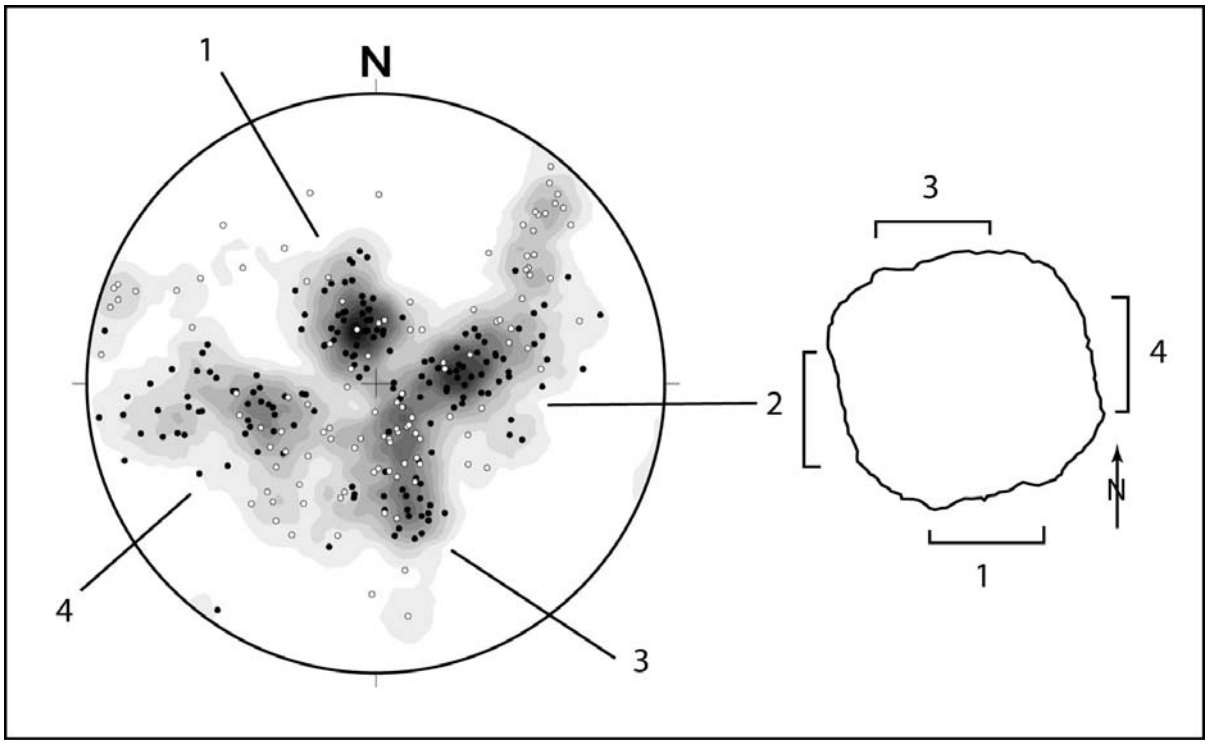

Figure 6: Stereographic projection (stereo plot) of 298 autochthonous bedding poles. White: corners; black: sides. Points represent surface normals (e.g. data from the S wall (“1”) is displayed in the N part of the plot). The sides of the crater are focused in four clusters that show differing amounts of scattering, indicating structural complexities beyond a simple, square-shaped deviation.

2. Concentric deviation

Reflecting the results displayed in the stereo plot above, the concentric deviation data of the autochthonous inner wall of Meteor Crater also show dispersions from radial symmetry, which appear to be stronger in the western half (Fig. 5a). The ejecta bedding data (Fig. 5b) was not sampled in a large enough quantity to be statistically meaningful, but still show the same rough trends apparent in the autochthonous data.

As opposed to stereo plots, concentric deviation diagrams allow a more detailed look into the bedding behavior relative to its azimuthal location in the crater wall. As can be seen in the polar plots, the orientation of strike does not directly reflect the square shape of the crater, but shows more complex rotation. This indicates an influence of faulting and folding that has deformed the crater wall and determined non-radial and non-squared shape orientation not only of bedding in the crater wall but also of the ejected material on top of it. The relationship between strike behavior to structural features is discussed in more detail in section “5. Uplift”.

3. Joints and radial faults in the crater corners

Joint sets form structurally weak zones along which vertical faults have propagated during crater formation. Two dominant joint orientations were recognized by Shoemaker [1960] and later quantified by Roddy [1978]. Roddy’s work was based largely on aerial photography and only to a small degree on field measurements. Nonetheless, his results suggest a strong correlation between the diagonals of the crater’s square shape and the average orientation of joints (Fig. 7). We were also able to observe small-scale orthogonal joints in rock units in the field (Fig. 3c). For a more recent, detailed study on joint sets and fractures in Meteor Crater, see Kumar and Kring [2008].

Vertical displacement of beds along faults in the crater wall is most strongly expressed in the four corners of the crater (Fig. 3a, 8a, b). Apparently these faults have utilized the two main vertical zones of weakness that the joint sets form. Shoemaker and Kieffer [1978] introduced the term “tear faults” to describe these faults. This term is a misnomer in the context of Meteor Crater. In conventional tectonics, tear faults are vertically oriented fault planes that occur perpendicular to the direction of deformation and are caused by differential amounts of displacement. In such a tectonic situation, the displacement is mainly lateral or strike-slip, with only minor vertical movement [Twiss and Moores, 1992]. At Meteor Crater we replace the term “tear faults” with “radial corner faults” as a purely descriptive term to express differential movement between blocks that occurred during rim uplift. The main component of movement displayed by these faults is vertical along with a rotational component or “scissors type of displacement” [Shoemaker, 1960] that tips the blocks outwards.

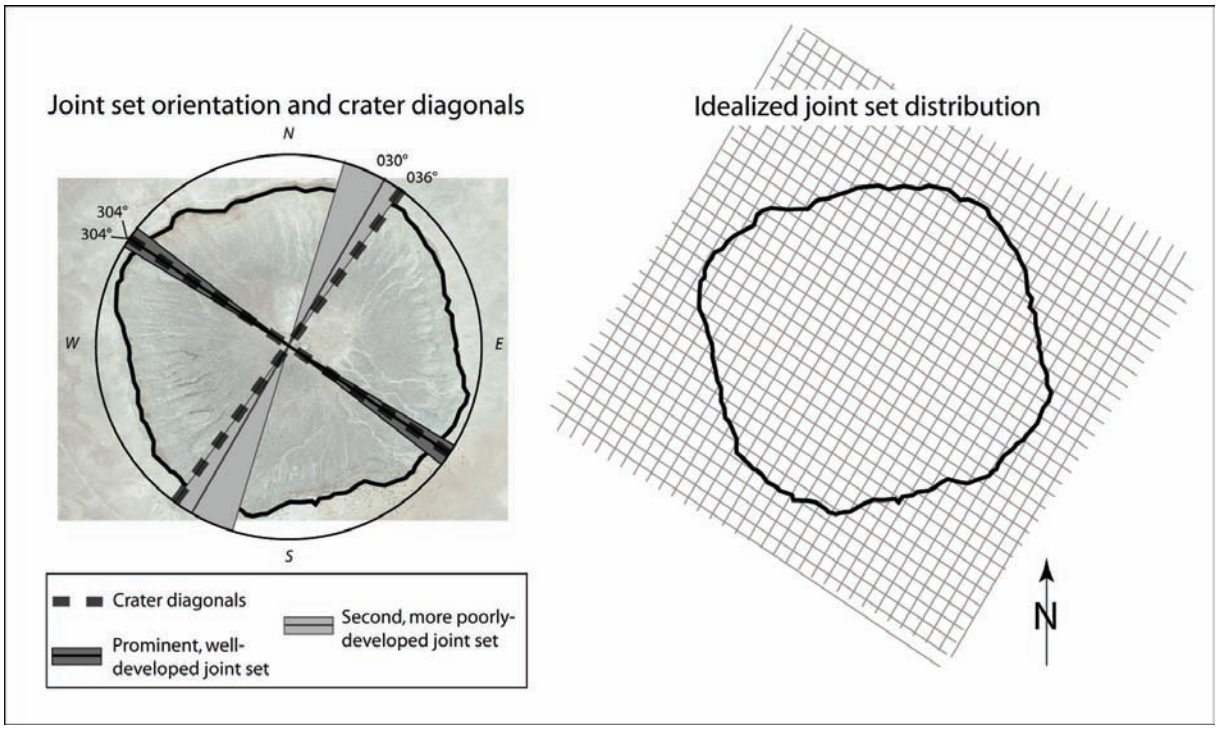

Figure 7: Field data from Roddy [1978] show a striking correlation between crater diagonals and the orientation of joint sets. The azimuth of the crater diagonals (36°; 304°) coincide with the average of joint sets measured in the crater and estimated in aerial photographs (30°; 304°). These joints have a spacing ranging between 0.5-10 m and have subdivided the target into small, square-shaped units.

The kinematics of the radial corner faults is comparable to mode III shear fractures. The main component of motion in these shear fractures is a sliding motion parallel to the fracture edge. In comparison, mode II shear fractures have a sliding motion perpendicular to the fracture edge, and mode I fractures are extensional [Twiss and Moores, 1992].

In Meteor Crater, radial corner faults displace rock beds by several decameters (Fig. 3a, 8b). Maximum displacement of ~45 m occurs along the SE radial corner fault, which cuts through all visible layers including the ejecta and exposes the largest segment of Coconino in the crater wall.

4. Interthrust wedges

Features that we have termed „interthrust wedges“ can be observed in the inner crater walls. They are isolated, horizontal, lensoid bodies of coherent strata that are terminated by faults on all sides and lead to a repetition of strata in the wall. While the base of the wedges is usually stratiform, the hanging wall contact shows unconformities. The outward extent of the lensoid bodies is undetermined, but it is expected that they also have a wedge shape in cross section. Shoemaker [1960] and Shoemaker and Kieffer [1974] first described these features, which they termed “thrust faults”, in the north and west sectors of the crater. They can also be observed in the south wall and in the SW corner (Fig. 8a).

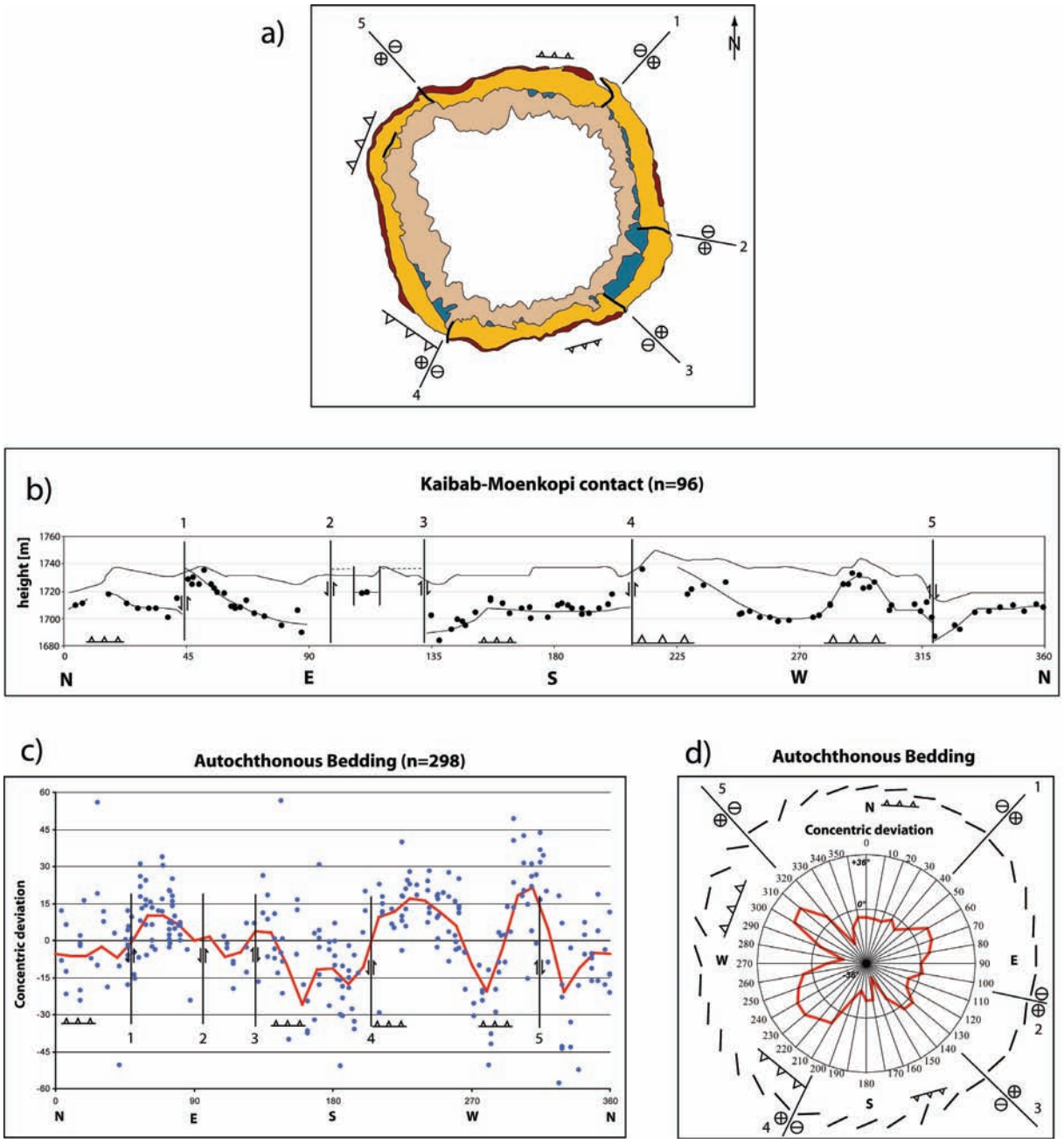

Figure 8: Structural control of bedding behavior. a) Simplified sketch of the main structural features, radial corner faults and interthrust wedges, in the crater wall. See Figure 1 for legend. b) The geological contact of the two highest units in the crater wall was measured with GPS. The elevation is plotted against the azimuth, giving a simplified profile with the topography of the rim (continuous bold line) and structural features. The trend lines of the data points are additionally based on field observations. Vertical exaggeration ~5x, estimated error is ±5 m. c & d) Deviation of concentric strike plotted against its azimuth, displayed in an x-y-plot (left) and polar plot with bars of average strike (right). Positive values quantify clockwise rotation of bedding strike (and vice versa). The curve displays data smoothed with the overlapping bins method (bin size 20°, step size 10°). The concentric deviation of bedding directly reflects the internal structure of the crater wall. The best example can be seen at 290°, where an interthrust wedge folds beds and creates an anticline at Barringer Point, causing the bedding strike to rotate. The rotation of strike bars in d) is exaggerated by a factor of 3.

We prefer the term interthrust wedges to thrust faults, as thrust faults incompletely describe the situation observed. While thrusting plays a major role in this process, the process is actually the injection of a wedge of bedrock between two rock layers, therefore resulting in a lower, crater-outward directed thrust at the bottom of the wedge, and an upper, crater-inward directed thrust bordering on top of the wedge.

Kenkmann and Ivanov [2006] have shown that weak spallation by interference of shock and release waves near the target surface leads to decoupling of the uppermost target layers in the early cratering stage. We expect that the wedges exploit these horizontal zones of weakness in the layering of rock beds. Thin interbeds of clay-siltstone in the Moenkopi Formation and marl beds in the Kaibab Formation are soft layers and preferential sites for displacements and rock decoupling.

The wedges have an effect on uplift. Where they occur, the top Kaibab and Moenkopi units are arched up and form anticlinal features, best represented by “Barringer Point” in the NW (Figs. 8a, b). Interthrust wedges only appear to occur in Kaibab. This observation may be due to the fact that Kaibab is the main unit exposed in the crater walls. However, it seems plausible that interthrust wedges occur at a level where overburden is low, utilizing weaker marl interbeds, thus allowing layers to be bent upwards in the formation process. A detailed model describing the injection and uplift is introduced below. Whereas at Barringer point we see a lensoid type termination of the sides of the interthrust wedge bodies, near the museum complex at the northern crater wall the eastern limb of a box fold is exposed that terminates an interthrust wedge.

5. Differential uplift

The rim of the crater stands around 50 m on average above the surrounding surface. This is caused mainly by bedrock uplift and partially by the thickness of the overturned ejecta flap. Differences in rim elevation between the highest point of the rim crest in the SW corner at ~1750 m and the lowest point in the NW at ~1716 m are connected to the structural features described above, which control differential uplift of the bedrock in the crater wall. The orientation of the radial corner faults and interthrust wedges in the crater are sketched out in a simplified structural map in Figure 8a, showing a tendency for both features to be located in or near the four corners of the crater.

As described in the methods section, the elevation of both the Kaibab-Moenkopi (KM) contact and the lower Coconino-Kaibab (CK) contact were measured for a better control of differential uplift in the crater wall. Average height of the CK contact where exposed within the crater is ~1645 m. Maximum elevation of the CK contact is higher in the corners of the crater (>1670 m) than along the sides (~1640 m). The pre-impact CK contact was located at ~1590 m elevation, based on an average thickness of overlying strata of 90 m and an average surface elevation of 1680 m outside of the crater [e.g. Kring, 2007]. Therefore, actual uplift of

the CK contact ranges from less than 40 m on the sides to a maximum of 80 ±10 m in the corners.

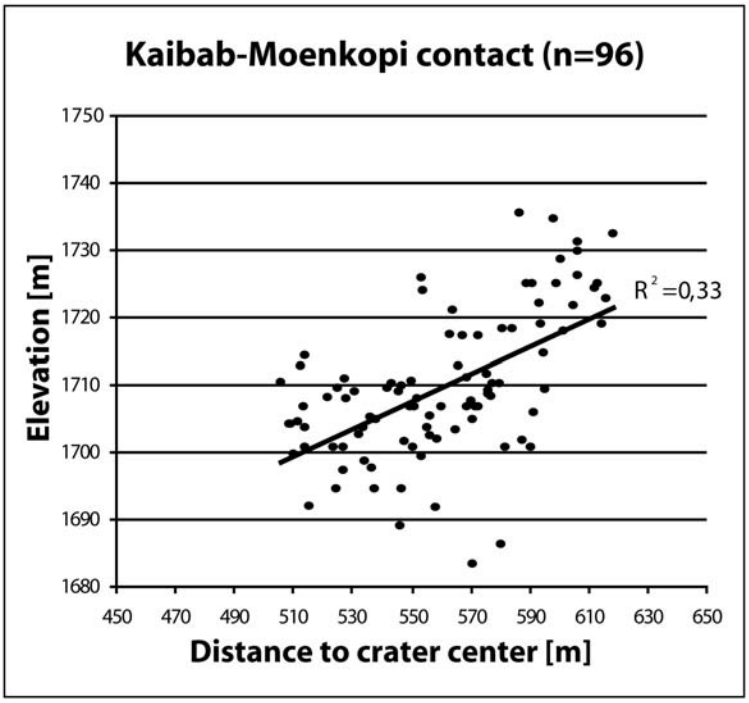

Figure 9: Elevation of the Kaibab-Moenkopi contact plotted against its radial distance from the crater center, based on GPS measurement. A rough trend can be seen for higher uplift to occur further away from the crater center.

Results from the KM contact are plotted as a profile in Figure 8b together with the main structural elements and topography of the rim. It becomes apparent how directly bedding elevation is controlled by radial corner faults and interthrust wedges. For example, in the NW at 320°, movement of the radial corner fault (5, Fig. 8b) has resulted in one of the lowest portions of the KM contact at 1690 m elevation, which is directly reflected as the lowest point in the topography of the rim crest (~1716 m). Slightly to the SW, the interthrust wedge at Barringer Point (290°) has uplifted the KM contact to 1730 m altitude and created a local topographical peak of 1744 m height. Based on a pre-impact elevation of the KM contact at 1670 m, measurable differential uplift ranges from 15 to 65 m (Fig. 8b, 9) and can be presumed to be over 70 m in eroded parts of the crater rim.

Differential uplift is also reflected in the concentric deviation data of the upper rim (Fig 8c,d). The interthrust wedge at Barringer Point created an anticline, folding strata outwards on either side and thus rotating the strike of bedding planes around this feature (best observed in the strike bars of the polar plot in Figure 8d). In the SW a combination of an interthrust wedge and a radial corner fault has led to a “slope” with a NW component of dip, which can be seen in the clockwise rotation of strike in this area.

In the x-y-plot in Figure 9, a trend can be seen for the KM contact to be in a higher position the further away it is from the crater center. This means that higher elevations are located in the corners of the quadrangular crater. The possibility that uplift, interthrust wedges and radial corner faults, and their concentration in the corners of the crater are interlinked is debated in the "Synthesis of data" section.

Results II: Data relevant to determining an impact direction

In this section we present and review different datasets that provide indications of an impact direction.

1. Deviation of strike from concentric orientation

The concept of the two corners model is described in the introduction and in Poelchau and Kenkmann [2008]. When compared to the two corners model rotated for a best fit, the concentric deviation data from the proximal ejecta and overturned flap of Meteor Crater show a rough fit that coincides with a direction of impact from the NNW at 330° (Fig. 10). Due mainly to erosion of the rim, the quality of this dataset is poorer than the autochthonous dataset, and parts of the concentric deviation curve are insufficiently supported by outcrop measurements. We are apparently close to the limit of detection for any oblique signatures in this dataset. Furthermore, target heterogeneity effects presented in Results I are not accounted for in the phenomenological two corners model.

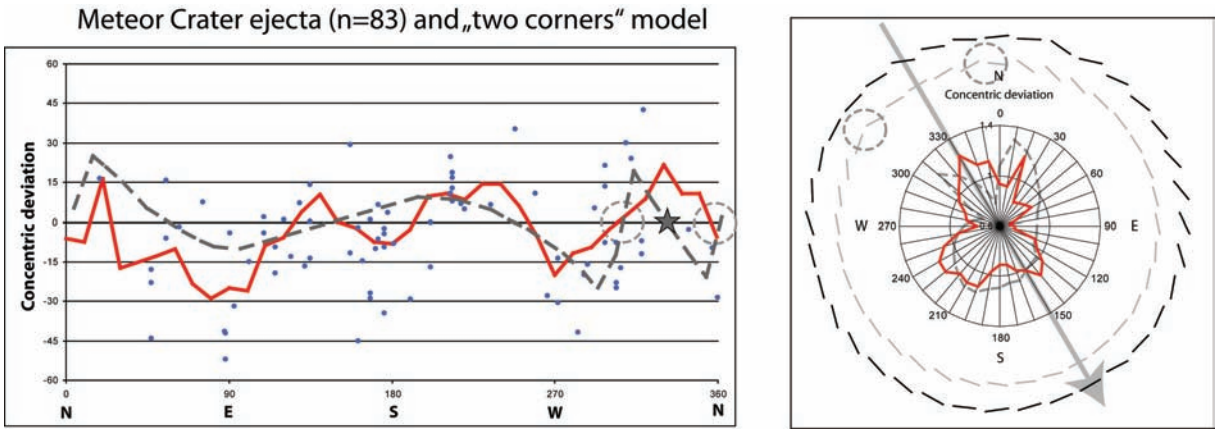

Figure 10: Analysis of possible obliquity of Meteor Crater. Concentric deviation data of Meteor Crater ejecta is plotted against its azimuth. Data was smoothed with the overlapping bins method (bin size 40°, step size 10°; solid curve). Data show a very rough correlation to the curve of the two corners model (dashed curve) with NNW orientation. The abrupt changes in the two corners model-curve from negative to positive concentric deviation values represent the two corners (dashed circles; compare also Fig. 2); the star marks the uprange direction of the model, the grey arrow marks the direction of impact.

2. Bedding dip and differential uplift

The stereographic projection (Fig. 4) of autochthonous bedding data shows a bilaterally symmetric pattern with a symmetric axis running NNW-SSE. While the E and W crater walls display comparable dip values, the N crater wall shows steeper dip data than the S crater wall. The symmetry plane may correlate with the trajectory axis in an oblique impact scenario. Steeper rim inclination would be expected in the uprange sector. Also, differential uplift (Fig. 8b) appears to be highest in the SE corner of the crater, where much of the KM contact has been eroded away. This may be an indicator for a downrange directed component of horizontal momentum from the impactor that could cause stronger uplift and deformation compared to the uprange sector.

3. Canyon Diablo Meteorite distribution

The distribution of the Canyon Diablo Meteorite around the crater was compiled by Barringer [1909] and is presented as a map in Figure 1a. Distal meteoritic material can be found predominantly in the SE and SW sectors to a distance of 6.5 km, including numerous specimens heavier than 5 kg. The NE sector has less distal material, reaching only to about 5 km and consisting of material under 5 kg, while distal meteorites in the NW can only be found as far as 3 km from the crater. It is notable that the N lacks any meteorites over 5 kg beyond a 1.5 km radius, while they can be found in the S, E and W at three times that distance. Erosion certainly plays a role in the distribution of the smaller fragments. Grant & Schultz [1993] estimate 1 m average vertical erosion over the bulk of the ejecta located outside of the steep, proximal rim, at ranges of 0.25-0.5 crater radii, or 125-250 m from the rim. It is questionable though how strongly the distribution of the heavier fragments is affected by erosion.

It is possible that the stronger concentration in the S reflects a direction of impact from the N, which would support the impact direction derived with the two corners model. On the other hand, the more proximal distribution of the Canyon Diablo meteorite shows a strong concentration of both heavy and light meteoritic mass in the NE sector of the crater up to a distance of 1 km (Fig. 1a). This has led previous workers [e.g. Nininger, 1956; Rinehart, 1958] to propose a projectile coming from the SW. It should be stressed though, that the distribution of the distal, not proximal, ejecta is the strongest indicator for impact trajectories on other planetary bodies.

4. Ejecta blanket

The ejecta blanket was drilled at several locations and results were published in Roddy et al. [1975]. Based on the data the “approximate end of the overturned flap in drill holes” was estimated, which is interpreted as the lateral extent of the ejecta blanket, averaging at around 1.5 km distance from the crater center (Fig. 1b). Based on this sketch, there is no observable offset pattern or forbidden zone that would infer an impact direction as described, for example, by Herrick & Hessen [2006] in ejecta blankets on Mars. The boreholes do reveal that on average the blanket is thicker in the S than in the N, which would support an impactor coming from the NNW. Ejected Coconino is found mainly in the S part of the blanket, and is missing in the W. Additionally, Barringer [1909] reports finding the deepest stratigraphic units of the Coconino sandstone in the SE ejecta, which would additionally support an impactor from the NNW, but this has not been confirmed by other workers.

5. Discussion of impact direction

Our analysis of bedding orientation of the proximal ejecta with the two corners model suggests an impactor coming from the NNW, which is supported by non-radial behavior seen in differential uplift, bilateral symmetry in the stereographic projection of bedding, distal distribution of meteoritic material, and ejecta blanket thickness. The proximal distribution of meteoritic material may contradict the NNW trajectory, while the lateral extent of the ejecta blanket appears to give no indication of the impact direction. One must also consider the possibility that the impactor could have struck at a high angle relative to the horizon, excluding any measurable horizontal components capable of inferring the direction of impact. The bedding dataset used for the determination of an impact direction may be too small to give a fit to the two corners model, even though our suggested direction coincides with other factors that lead to speculation on the impact direction. Additionally, there is always the problem of noise obscuring the patterns we are searching for, but, as explored in Results I, we discovered that faulting and folding in the crater wall have a much stronger control on the deformation of bedding and strike orientation than the diluted, oblique signals we were originally searching for.

Synthesis of data

We discuss the indications our results have on rim uplift and crater shape, and the effects that an oblique angle of impact and target heterogeneities have on the cratering process.

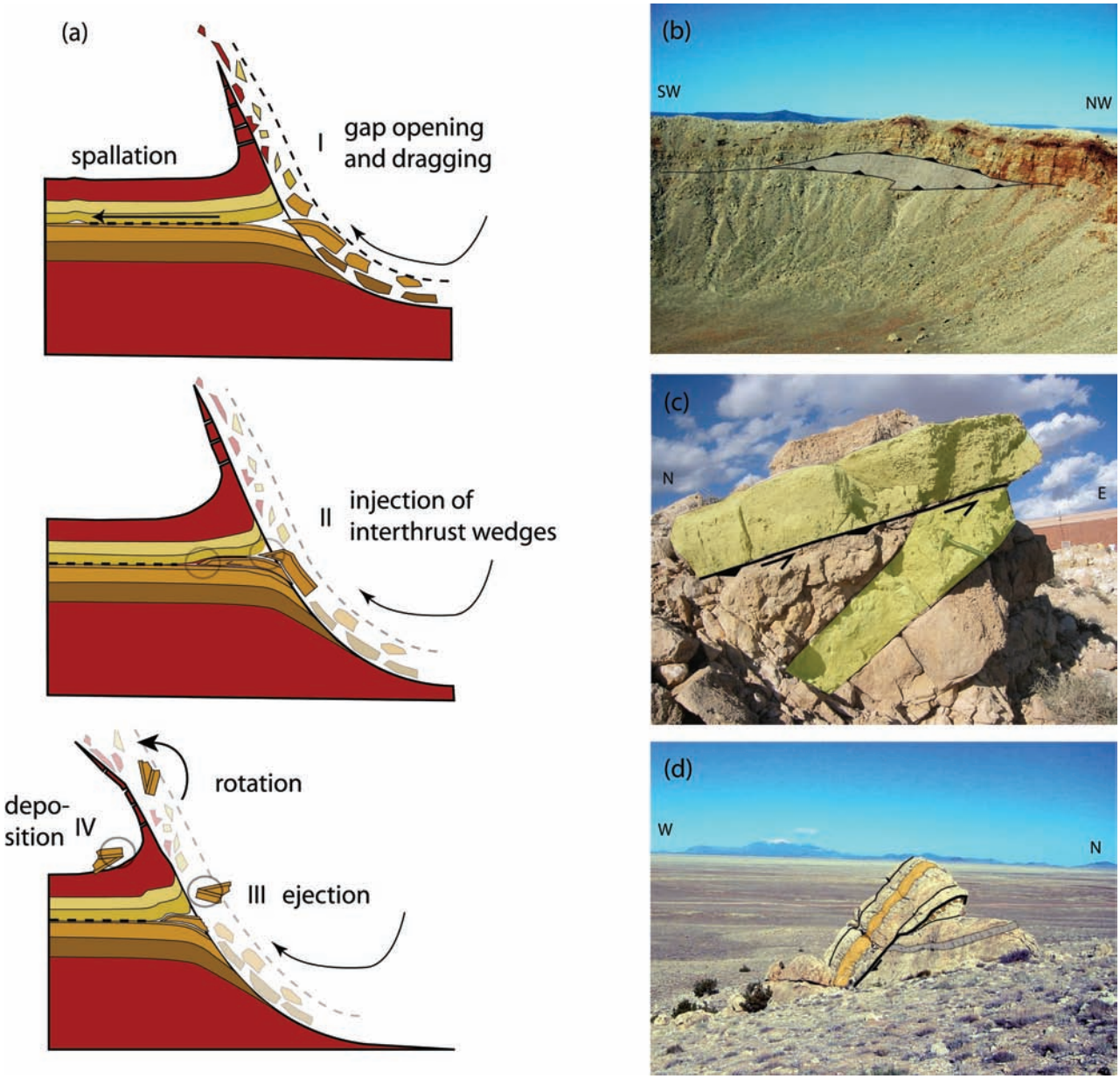

Figure 11: Field observations and a mechanism for the formation of “interthrust wedges”. a) Four stages of the interthrust wedge formation. I) After spallation induces horizontal zones of weakness, small gaps are formed during the excavation process while thrust ramp are formed in rock beds. II) Wedges of rock are thrust outward into the crater wall, warping up overlying beds. III) Some of the thrust ramps formed are ejected during crater excavation, while others remain embedded in the crater wall as interthrust wedges. IV) The ejected incipient thrust ramps are deposited as ejecta. b) Barringer Point, one of the most prominent topographical peaks at Meteor Crater, is caused by an interthrust wedge that has folded the top beds in an anticline. c) An incipient thrust ramp of an interthrust wedge found in Kaibab ejecta near the museum complex, showing obliquely terminating bedding planes and an inferred direction of movement. The upper rock unit is ~3 m wide. d) Whale Rock in the W of the crater, another possible ejected thrust ramp of an interthrust wedge.

1. A mechanism of rim uplift formation

The emplacement of interthrust wedges is a mechanism of rim thickening and uplift (Fig. 11a). This is documented in Figure 8b and leads to anticlinal doming above interthrust wedges, e.g. at Barringer Point (Fig. 11b). Certain ejected Kaibab boulders found on the crater rim (Fig. 11 c, d) provide an important observation that is relevant to understanding the formation of interthrust wedges. Within a single block two Kaibab beds are in 30° contact and have a brecciated unconformity plane which is most likely a fault plane. As no thrust ramps can be expected from the regional, pre-impact geological context, we interpret these as ejected thrust ramps formed during the emplacement of the interthrust wedges.

Based on these observations, we propose a model for the formation and excavation of interthrust wedges (Fig. 11a). We assume that during the cratering process, spallation delaminates horizontal areas of weakness in upper stratigraphic units along bedding planes, e.g. clayey interbeds [Kenkmann and Ivanov, 2006], then outward and upward directed excavation flow opens small gaps along these weakened zones (Fig. 11a-I), which are exploited by the tips of incipient interthrust wedges (II). Further thrusting of these wedges into the gaps creates additional uplift, raising overlying units to a higher elevation than neighboring beds. As the transient crater continues to grow, the early stage interthrust wedges get incorporated in to the excavation flow (III) and are deposited as ejecta boulders (IV). Rim uplift by this mechanism appears to be specifically active near the radial corner faults.

2. A model of formation of quadrangular crater shapes

In an attempt to understand the mechanical processes behind the formation of the square shape of Meteor Crater, we suggest a simplified, qualitative model that compares surface stress to the excavation force exerted on rock units (Fig. 12). In this model we divide the target rock into discrete cubes, based on the two joint sets, plus horizontal layering planes. During cratering, the excavation flow field that ejects rock is directed outward and upward in the upper part of the crater. For simplification, we assume the flow field is oriented radially from the crater center and upwards at 45°. We can observe two situations in this model, one where the flow field is directed parallel to one of the joint sets (Fig. 12-1), and one which is directed at a 45° angle to both joint sets (Fig. 12-2). The flow field exerts a force on the cube, which is proportional to the exposed surface of the cube, thus resulting in a force that is 1.41 times stronger in 2. The force is calculated as the surface area component that is orthogonal to the flow field. While the cube is cut in half along its diagonal for a better overview in Figure 12-2, the surface area component orthogonal to the flow field remains the same for a complete cube. This force can be split into horizontal and vertical components that correspond to normal stress (σ_x, σ_y) and shear stress (τ_z), respectively. Vector addition (Fig. 12) shows that the ratio of normal stress to shear stress in situation 1 is $\sigma_y : \tau_z = 1$. In situation 2 the ratio is $(\sigma_x + \sigma_y) : \tau_z = \sqrt{2}$, due to the larger surface area exposed to the flow field and the

circumstance that shear stress is exerted on two surfaces of the cube (marked in gray in Figure 12-2), as opposed to one surface in situation 1. As less shear stress is resolved in situation 1, excavation should progress faster and further, and the initial circular crater shape should start developing corners, resulting in the final square shape seen in Meteor Crater. Interestingly, the crater radius in the corners of a square is $\sqrt{2}$ times larger than perpendicular to the sides. It should be noted that target anisotropies such as joints become important mainly in the final stages of crater excavation, when the stresses induced by the excavation flow are in the order of the strength of the target material. We discuss this further in the crater hinge model below.

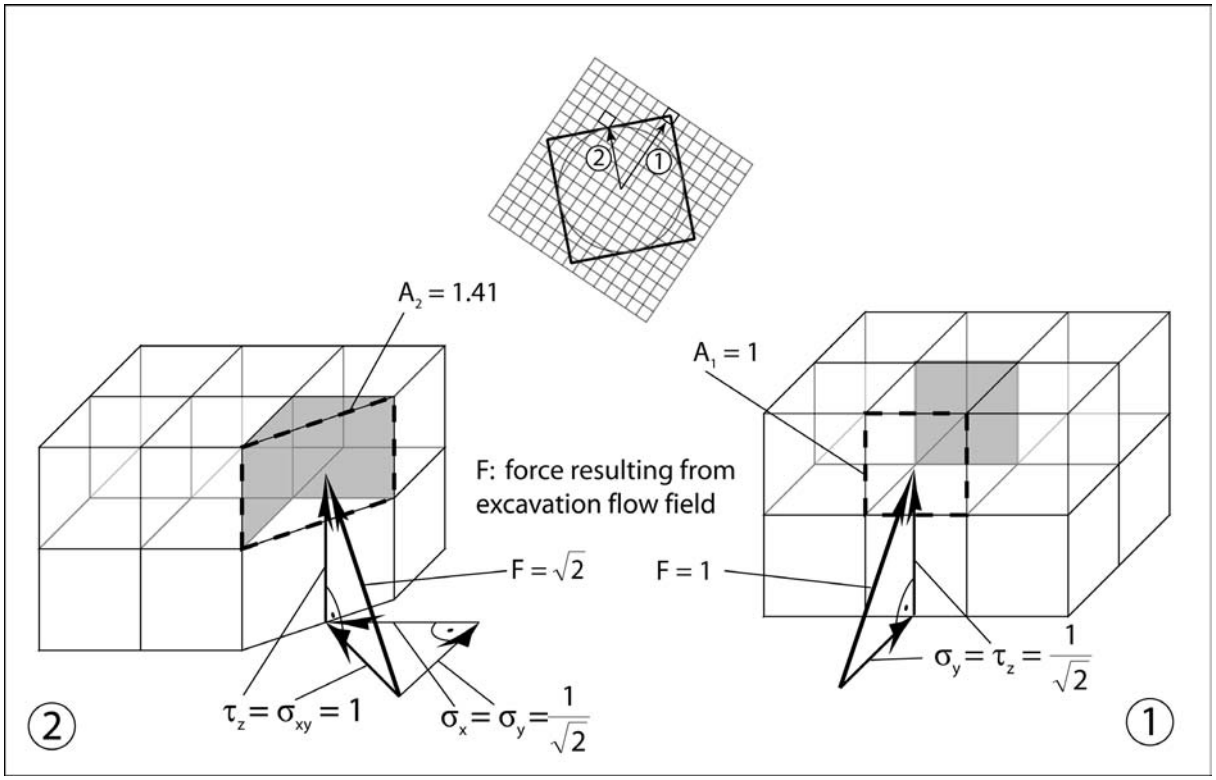

Figure 12: A simplified model correlating joint sets and bedding planes with crater formation. 1 and 2 represent blocks during crater excavation oriented parallel (1) or at a 45° angle (2) to excavation flow. While the force of the excavation flow exerted on 2 is $\sqrt{2}$ times stronger than on 1 due to the exposed surface (dashed line), the shear stress exerted on the back of the cube (grey area) is twice as strong in 2 compared to 1. This results in more effective crater excavation parallel to the joint sets (1), forming a square shaped crater. See text for details.

3. Differential rim uplift in quadrangular craters

Figure 8b shows that differential rim uplift is affected by the formation of interthrust wedges and is also controlled by the radial corner faults. There is a rough spatial relation of radial corner faults and interthrust wedges that suggests a connection between the two. Figure 13 illustrates how both mechanisms could be interconnected and controlled by the quadrangular crater shape.

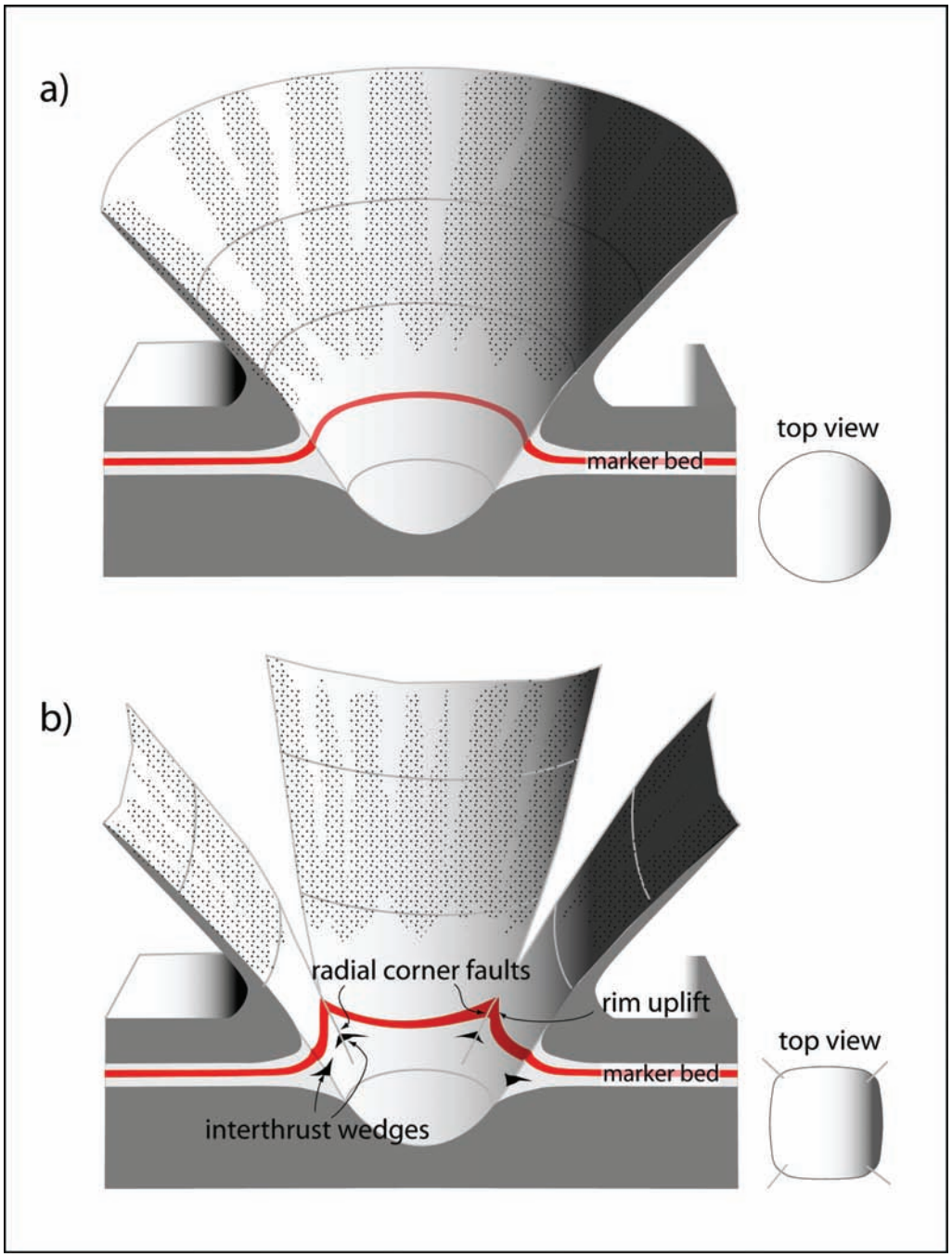

Figure 13. The crater hinge model contrast two scenarios: a) a homogenous target resulting in a circular crater shape and b) a target with perpendicular zones of weakness, resulting in a structurally complex, quadrangular crater with stronger rim uplift in the corners, as shown by the marker bed. The resulting geometry in b) must be compensated by the formation of radial corner faults and interthrust wedges.

The ejection is more effective parallel to joints and the crater grows faster within the corners of the crater, as demonstrated in the previous section. As an example, the marker bed is originally uniform in Figure 13a, and is uplifted further in the corners of the crater in Figure 13b, as the excavation is $\sqrt{2}$ times more effective. If the marker bed remains coherent and

intact, this flow would create marker bed highs in the corners. This fits perfectly to Figure 9, in which the correlation of uplift and radial distance of a marker bed is plotted. The model only works if the strata remain coherent. This describes only the late cratering stages, when the stresses induced by the excavation flow are in the same order of magnitude as the strength of the rocks involved. As the uplift is enhanced in and near the crater corners, these are also likely sites where gaps parallel to weak interbeds open that could subsequently be filled by interthrust wedges. The accentuation of the square crater shape is a process that is induced by the more effective excavation flow parallel to the joints. Once this process is initiated this facilitates the formation of straight fold hinges of the overturned flap parallel to the crater walls, as can be observed at Meteor Crater (Fig. 3a). In contrast, concentrically striking fold hinges require the tensile breakup of the ejected rock in the overturned limbs.

Conclusions

We present a comprehensive dataset of bedding strike and dip combined with positional data based on GPS measurements for Meteor Crater. Application of a method devised in Poelchau and Kenkmann [2008] to infer an impact direction from bedding data, in combination with data on the spatial extent of the ejecta blanket and distribution of meteoritic material, did not lead to unambiguous results for an impact direction, due in part to a weak database of sampled ejecta. Although a projectile coming from the NNE is suggested from the data, the orientation of bedding is more strongly controlled by (1) pre-impact joint sets resulting in radial corner faults and (2) horizontal weaknesses in the planes of rock strata that are exploited by anticlinal interthrust wedges; thus, any weaker signals of an impact direction appear to be concealed and superimposed by these features. The complete dataset enables us to quantify differential uplift, folding, faulting and rotation of specific areas of the crater wall and display an azimuthal profile of the crater wall.

Structures in ejected boulders were observed that were interpreted as ejected remnants of incipient ramp thrusts, leading to the formulation of a model describing the process of rim uplift by interthrust wedge formation. This model postulates interthrust wedge formation as an ongoing process of crater excavation with coherent rock material being thrust into the crater wall, only to be ejected shortly afterwards.

In our second model, a comparison of surfaces stress to the excavation force exerted on arbitrarily defined rock units parallel and at a 45° angle to orthogonal joints shows that 1.41 times less force is needed to eject rock units parallel to joint sets, suggesting a possible mechanical factor responsible for preferred ejection along the joint sets, which should result in a square-shaped crater with its diagonals parallel to the joints.

Both models are confined to the late stages of crater excavation. We assume that the target rock in the models is sufficiently far away from the point of impact to form coherent units that are not dominated by impact-induced damage. This assumption also implies that for simple craters the effects of obliquity prevail during the early stages of crater excavation and

give way to the effects of pre-existing target features like joint sets as the shock wave diminishes and causes less homogenization of the target material. Target heterogeneities start to influence the cratering flow when the stresses induced by the flow are in the same order of magnitude as the strength of the target rock. In this case, planes of weakness, such as joints or bedding surfaces become zones of deformation localization.

The effect of target heterogeneity on the crater shape increases with time and progressing crater excavation, while the effect of obliquity decreases with time. This affects the ejecta patterns in different ways. Obliquity is seen most strongly in the early, distal ejecta, whereas target heterogeneity, as a factor that has an effect on the later stages of cratering, becomes visible in the late, proximal ejecta.

Acknowledgements

We are very grateful to P. Senthil Kumar, who was kind enough to coordinate the publication of his structural data of Meteor Crater with ours. M.H.P. is grateful to the Barringer Family for awarding a travel grant to present the ideas in this paper at the LMI 2008, and to the Dallas Family Fund for further aid. We are additionally grateful to the Barringer Family for granting us permission to perform research on the crater. We appreciate the efforts John Spray and an anonymous reviewer have made to improve the content and style of this paper. Finally, we would like to thank the DFG for funding this project (KE 732-11/1). This is LPI Contribution No. 1427.

References

Aittola, M., T. Öhman, J.J. Leitner, and J. Raitala (2007), The characteristics of polygonal impact craters on Venus, *Earth, Moon and Planets*, *101*, 41-53.

Anderson, J.L.B., P.H. Schultz, and J.T. Heineck (2003), Asymmetry of ejecta flow during oblique impacts using three-dimensional particle image velocimetry, *J. Geophys. Res.*, *108*(E8), 13-1, doi:10.1029/2003JE002075.

Barringer, D.M., Coon Mountain and its crater (1905), *Proceedings of the Academy of Natural Sciences of Philadelphia*, *57*, 861-886.

Barringer, D.M., Meteor Crater in Northern Central Arizona (1909), *Pap., Autumn Meeting of the National Academy of Sciences at Princeton Univ*.

Elston, W.E., A.W. Laughlin, and J.A. Brower (1971), Lunar near-side tectonic patterns from Orbiter 4 photographs, *J. Geophys. Res.*, *76*, 5670-5674.

Eppler, D.T., R. Ehrlich, D. Nummedal, and P.H. Schultz (1983), Source of shape variation in lunar impact craters: Fourier shape analysis, *Geological Society of America Bulletin*, *94*, 274-291.

Fulmer, C.V., and W.A. Roberts (1963), Rock induration and crater shape, *Icarus*, *2*, 452-465.

Gault, D.E. (1968), Impact cratering mechanics and structures, in *Shock metamorphism of natural materials*, edited by B.M. French, and N.M. Short, pp. 87 - 100, Mono Book Corp., Baltimore.

Gault, D.E., and J.A. Wedekind (1978), Experimental studies of oblique impact, in *Proc. Lunar Planet. Sci. Conf., 9th*, pp. 3843 - 3875, Pergamon Press, Inc., Houston, Tex.

Grant, J.A., and P.H. Schultz (1993), Erosion of ejecta at Meteor Crater, Arizona, *J. Geophys. Res., 98*, 15033-15047.

Herrick, R.R., and K.K. Hessen (2006), The planforms of low-angle impact craters in the northern hemisphere of Mars, *Meteorit. Planet. Sci*, *41*, 1483-1495.

Kring, D.A. (2007), Guidebook to the geology of Barringer Meteorite Crater, Arizona (a.k.a. Meteor Crater), *LPI Contrib., 1355*, 150 pp., Lunar and Planet. Inst., Houston Tex.

Kenkmann, T., and B.A. Ivanov (2006), Target delamination by spallation and ejecta dragging: An example from the Ries crater's periphery, *Earth Planet. Sci. Lett.* 252, 15-29.

Kumar, P.S., and D.A. Kring (2008), Impact fracturing and structural modification of sedimentary rocks at Meteor Crater, Arizona, *J. Geophys. Res.*, 113, E09009, doi:10.1029/2008JE003115.

McDonald, M.A., H.J. Melosh, and S.P.S. Gulick (2008), Oblique impacts and peak ring position: Venus and Chicxulub, *Geophys. Res. Lett., 35* (7), L07203.

Nininger, H.H. (1956), Arizona's Meteorite Crater; past, present, future, *American Meteorite Museum*, 1 - 232.

Öhman, T., M. Aittola, V.P. Kostama, M. Hyvärinen, and J. Raitala (2006), Polygonal impact craters in the Argyre region, Mars: Evidence for influence of target structure on the final crater morphology., *Meteorit. Planet. Sci*, *41*, 1163-1173.

Poelchau, M.H., and T. Kenkmann (2008), Asymmetric signatures in simple craters as an indicator for an oblique impact direction, *Meteorit. Planet. Sci.43*, 2059-2072.

Rinehart, J.S. (1958), Distribution of meteoritic debris around the Arizona meteorite crater, *Smithsonian Contributions to Astrophysics*, *2*, 145-160.

Roddy, D.J., J.M. Boyce, G.W. Colton, and A.L. Dial (1975), Meteor Crater, Arizona, rim drilling with thickness, structural uplift, diameter, depth, volume, and mass balance calculation, in *Proc. Lunar Sci. Conf., 6th*, pp. 2621-2644, Pergamon Press, Inc., Houston, Tex.

Roddy, D.J. (1978), Pre-impact geologic conditions, physical properties, energy calculations, meteorite and initial crater dimensions and orientations of joints, faults and walls at Meteor Crater, Arizona., in *Proc. Lunar Planet. Sci. Conf., 9th*, pp. 3891-3930, Houston, Tex.

Shoemaker, E.M. (1960), Penetration mechanics of high velocity meteorites, illustrated by Meteor Crater, Arizona, *Rep, Int. Geol. Congr., XXI Session*, 418-434.

Shoemaker, E.M. (1963), Impact mechanics at Meteor Crater, Arizona, in *The Moon, Meteorites and Comets*, edited by B.M. Middlehurst, and G.P. Kuiper, pp. 301-336, University of Chicago Press, Chicago.

Shoemaker, E.M., and S.W. Kieffer (1974), Guidebook to the geology of Meteor Crater, Arizona, in *37th Ann. Meeting of the Meteoritical Soc.*

Twiss, R.J., and E.M. Moores (1992), *Structural Geology*, 532 pp., W. H. Freeman and Company, New York.

4. Low-angle collision with Earth: The elliptical impact crater Matt Wilson, Northern Territory, Australia

This chapter has been published as the following peer-reviewed article:

Kenkmann, T. and Poelchau, M. H., 2009. Low-angle collision with Earth: The elliptical impact crater Matt Wilson, Northern Territory, Australia. Geology 37, 459-462.

Abstract

Nearly all meteorite impact craters on Earth are circular. However, ~4% of craters should be formed by impacts at angles lower than 12° from the horizontal, which should result in elongated crater structures. The crater-forming process that produces elliptical shapes is poorly understood. We document the first elliptical crater on Earth that contains a central uplift and that provides insights into the mechanisms of crater formation at a critical threshold angle of 10°–15°. The dimensions of the Proterozoic Matt Wilson impact structure, Northern Territory, Australia, are 7.5 by 6.3 km, corresponding to an aspect ratio of 1.2, with its long axis trending northeast-southwest. The exposed crater floor shows a preferred stacking of thrust sheets within the central uplift and in the surrounding syncline, indicating northeast-southwest shortening and a material transport top-to-the-SW. This is consistent with an uprange to downrange motion of rock, caused by remnant horizontal momentum transferred from the impacting projectile to the target. This preferential deformation interferes with a radially oriented convergent material flow characteristic for crater collapse. The Matt Wilson crater provides evidence for the usefulness of structural asymmetries as a diagnostic tool to infer impact vectors. The new impact crater is confirmed by the presence of planar deformation features, planar fractures in quartz grains, and its structural inventory.

5. Signatures of an Oblique Impact in the Central Uplift of Martin Crater, Mars.

Introduction

The highly oblique, elliptical Matt Wilson crater shows that bedding strike is perpendicular to the long axis of the ellipse, thus giving a possible independent indicator for an impact direction. This imbrication is interpreted as the expression of the horizontal component of momentum transferred from the projectile to the target during an oblique impact. 3D numerical modeling results of oblique impacts (Shuvalov and Dypvik, 2004, Elbeshausen and Wünnemann, 2008) confirm this interpretation and show a downrange shift of the rising central peak during crater modification.
Due to constant erosion on Earth, the ejecta blanket can not be used to confirm the impact direction inferred by the imbrication and thrusting seen in terrestrial central peaks, therefore other planetary surfaces where the ejecta blanket is preserved need to be observed. Results of mapping performed on the central uplift and ejecta blanket of Martin Crater, Mars (Fig. 1), are presented here and suggest imbrication and strike orientation as a possible indicator for an impact direction.

Method

Layered bedrock is well exposed in Martin Crater's central uplift, has excellent coverage with MOC and HiRISE imagery (Malin et al., 1992, McEwen et al. 2007), and can thus be used to control details of how the central uplift was formed during crater modification, as was first observed by Milam (2008). A GIS-based map of Martin Crater was created with an emphasis on the structural deformation of the layered units. Strike, dip and structural trends of folding and faulting were inferred from rock layers.

Geological Overview

Martin Crater is located at 21.4° S 69.2° W, south of Valles Marineris in Thaumasia Planum, part of the volcanic Thaumasia plateau (Fig. 1). Thaumasia Planum is mapped as older ridged plains material of late Noachian to early Hesperian age, which is interpreted as plains volcanism by Dohm and Tanaka (1999). Wrinkle ridges of late Noachian to early Hesperian age have permeated the relatively flat plains material and are interpreted as contractional folds or thrust faults (Dohm and Tanaka, 1999). The central uplifts of Martin Crater and numerous other craters throughout the Thaumasia plateau have exposed layered bedrock from deeper crustal levels, as seen in MOC and HiRISE imagery. These rocks are assumed to be layered

deposits of volcanic or sedimentary origin, similar to those in Valles Marineris, and must have been deposited as horizontal layers. Where exposed in coherent, undeformed blocks, beds are in parallel to sub-parallel layers, and the thickness of individual layers varies between several tens of meters down to 1 m (Fig. 2).

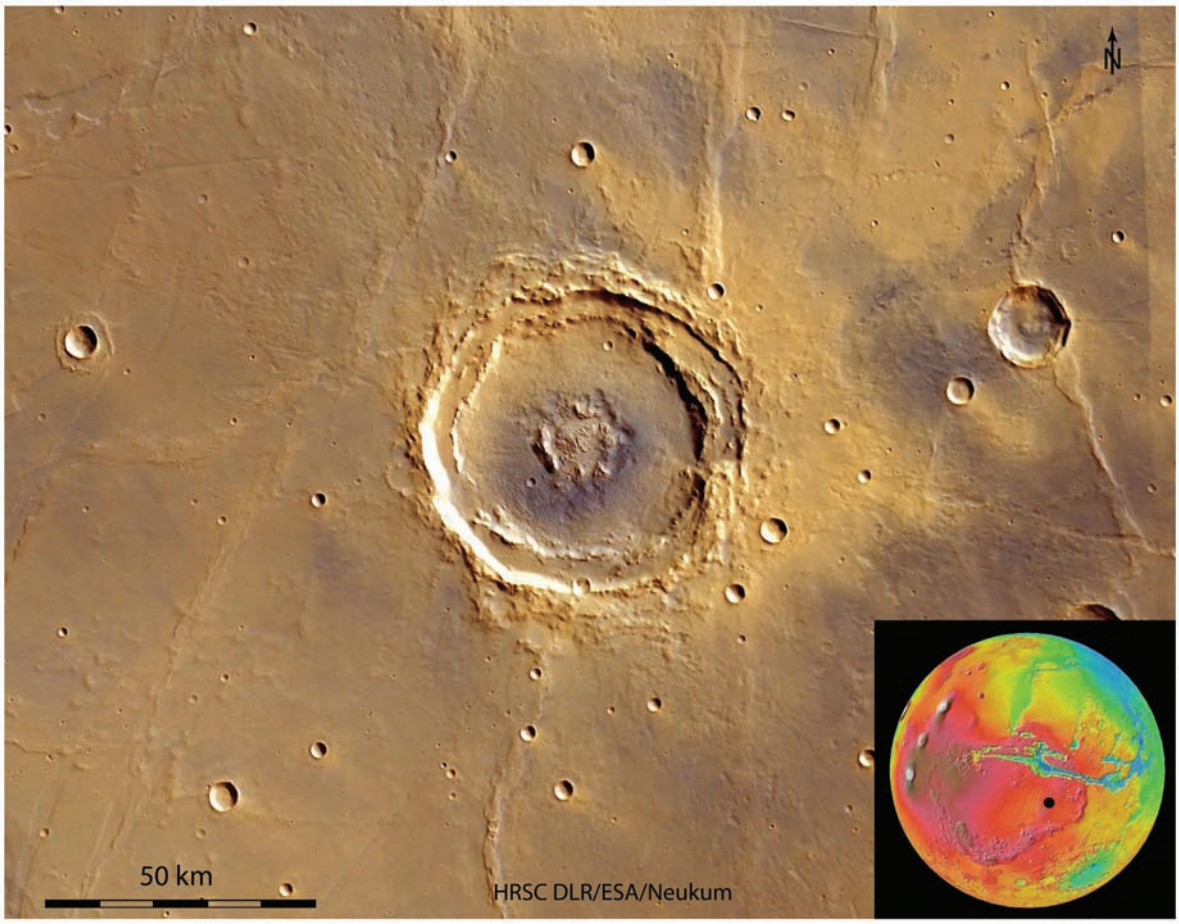

Fig. 1: Martin Crater, Mars, located in the volcanic Thaumasia Planum region south of Valles Marineris.

The ~60 km diameter Martin Crater has a terraced rim and a ~16 km diameter central uplift (Fig. 1), which consists of an outer group of massive rock units forming several peaks, and a more highly disrupted inner group. Impact melt encompasses the uplift on all sides, and blocks of layered rock have been observed “floating” in the melt.

Results

Good structural control of rock deformation in remote sensing imagery of Martin Crater is mainly due to the fact that the rock layers have rotated from the horizontal by ~90° during central uplift formation, exposing their cross-sections to the surface (Fig. 2). Most rock units mapped were estimated to be nearly vertical (65% at 75-90° dip). The percentage of non-vertical layers (35%, <75° dip) appears to be randomly distributed throughout the central uplift. Strike is shown in Fig. 3b, and reveals a dominant NW-SE trend in all parts of the central uplift. Similarly, non-vertical layers normally dip to the SW. Two km-scale folds

dominate the western half of the uplift, with vertically plunging fold axes (Fig. 2). Fold formation is largely accommodated by fracturing.

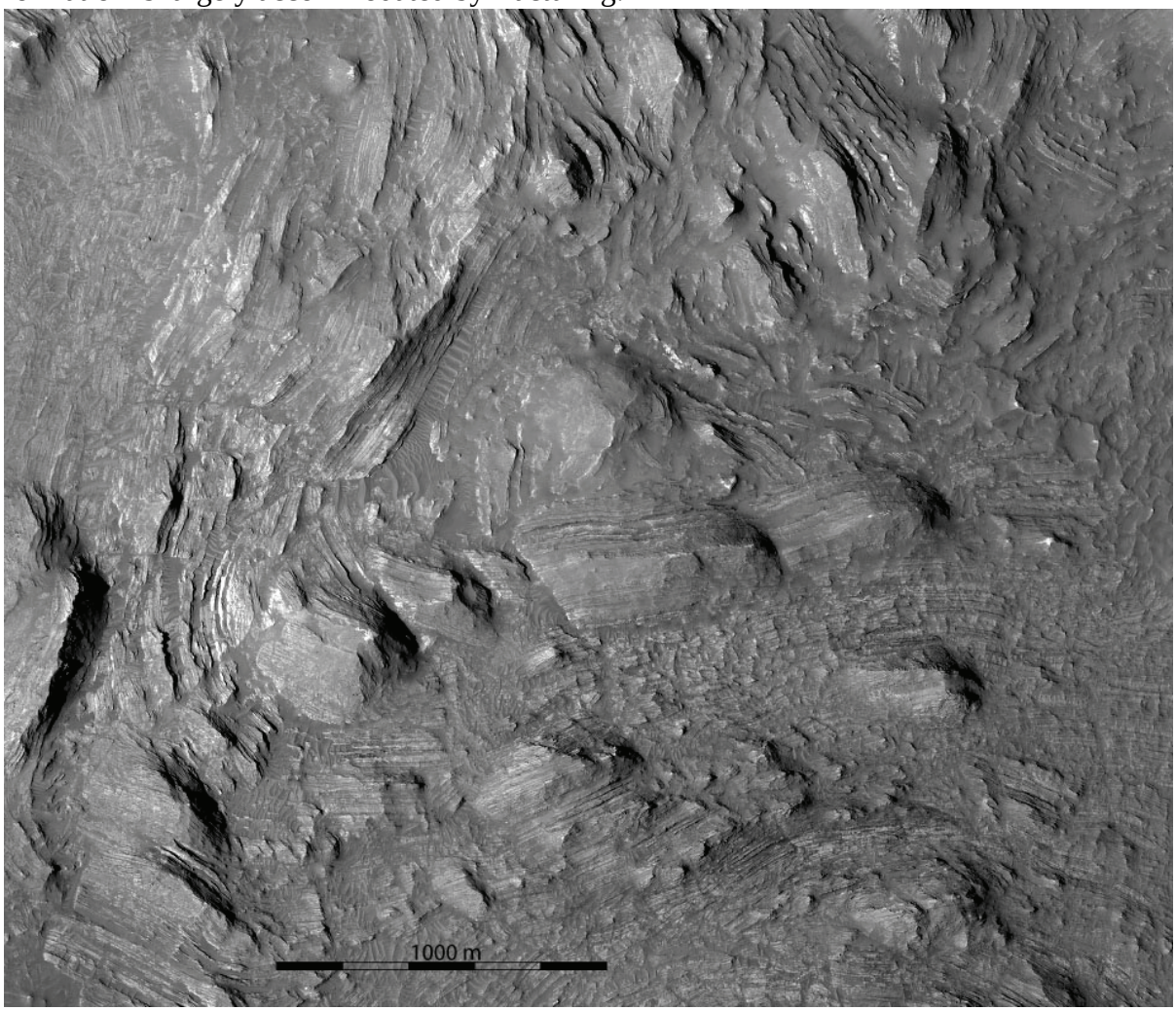

Fig. 2: Folded and fractured bedrock in the central uplift of Martin Crater. HiRISE imagery.

The ejecta blanket was mapped to determine the impact vector independently (Fig. 3a). Best visualization was achieved with THEMIS nighttime IR images. Two ejecta layers are visible, an outer, radial-shaped blanket and an inner, infrared-bright blanket that shows a bilateral symmetry axis running NE-SW and a stronger concentration of ejecta in the SW.

Discussion of Martin Crater results

The obvious NW-SE strike throughout the central uplift indicates that the originally horizontal layered bedding must have been folded and thrust upward by a dominant force perpendicular to the strike, as opposed to a radially inward converging force that would have led to concentric strike behavior. Based on the flat appearance of Thaumasia Planum and the lack of any obvious large scale structural heterogeneities visible on the surface, it seems plausible that the structural deviation from radial behavior can be linked to an oblique impact coming either from the NE or SW. The shape of the inner ejecta layer suggests that the

impactor came from the NE (Fig 3a), thus independently confirming that strike of central uplifts is oriented perpendicular to the impact direction, as was also demonstrated in the case of Matt Wilson in the previous chapter. The SW (downrange) dip direction trend contradicts what would be expected during the imbrication of a central uplift that shifts downrange as it rises upwards; i.e., stacked layers should dip in uprange direction, reflecting thrusting in downrange direction. The possibility that N-S trending, west dipping wrinkle ridges have influenced central peak behavior cannot be ruled out, but seem highly improbable based on the striking correlation of the two axes of ejecta and deformation orientation.

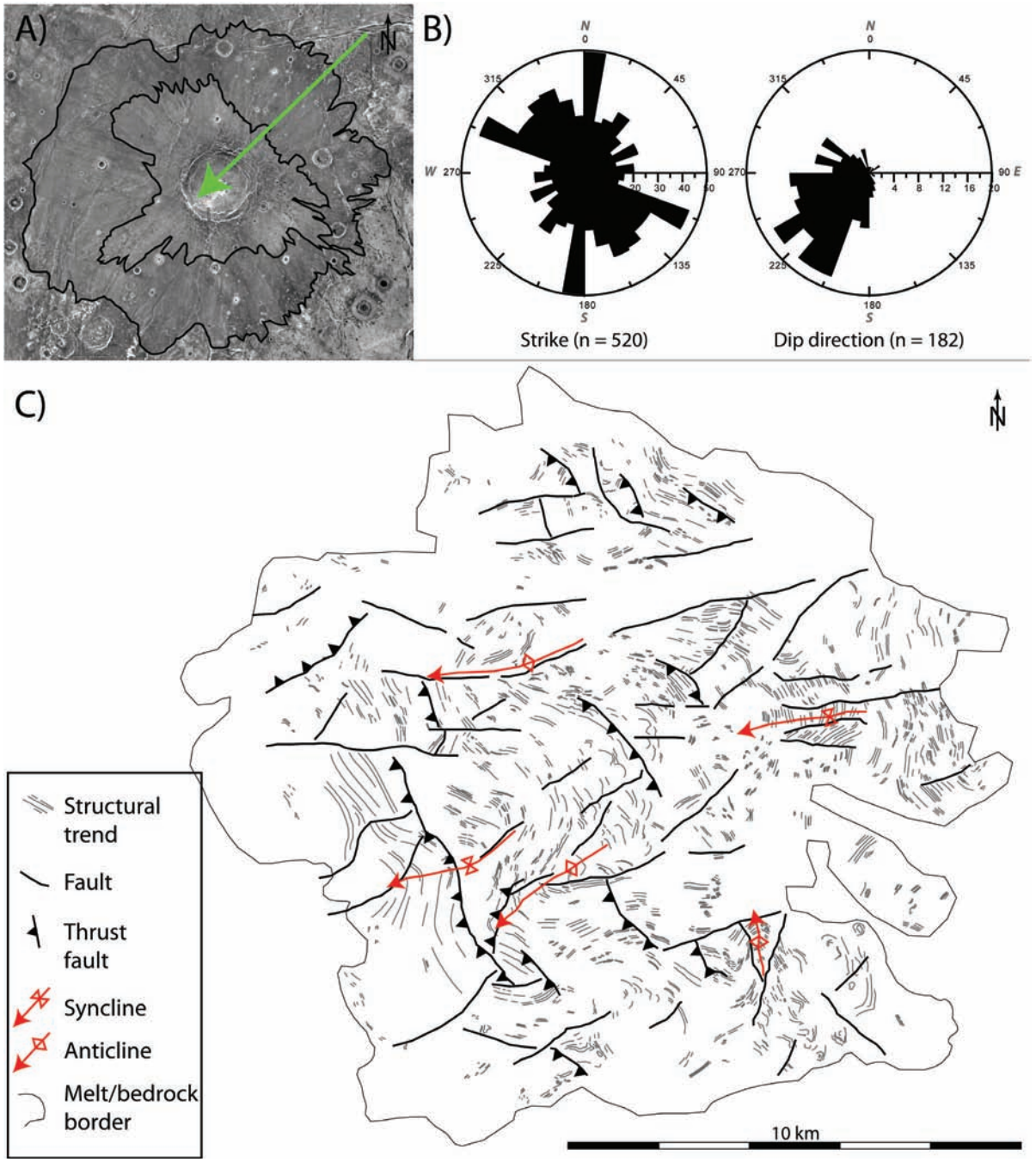

Fig. 3: Results of structural mapping. A) THEMIS nighttime IR imagery of Martin Crater's ejecta blanket implies an impact from the NE. B) Polar plots of strike and dip measurements of bedding planes in the central uplift show an obvious trend, inferring deformation from the SW. C) Structural map of the central uplift.

Numerical Modeling of oblique impacts

Recent advances in the numerical modeling of 3D oblique impacts give insights into the details of central uplift formation and deformation. The model in Fig. 4 summarizes the results of a 3D simulation performed by Dirk Elbeshausen (Elbeshausen and Wünnemann, 2008). In this model, a 5 km diameter granite projectile struck a granite target at an angle of 30° and a velocity of 6.5 km/s. Gravitational acceleration was 9.81 m/s², and a Tillotson equation of state, a strength model and acoustic fluidization were applied. The obliquity of the impact has a strong effect on the formation of the transient crater, which is lop-sided. In particular, the downrange crater wall has a more shallow slope than the uprange wall, and the excavation flow field is stronger downrange than uprange. This leads to an unequal transition from crater excavation to crater modification in different parts of the crater. While the excavation flow field is still active downrange, it has stopped uprange in the steeper crater wall. Crater rim collapse and slumping are then initiated first uprange, with material shifting downrange to the crater center. This movement affects the central peak, pushing it further downrange as rebounds and rises upwards. In this simulation, the slumping of the downrange sector is a late stage process with less force than the uprange slumping, and thus has a much smaller effect on the deformation of the central uplift.

This model indicates that the non-radial deformation observed in central uplifts is not simply caused by the transfer of horizontal momentum from the projectile to the target, but is connected to a more complex chain of events. The asymmetrical excavation of the transient crater is a major feature, effecting not only *structural* asymmetries of crater modification, but, perhaps most importantly, *temporal* asymmetries.

The model does not directly explain the apparent contradiction observed in Martin Crater. In models performed by Shuvalov and Dypvik (2004), a similar downrange shift of the central uplift is observed, followed by a late-stage uprange shift, which is strongest in the top layers of the uplift. Presumably, this is caused by the late stage slumping of the downrange walls in uprange direction that had a stronger effect than in D. Elbeshausen's model. Therefore, the "reverse" structural orientation of Martin Crater may be affected by oscillating movements of late stage, uprange directed slumping that vary based on impact cratering conditions chosen in the model. Furthermore, the orientation of deformation may change with depth, with top layers deformed in uprange direction in fresh craters, and lower layers deformed in downrange direction in highly eroded craters like Matt Wilson.

The amount of asymmetric deformation caused by an oblique impact may be most strongly related to the cratering efficiency of the impact event. Cratering efficiency is defined as the ratio of mass displaced from the (transient) crater to the mass of the projectile (Melosh, 1989). Previous studies have already shown a connection between cratering efficiency and the threshold angle for elliptical crater formation (10-15° for planetary scales), in which poor

cratering efficiency increases the threshold angle (i.e., higher-angle impacts are elliptical; Bottke et al., 2000). Similar effects should then be expected for asymmetric transient crater excavation. Cratering efficiency increases with increasing projectile velocity and with increasing target density, while it decreases with increasing projectile diameter for a constant velocity (Melosh, 1989). Thus, large, slow impacts into sedimentary rocks or similar low density target material should cause greater asymmetry effects. It should also be noted that the vertical component of projectile velocity decreases with decreasing impact angle, indicating that oblique impacts have poorer cratering efficiency than vertical ones.

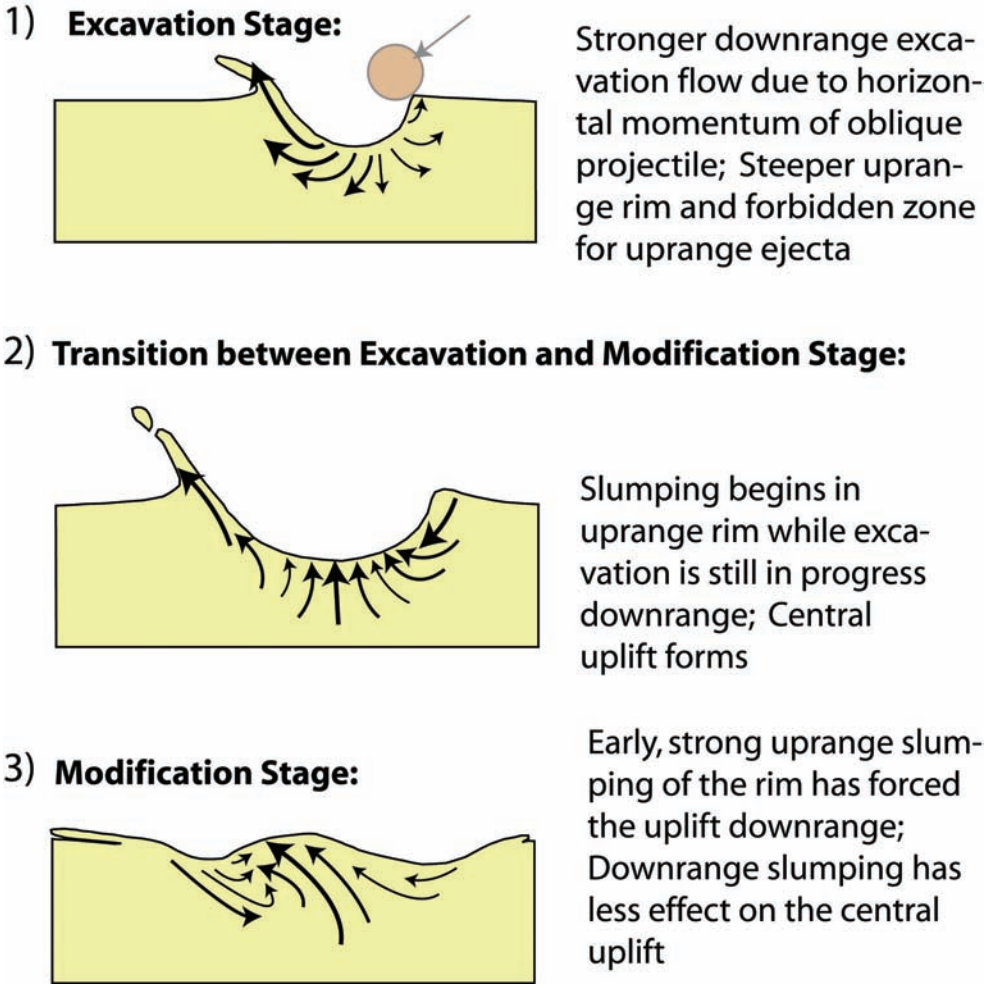

Fig. 4: Model based on 3D numerical modeling results of oblique impacts.

Conclusions

The success of structural mapping in Martin Crater shows the value and potential of high resolution planetary remote sensing for the understanding of impact cratering phenomena. The synthesis of terrestrial field work, planetary remote sensing, and numerical modeling has led to a deepened understanding of how oblique impacts form craters, and which structural features are specific to oblique impacts. Of course, further work is desirable to solidify these findings and reveal possible new and unexpected insights. Future plans beyond this thesis are

focused on gathering structural information from more oblique impacts on Mars, now that high resolution coverage is becoming increasingly available. In particular, craters with a well defined ejecta blanket indicating an impact direction, in combination with good exposure of layered bedrock in the central uplift will be mapped in detail. These further studies would benefit from additional results in 3D numerical modeling, which explore the influence that factors like projectile speed or target density have on the oblique cratering process.

References

Bottke W. F., S. G. Love, D. Tytell, T. Glotch, 2000. Interpreting the Elliptical Crater Populations on Mars, Venus, and the Moon. Icarus 145: 108-121.

Dohm, J. M., K. L. Tanaka, 1999. Geology of the Thaumasia region, Mars: Plateau development, valley origins, and magmatic evolution. Planetary and Space Science 47: 411-431.

Elbeshausen D., K. Wünnemann, 2008. Asymmetries in complex craters due to oblique meteorite impacts? Large Meteorite Impacts IV Abstract #3080

Malin, M. C., G. E. Danielson, A.P. Ingersoll, H. Masursky, J. Veverka, M. A. Ravine, T. A. Soulanille, 1992. Mars Observer Camera. Journal of Geophysical Research, 97: 7699-7718.

McEwen, A. S., E. M. Eliason, J. W. Bergstrom, N. T. Bridges, C. J. Hansen, W. A. Delamere, J. A. Grant, V. C. Gulick, K. E. Herkenhoff, L. Keszthelyi, R. L. Kirk, M. T. Mellon, S. W. Squyres, N. Thomas, C. M. Weitz, 2007. Mars Reconnaissance Orbiter's High Resolution Imaging Science Experiment (HiRISE) Journal of Geophysical Research, 112. E05S02, doi:10.1029/2005JE002605

Melosh, H.J., 1989. Impact Cratering: A Geologic Process. Oxford University Press, U.K. Paperback, 245 pp.

Milam, K., 2008. Petrogenesis of Central Peak Formation on Mars. Large Meteorite Impacts IV Abstract #3089.

Shuvalov, V.V., H. Dypvik, 2004. Ejecta formation and crater development of the Mjølnir impact: Meteoritics & Planetary Science, 39: 467–479.

6. Feather Features: A Low Shock Pressure Indicator in Quartz

This chapter has been submitted as a manuscript:

Poelchau, M.H., and T. Kenkmann, 2010. Feather Features: A Low Shock Pressure Indicator in Quartz. Submitted to Earth and Planetary Science Letters.

7. General Conclusions

As the acceptance of impact cratering as a terrestrial phenomenon continues to grow among geologists, more craters are expected to be found on all continents, thus showing the need for a deeper understanding of the impact cratering process and a deeper understanding of how features of impact cratering can be recognized on Earth. As stressed in this thesis in chapter 1, while oblique impacts occur commonly on all bodies in the solar system, little work, particularly ground-truth structural research, has been done so far to categorize indicators of impact obliquity, as to differentiate these features from other aspects of cratering. The main goal of this thesis was to focus on structural effects of oblique impacts.

In chapters 2 and 3, it was proposed that the asymmetry commonly seen in ejecta blankets of oblique impacts on the Moon and Mars should be structurally traceable to the most proximal parts of the ejecta blanket up to the overturned flap in the crater rim, where the excavation process came to a halt. The motivation for this first study is based on the fact that the ejecta blanket is not well preserved in terrestrial craters and thus is normally useless for indicating an impact direction, while, on the other hand, three dimensional structural data are easily acquired in the field on Earth and difficult to obtain from remote sensing data. For the evaluation of the data collected in the two terrestrial craters, Wolfe Creek and Meteor Crater, a novel approach was introduced which combined the azimuthal position of data relative to the crater center together with the deviation of bedding strike from tangential or concentric orientation, termed concentric deviation. The visualization of these data in x-y- and polar plots was very useful for revealing structural trends of the rim, and resulted in proposed impact directions for both craters, based on a “two corners” pattern derived from radial grooves observed on Tooting Crater, Mars. A similar pattern based on lunar and Martian crater rays, the “cardioid pattern”, was proposed by Schultz et al. (2007).
While the proposed impact directions are constrained by other possible indicators, e.g. meteorite distribution and ejecta thickness, the method does have weaknesses that need to be refined. The datasets show a strong degree of scattering or “noise”, which impedes the recognition of the “two corners” pattern, and it appears that the trends are close to the limit of detection needed for a confirmation. The method for smoothing the datasets (the “overlapping bins” method), which is needed to fit the data curve to the “two corners” pattern, requires further work before it can be used as a quantitative method. For example, changing the bin size may strongly alter the shape of the curve, the choice of bin size is arbitrary, and a statistical discussion of error margins for the fit of the data curve to the “two corners” pattern is necessary. Additionally, the shape of the “two corners” pattern is based on theoretical considerations and has only been confirmed for one crater on Mars. For the “two corners” pattern to be quantitatively useful, it at least needs to be constrained to a specific range of impact angles, as highly oblique or more vertical impacts are expected to alter its shape.

Further remote sensing studies of ejecta blankets would therefore help to improve the “two corners” pattern. Cratering efficiency, which itself is governed by projectile size and mass along with target properties, may also have an effect on the pattern.
The effect of preimpact target heterogeneities on the cratering process was thoroughly discussed for Meteor Crater and was shown to influence differential crater rim uplift, which in turn affects the structure of the proximal ejecta blanket. This aspect has so far not been researched for Matt Wilson, and, if done so, may also affect the current results. The results for Meteor Crater do offer a perspective for the application of the analysis of strike data to the high resolution remote sensing images of Mars and the Moon. There, evaluation of strike of layers now readily visible in the lower parts the rims of simple crater could be used to indicate possible preimpact structural trends similar to those at Meteor Crater that are otherwise concealed by the topmost regolith layers.

In chapters 4 and 5, the focus on the effects of obliquity were shifted from the crater rim to the central uplift, and thus from the excavation stage to the modification stage. In a previous study (Scherler et al., 2006) asymmetries observed in the internal structure of central uplifts in several terrestrial craters were proposed to be the result of oblique impacts transferring a non-radial component of momentum to the target. The Australian Matt Wilson structure was mapped to confirm this and proved to be the optimal choice. Its elliptical shape constrained the impact trajectory to two possible directions and showed that the structure was formed by a highly oblique impact, providing independent indicators of obliqueness that were lacking from other studied terrestrial craters. Mapping confirmed that the structural asymmetries of the central uplift, i.e., thrusting and imbrication of bedding in a preferred direction, coincided with the long axis of the crater ellipse, thus giving strong evidence for a connection between preferential deformation and impact obliqueness. In the second study, structural mapping of the central uplift of the Martian Martin Crater showed that non-radial preferential thrusting also coincides with the asymmetric distribution of the ejecta blanket, but also that the thrusting is in the exact opposite direction as expected and originally proposed. These surprising results also contradict 3D numerical models, which demonstrate how oblique impacts form asymmetric transient cavities that preferentially slump in the uprange sector, thus pushing the central uplift downrange as it rises.
The ground truth results show that the numerical models do not correctly describe the situation observed in Martin Crater. This means that the results of this study have a qualitative value in connecting structural deformation with obliqueness, but that more work is needed for quantitative constraints. Specifically, more studies are needed to show how asymmetric crater excavation, preferential slumping and central uplift movement are influenced by different parameters. The degree of asymmetry in crater excavation is most likely governed by the ratio of radial excavation initiated by the shock wave, to preferential horizontal momentum of the impactor. Therefore several factors, including projectile size, speed and angle, target density

and gravity must be taken into consideration, which all influence how efficiently a crater is excavated. Preferential slumping appears to be affected by an asymmetric transient crater, although temporal aspects make this process more complex. If slumping occurs too early, the slumped rim may pass over the central uplift before it begins to rise. If it is too late, it will have little effect on the deformation of the central uplift. Additionally, the relationship between uprange and downrange excavation flow and rim steepness should result in different amounts and styles of crater rim slumping. Numerical models by Shuvalov and Dypvik (2004) show how the downrange movement of the central uplift is followed by a late-stage uprange shift. Although no explanation for this is given in the paper, uprange slumping followed by a more effective downrange slumping than in the model discussed above seems plausible as a driving mechanism. Preimpact target heterogeneities like large-scale joint sets, faults, or sloped terrains should also affect the orientation of slumping, although in the case of Martin Crater, the fact that the ejecta blanket and the imbrication of the central uplift are aligned along the same axis speaks against the influence of target heterogeneities. Target properties should also influence the style of structural deformation in the central uplift. Imbrication and thrusting are expected to be facilitated in horizontally layered targets. The relationship of competent and incompetent beds, e.g. sandstone or clays, must affect how deformation is compensated, while in massive, unlayered plutonic or volcanic rocks, the imbrication in the central uplift should be less pronounced.

Currently, only the two craters in this thesis: Matt Wilson and Martin Crater have been described as having imbricated uplifts together with independent indicators for the impact direction, or at least the axis of the impact direction. Therefore, future studies of central uplifts on Mars are planned for better quantitative control on the oblique cratering process. Craters with asymmetric ejecta blankets in layered targets will be selected, the impact angle and direction will be estimated based on the ejecta shape, crater size will be taken into account, and, if possible, differential slumping of crater rims and the distribution of terraces will be inspected and quantified.

Chapter 7 originated from the search for, and general lack of, PDFs as shock deformational features in quartz from collected samples, needed to confirm that the Matt Wilson structure is indeed an impact crater. The later discovery of rare PDFs proved to be of secondary importance for this study in comparison with the occurrence of “feather features” in numerous samples from Matt Wilson and other craters. Feather features, or FFs, are sets of lamellae with similar appearance to PDFs that emanate from planar fractures in quartz. Their occurrence in numerous craters and their generation in shock experiments suggest they are uniquely shock metamorphic features formed at low shock pressures.

FFs are shear induced features that require high differential stresses to form. While these stresses can occur through the heterogeneous expansion of the shock wave through a non-uniform target, their generation may be greatly facilitated by projectiles striking at oblique or

highly oblique angles, shearing as they contact the target and compress. This means that, although it would go too far to suggest that FFs are oblique impact indicators, they can be used to point out localized shear stresses and define the orientation of the stress field, thus giving possible insights into the development and propagation of the shock wave under varying conditions.

To conclude, this thesis has successfully shown that structural deformation of the central uplift of impact craters can be tied to oblique impacts. The structural deformation of crater rims may also show effects of oblique impacts, but these effects can be concealed by the level of "noise" in the data and by the influence of preimpact target heterogeneities. Shear induced microstructural feather features that occur in shocked quartz were analyzed, and their occurrence may be affected by the amount of shearing caused by obliquely striking projectiles.
This thesis has contributed to the knowledge of the structural inventory of impact craters in a qualitative sense and has shown the need for further work focusing on quantitative constraints. It is hoped that the results of this thesis will find use and application in remote sensing studies of impact craters, giving insights into the cratering process and the target subsurface, as well as aiding the structural study of known terrestrial impact craters and the identification of unknown ones.

References:

Scherler D., Kenkmann T. and Jahn A. 2006. Structural record of an oblique impact. Earth and Planetary Science Letters 248:43-53.

Schultz P. H., Eberhardy C. A., Ernst C. M., A'Hearn M. F., Sunshine J. M. and Lisse C. M. 2007. The Deep Impact oblique impact cratering experiment. Icarus 190:295-333.

Shuvalov V. and Dypvik H. 2004. Ejecta formation and crater development of the Mjølnir impact. Meteoritics & Planetary Science 39:467- 479.

The curriculum vitae is excluded from the online version due to protection of privacy laws.

Danksagung

Ich bin sehr vielen Leuten dankbar.

Dank gilt meinem Betreuer Thomas Kenkmann, für seine unglaubliche Unterstützung, Energie, Motivation und Hingabe zu dem Thema meiner Doktorarbeit. Für seine Bodenständigkeit, und dafür, dass er Tacheles reden konnte. Dass seine Kritik direkt war und immer wieder zeigte, wie sehr er an meinem Vorankommen interessiert war. Für die Abenteuer auf sage und schreibe 6 Kontinenten und das Seemannsgarn, das wir daraus gesponnen haben. Für meine Weiterbeschäftigung. Und insbesondere dafür, dass ich mir keinen besseren Betreuer vorstellen kann als ihn, und jedem Doktoranden die Betreuung wüsche, die ich in den 3 ½ Jahren erhalten habe. Auf ein erfolgreiches Weiterarbeiten in Freiburg, und danke nochmals für Alles!

Dank an Silke Jahn-Awe und Thorsten Sander, die mir den Weg zum DLR gebahnt haben und damit mein Interesse an Planetologie gestärkt haben; Dennis Reiss, der mir diese Doktorarbeit vermittelt hat und mich sehr gut während meines Praktikums am DLR betreut hat, und nachher während der Doktorarbeit immer wieder fachlich und menschlich unterstützt hat.

Dank gilt dem Museum für Naturkunde, altes Haus, für seine faszinierende Geschichtsträchtigkeit und seine Dinos, die mich morgens begrüßt und mir nachts Gesellschaft geleistet haben; den Leuten im Museum, ohne die das Museum einfach nur ein altes Haus gewesen wäre. Uwe Reimold, für Leitung unserer Gruppe. Auf ihn war immer Verlass, wenn man Unterstützung jedweder Art brauchte. Dann Dieter Stöffler, Kai Wünnemann, Lutz Hecht, Ansgar Greshake, Ralf Schmitt, Jörg Fritz, die immer ein offenes Ohr für meine Probleme und Fragen hatten, und die unsere Gruppe so dynamisch und aktiv gehalten haben. Dank an die vielen alten und neuen Doktoranden, Diplomanden, TAs, Hiwis und Sekretärinnen, mit denen man alles Mögliche besprechen und zum Teil Pferde stehlen konnte (in ungewichteter Reihenfolge: Andi, Tanja, Conny, Astrid, Dirk, Daniel, Sarah, Nina, Michael, Alex, Martin, Claudia, Ulli, Hans, Daniela, Harold, Siya, Birgit, Kirsten, Peter, Katrin, Anthony, Max, Tobias, Frank, Axel, Roald, Daniel, Frederike, Frau Gerhard, und viele mehr). Den ganzen Kollegen außer Haus und z. T. im Haus, die dafür gesorgt haben, dass Impaktkrater ein spannendes und internationales Thema geblieben sind. Komischerweise bin ich auch dem Subway an der Chausseestr. dankbar, da dort wesentliche Teile dieser Arbeit entstanden sind.

Meiner Familie (aka „The Dallas Family Fund“) gilt Dank für die Unterstützung und Liebe, und für viele weitere Sachen, die man gar nicht hier alle auflisten kann. Meinem Vater, dafür, dass er mich zur Geologie geführt hat; meiner Mutter für die Musik, die mir Ablenkung und Perspektive gab.

Und meiner Freundin Silke, die de janze Driss mitgemacht hat und immer da war, wenn ich sie brauchte; die mein ständiges Geschwätz über dieses Thema anhören musste; die meinen Sinn für Humor ertrug; die mich unterstützte, und wichtiger noch, ablenkte und mir ein Leben neben der Doktorarbeit ermöglichte. Danke, Babe!

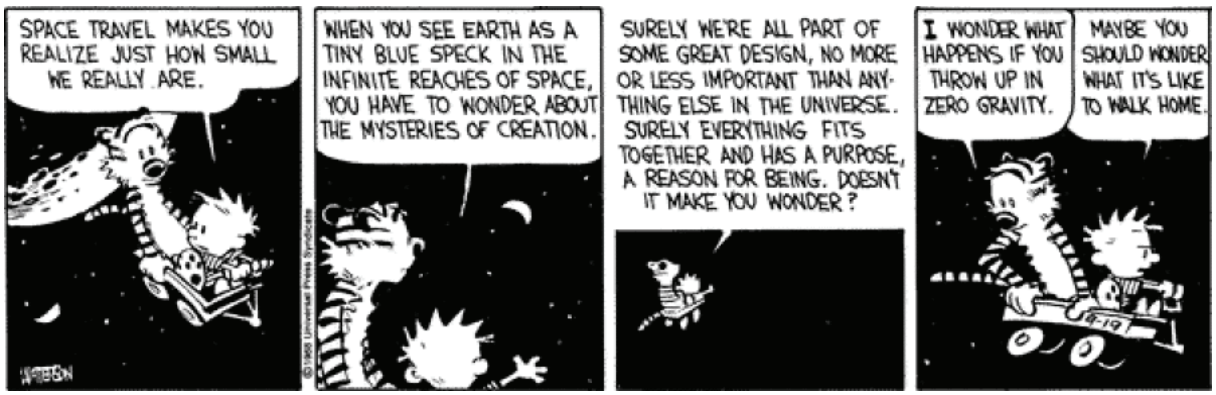
SPACE TRAVEL MAKES YOU REALIZE JUST HOW SMALL WE REALLY ARE.
WHEN YOU SEE EARTH AS A TINY BLUE SPECK IN THE INFINITE REACHES OF SPACE, YOU HAVE TO WONDER ABOUT THE MYSTERIES OF CREATION.
SURELY WE'RE ALL PART OF SOME GREAT DESIGN, NO MORE OR LESS IMPORTANT THAN ANYTHING ELSE IN THE UNIVERSE. SURELY EVERYTHING FITS TOGETHER AND HAS A PURPOSE, A REASON FOR BEING. DOESN'T IT MAKE YOU WONDER?
I WONDER WHAT HAPPENS IF YOU THROW UP IN ZERO GRAVITY.
MAYBE YOU SHOULD WONDER WHAT IT'S LIKE TO WALK HOME.